Hydrodynamic Modeling of Dielectric Response in Graphene and Carbon Nanotubes

by

Jorge Zuloaga

A thesis
presented to the University of Waterloo
in fulfilment of the
thesis requirement for the degree of
Master of Mathematics
in
Applied Mathematics

Waterloo, Ontario, Canada, 2006

I hereby declare that I am the sole author of this thesis. This is a true copy of the thesis, including any required final revisions, as accepted by my examiners.

I understand that my thesis may be made electronically available to the public.

Abstract

This thesis studies two important carbon structures, graphene and carbon nanotubes, with the purpose of understanding how their three-dimensional electron density distribution affects the way fast ions interact with them.

A brief introduction to research in pure carbon structures is made. We then use different models to calculate the equilibrium electron density distribution in graphene and carbon nanotubes.

In the second part of the thesis we investigate fast ions moving parallel to a graphene sheet and experiencing forces due to the dynamic polarization of carbon valence electrons. Using the three-dimensional electron density distribution of graphene, we calculate the force directly opposing the ion's motion (stopping force), as well as the force which bends the ion's trajectory towards the sheet (image force). It is our purpose to compare these results with those based on a two-dimensional hydrodynamic model of graphene, which approximates the electron distribution of graphene by a charged fluid confined to the two-dimensional plane of the sheet.

The results obtained for interactions of ions with a single graphene sheet should be useful for a further analysis of ion channeling through carbon nanostructures.

Acknowledgements

I would like to thank my supervisors Dr. Mišković and Dr. Goodman for their help and support throughout my studies. Thanks also to Duncan Mowbray for helpful discussions and advice.

I also want to thank all my friends at Waterloo for helping make my time here so enjoyable. And of course thanks to my family for their encouragement.

Dedication

Para Daddy.

You took off while I was working on this, but thanks for all the good times.

Contents

List of Figures

Chapter 1

Introduction

1.1 Motivation

In the final decades of the 20th century, condensed matter physics was marked by a revival of research interest in carbon-based materials. In addition to the conventional forms in which pure carbon was known to exist (graphite and diamond), new forms were discovered. The first shock to the scientific community came in 1985, when C_{60} molecules were first discovered in laboratories by Sir Harold Kroto, Richard E. Smalley and Robert F. Curl [1]. The C_{60} molecule is an arrangement of 60 carbon atoms in a highly symmetrical hollow polygon structure that resembles a soccer ball (see figure 1.1). The search for new carbon nanostructures drove scientific research in the field and in 1991 Iijima first produced carbon nanotubes [2], pure carbon cylinders with walls just one atom thick (see figure 1.2). These new macromolecules immediately sparked much excitement because of their remarkable shape and structure; they are only a few nanometers in diameter, yet (presently) up to a few millimeters long.

Carbon nanotubes have now been found to have a broad range of intriguing electronic, thermal, and structural properties, that change depending on the different

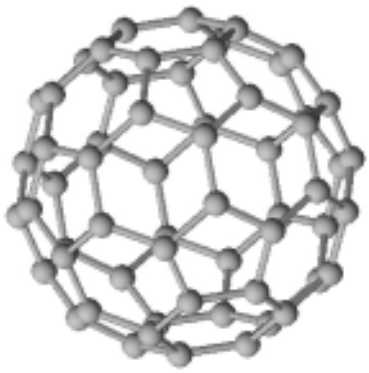

Figure 1.1: C_{60} molecule, called Buckminsterfullerene, or "buckyball".

kinds of nanotube (defined by diameter, length, and orientation of the hexagonal lattice forming their walls). They are 100-1000 times stronger than the strongest steel, and can be either metallic or semiconducting. They are also excellent thermal conductors. Because of their shape and size, carbon nanotubes are currently being used as probes in extremely sensitive scanning microscopes. They have also been used to reinforce ordinary materials, yielding compounds with greatly increased strength and heat conducting properties.

Nanotubes are now being grown on glass in a well aligned manner, resembling a wheat field, and they are expected to be used in flat panel displays such as laptop and desktop computers. Researchers have also envisioned these miniature hose-like molecules as current conductors in ever-smaller electrical circuits. Their immense field of applications has made them the "hottest topic in physics" in 2006 [3].

All these newly discovered pure carbon structures, including C_{60}, carbon nanotubes, and other polygon shaped, cage-like molecules are collectively referred to as fullerenes. Fullerenes can be thought of as wrapped up sheets of graphite (see figure 1.2). For decades scientists believed that a two-dimensional (2D) sheet of graphite (know as graphene) could not exist in its free state; they presumed that its planar structure would be thermodynamically unstable. In 2004, however, An-

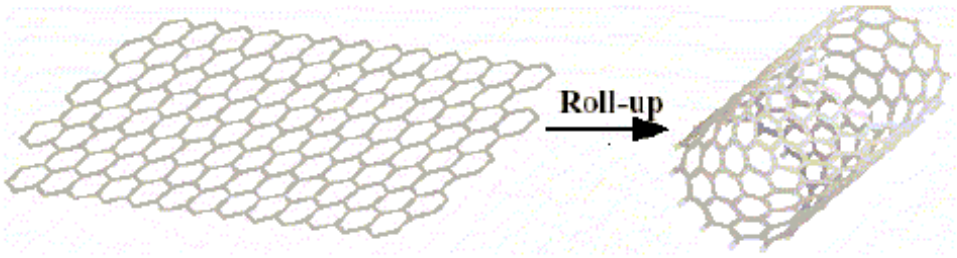

Figure 1.2: A graphene sheet and a carbon nanotube, which can be thought of as a graphene sheet rolled up into a cylinder.

dre Geim and colleagues at the University of Manchester and at the Institute for Microelectronics Technology in Chernogolovka, Russia, succeeded in isolating single graphene sheets. Their work showed that graphene is stable, chemically inert, and crystalline under ambient conditions. Graphene has also been found to tolerate huge current densities–about 10^8 A/cm^2, roughly two orders of magnitude greater than copper. Electrons in graphene can move at high speeds and suffer little energy loss. The one-atom-thick sheets of carbon have aroused much interest and are currently being studied extensively because of their fascinating physical properties and their large range of potential applications. Walt deHeer and his research group at Georgia Tech have built graphene structures (including a graphene transistor) as small as 80 nm, and expect to get down to the 10 nm size. They believe graphene will provide a more controllable platform for integrated electronics than is possible with carbon nanotubes, since graphene structures can be fabricated lithographically as large wafers.

1.2 Physical Model of the Problem

Researchers are currently trying to learn more fullerene physics. This is where the purpose of this work lays. We are primarily interested in the interactions of ions

with graphene and nanotubes under channeling conditions, where the ion (typically a proton) is represented by a point charge moving (almost) parallel to the plane with carbon atoms in the case of graphene, or to the axis of a cylinder representing a nanotube with single wall. These ions typically move at the speeds in excess of the Bohr velocity, and are striking the walls of these carbon structures under the angles of the order of 1^o. In the case of graphene, one can think of the so-called planar channeling, where the ions move between the parallel planes of graphene which are stuck at a separation of about 3.4 Å to form a crystal known as highly oriented pyrolytic graphite (HOPG). As for the carbon nanotubes, channeling can occur in three different ways: through the hollow cylindrical region of either a single-wall carbon nanotube (SWNT) or a multi-wall carbon nanotube (MWNT), between the concentric cylinders of a MWNT (which are separated by approximately 3.4 Å), and in the regions outside the cylinders representing SWNTs stuck into a rope or a bundle with the nearest carbon walls again separated by about 3.4 Å. Rather intense studies of ion channeling through carbon nanotubes have been underway over the past several years (see the review by X. Artru et al. [4]. The main interest in ion channeling through carbon nanotubes comes from their possible applications in several areas, such as

- creating and transporting highly-focused nano-beams of ions
- nano-implantation of particles in electronics, biology, and medicine
- beam steering and collimation at particle accelerators
- sources of hard X– and gamma – rays by channeled particles

While we do not pursue in this thesis any detailed study of ion channeling per se, the results obtained for the interactions of ions with a single sheet of graphene are the important first step towards full analysis of ion channeling through carbon nanostructures.

Under the channeling conditions, an ion undergoes a sequence of small-angle deflections from a large number of carbon atoms in a wall by their repulsive atomic potentials. This superposition of atomic potentials, as seen by the incident ion, results in a natural "smearing-out" of the distribution of carbon atomic positions into a continuous sheet of positive charge, which then amounts to the well-known "jellium" model for calculations of the carbon valence electron distributions in the ground (unperturbed) state. For this purpose, we use generalizations of the well-known Thomas-Fermi (TF) model for a single atom to the planar and cylindrical geometries corresponding to the cases of graphene and a single wall nanotube, respectively. Besides obtaining the exact solutions of the relevant TF equations, we also use variational methods with simple trial forms for electron densities based on minimizing the electron energy functional. In addition, we also use the Poisson equation to derive the ground-state electron distribution from the well-known atomic repulsive potentials (such as Molière's approximation to the TF potential), which are commonly used in the standard theory of ion channeling through solid crystals.

Given that the projectile charges move at the speeds in excess of the typical speeds of carbon valence electrons in the graphene or nanotube, the dynamic polarization of such electrons can be modeled by a hydrodynamic model which represents the four carbon valence electrons by a continuous charged fluid whose internal quantum degrees of freedom can be described by an equation of state resulting from TF model. Our main goal is to calculate forces acting on fast ions under channeling conditions coming from the dynamic perturbation of the three-dimensional (3D) electron distributions obtained from the above mentioned TF models for the electron density in the ground state. To this end, we employ a high-frequency approximation for the dielectric function of a non-homogeneous electron gas, which was developed by Mukhopadhyay and Lundqvist [5], rediscovered in the

classical limit by Kitagawa [6], and recently used by Apel, Sabin and Trickey [7]. In Appendix A, we present a derivation of this approximation for the dielectric function which is consistent with the TF model of electrons in the ground-state. In this way, we are able to ensure that the dynamical polarization forces are obtained in a manner consistent with modeling of the repulsive forces coming from the carbon atoms in the graphene or nanotube walls. Such consistency is very important for ion channeling since the ion trajectories are known to be extremely sensitive to the details of all the forces involved.

1.3 Purpose and Outline

We have studied both graphene sheets and carbon nanotubes. Our goal has been to study the electron density distribution in these structures and how this affects the way fast moving ions interact with them.

The first part of this work (chapters 2 and 3) is devoted to the study of equilibrium electron densities. In chapter 2, the three-dimensional equilibrium electron density for graphene is computed using different models. Chapter 3 shows calculations of the three-dimensional equilibrium electron density for carbon nanotubes.

In the second part of this work we study fast ions moving parallel to a graphene sheet and experiencing forces due to the dynamic polarization of carbon valence electrons.

When studying the energy loss of such ions, it is important to look at the force which directly opposes the ion's motion, called the stopping force. In chapter 4 we develop the theory used to calculate the stopping force. Chapter 5 shows results for calculations of the stopping force using the three-dimensional electron density distribution of graphene.

It is also of interest to study the force which bends the ion's trajectory towards

the sheet (image force), which plays a major role in the study of ion channeling. In chapter 6 we develop the theory used to calculate the image force, and in chapter 7 we show results for calculations of the image force using the three-dimensional electron density distribution of graphene.

It is our purpose to compare our calculations of stopping and image forces with calculations based on a two-dimensional hydrodynamic model of graphene, which approximates the electron distribution of graphene by a charged fluid confined to the two-dimensional plane of the sheet. In this way we intend to better appreciate the effect of having a three-dimensional electron density distribution on the interactions of fast ions with graphene. The calculations of the stopping and image forces based on the two-dimensional hydrodynamic model are well known in the literature, so we have only briefly summarized the main results in Appendix B.

Finally, we conclude with a discussion of the results and suggestions for future work in the last chapter.

Chapter 2

Equilibrium Electron Density In Graphene

In this chapter we compute the three dimensional equilibrium electron density for graphene. We shall use various models to calculate this electron density and then compare the results.

In graphene, carbon atoms form a hexagonal lattice with inter-atomic distance $d \approx 1.421$ Å[8]. The surface density of atoms is $n_a = 4/(3\sqrt{3}d^2)$ Å^{-2}. We use the jellium model to study graphene. In this model, the sheet made of individual nuclear cores is modeled by a sheet of uniform charge density σ. Considering each carbon atom to have 4 valence electrons, the surface charge density for our jellium model is given by $\sigma = 4en_a \approx 0.428$ in atomic units (a.u.). We then consider an electron gas around our positive sheet to account for the valence electrons in graphene. We shall be interested in finding the equilibrium electron density distribution around the positively charged sheet.

2.1 Equilibrium Density

In many-electron systems, equilibrium electron behavior is defined in terms of the following energy functional [9]

$$E\left[n\left(\mathbf{r}\right)\right]=\int d\mathbf{r}\left[C_{F}n^{5/3}(\mathbf{r})+C_{vW}\frac{\left[\vec{\nabla}n(\mathbf{r})\right]^{2}}{n(\mathbf{r})}-C_{x}n^{4/3}(\mathbf{r})\right]$$

$$+\frac{1}{2}\frac{e^{2}}{\left(4\pi\epsilon_{0}\right)}\int d\mathbf{r}\int d\mathbf{r}'\frac{n(\mathbf{r})n(\mathbf{r}')}{|\mathbf{r}-\mathbf{r}'|}-e\int d\mathbf{r}\ V_{+}(\mathbf{r})n\left(\mathbf{r}\right), \tag{2.1}$$

where $n(\mathbf{r})$ is the electron density and $V_{+}(\mathbf{r})$ is the electrostatic potential produced by the positive ion cores. The first two terms are the Thomas-Fermi kinetic energy functional and its von Weizsäcker correction, respectively. The third term is the Dirac exchange energy. The coefficients are given by

$$C_{F}=\frac{3}{10}\frac{\hbar^{2}}{m}\left(3\pi^{2}\right)^{2/3},\ C_{x}=\frac{3e^{2}}{4}\left(\frac{3}{\pi}\right)^{1/3},\ C_{vW}=\frac{1}{72}\frac{\hbar^{2}}{m}, \tag{2.2}$$

with $\hbar$, m, and e being Planck's constant divided by 2π, the electron mass, and the proton charge, respectively. We shall be working in atomic units (a.u.) so that $\hbar=m=e=1$, as well as in Gaussian units of electrostatics, so that $1/(4\pi\epsilon_{0})=1$. In (2.1) the fourth term represents the Coulomb interaction of the electrons with each other, while the fifth term represents the Coulomb interaction between the electrons and the positive ion cores.

2.2 Thomas-Fermi Analytical Solution

When using a Thomas-Fermi (TF) model to describe the electron density around graphene, we consider only the Thomas-Fermi term in (2.1), as well as the last two

terms describing the Coulomb interaction. If we set $C_x = C_{vW} = 0$ in (2.1) we have

$$E\left[n\left(\mathbf{r}\right)\right] = \int d\mathbf{r}\ C_F n^{5/3}(\mathbf{r}) + \frac{1}{2}\int d\mathbf{r}\int d\mathbf{r}'\frac{n(\mathbf{r})n(\mathbf{r}')}{|\mathbf{r}-\mathbf{r}'|} - \int d\mathbf{r}\ V_+(\mathbf{r})n\left(\mathbf{r}\right). \tag{2.3}$$

We want to find the electron density $n(\mathbf{r})$ that minimizes the energy functional (2.3). To do this, we perform a functional derivative of (2.3) and obtain

$$\frac{\delta E}{\delta n} = \frac{5}{3}C_F n^{2/3}(\mathbf{r}) - V_e(\mathbf{r}) - V_+(\mathbf{r}) = 0, \tag{2.4}$$

where

$$V_e(\mathbf{r}) = -\int d\mathbf{r}'\frac{n(\mathbf{r}')}{|\mathbf{r}-\mathbf{r}'|}. \tag{2.5}$$

The total electrostatic potential at point $\mathbf{r}$ is

$$\Phi(\mathbf{r}) = V_e(\mathbf{r}) + V_+(\mathbf{r}), \tag{2.6}$$

so we may write (2.4) as

$$\frac{5C_F}{3}n^{2/3}(\mathbf{r}) - \Phi(\mathbf{r}) = 0, \tag{2.7}$$

or solving for $n(\mathbf{r})$

$$n(\mathbf{r}) = \left(\frac{3}{5C_F}\Phi(\mathbf{r})\right)^{3/2}. \tag{2.8}$$

Now, Poisson's equation reads

$$\nabla^2\Phi(\mathbf{r}) = -4\pi\rho(\mathbf{r}), \tag{2.9}$$

where $\rho(\mathbf{r})$ is the total charge density. We may write (2.9) as

$$\nabla^2\Phi(\mathbf{r}) = -4\pi\left[-n(\mathbf{r}) + n_+(\mathbf{r})\right], \tag{2.10}$$

where $-n(\mathbf{r})$ is the charge density due to the electrons and $n_+(\mathbf{r})$ is the charge density due to the positive ion cores. Since for a graphene sheet the charge density due to the positive ion cores is zero everywhere except at the sheet [1], we may write (2.10) as

$$\nabla^2\Phi(\mathbf{r}) = 4\pi n(\mathbf{r}) \tag{2.11}$$

for all $\mathbf{r}$ that are not on the sheet.

Now, using (2.11) together with (2.8), we have

$$\nabla^2\Phi(\mathbf{r}) = \frac{2^{7/2}}{3\pi}\Phi^{3/2}(\mathbf{r}), \tag{2.12}$$

which is known as the Thomas-Fermi (TF) equation.

By symmetry the electron density around an infinite graphene sheet depends on only the distance $|z|$ from the sheet. To calculate this density using a Thomas-Fermi approach, we write down the TF equation (2.12) for $z \neq 0$ in one dimension

$$\frac{d^2\Phi(z)}{dz^2} = \xi\Phi(z)^{3/2}, \tag{2.13}$$

where we have let

$$\xi = \frac{2^{7/2}}{3\pi}, \tag{2.14}$$

and where $\Phi(z)$ is the electric potential a distance z from the sheet. Notice that by symmetry, $\Phi(z)$ is an even function. On the other hand, the electric field in the vicinity of the sheet is given by $\mathbf{E} = (0, 0, E_z(z))$, where $E_z(z)$ is an odd function given by $E_z(z) = -d\Phi/dz$.

---

[1] Recall that in our jellium model the nuclear cores are modeled by a uniform charge density σ, so that the charge density due to the protons is $n_+(\mathbf{r}) = \sigma\delta(z)$.

Multiplying both sides of (2.13) by $\Phi' = d\Phi/dz$, we have

$$\Phi'\Phi'' = \xi\Phi^{3/2}\Phi', \tag{2.15}$$

and integrating with respect to the distance z, we get

$$\frac{1}{2}\left(\Phi'\right)^2 + C_0 = \xi\frac{2}{5}\Phi^{5/2} \tag{2.16}$$

$$E_z^2 + 2C_0 = \xi\frac{4}{5}\Phi^{5/2} \tag{2.17}$$

$$\left(E_z^2 + 2C_0\right)^{3/5} = \left(\frac{4}{5}\xi\right)^{3/5}\Phi^{3/2}. \tag{2.18}$$

Since we define the electric field E_z and the electric potential Φ to be zero at infinity, the constant of integration $C_0 = 0$, and we write

$$\left(E_z\right)^{6/5} = \left(\frac{4}{5}\xi\right)^{3/5}\Phi^{3/2}. \tag{2.19}$$

Since the electric field is given by the negative gradient of the electric potential, from (2.13) we have that

$$-\frac{dE_z}{dz} = \xi\Phi^{3/2}, \tag{2.20}$$

and using (2.19) we get

$$-\frac{dE_z}{dz} = \xi\frac{\left(E_z\right)^{6/5}}{\left(\frac{4}{5}\xi\right)^{3/5}} \tag{2.21}$$

or

$$-\frac{dE_z}{dz} = \zeta\left(E_z\right)^{6/5}, \tag{2.22}$$

where we have set

$$\zeta = \left(\frac{250}{9\pi^2}\right)^{1/5} \tag{2.23}$$

Integrating (2.22) with respect to the distance z we get an expression for the

magnitude of the electric field a distance z from the graphene sheet

$$E_z = (C_0 + \zeta z/5)^{-5}, \tag{2.24}$$

where C_0 is a constant of integration.

To calculate the electric field at an infinitesimal distance away from the graphene sheet, we use Gauss's law:

$$\oint \mathbf{E} \cdot d\mathbf{A} = 4\pi Q_{enc}, \tag{2.25}$$

where Q_{enc} is the charge enclosed by whatever Gaussian surface we choose. Using a so-called "Gaussian pillbox"[2], which is a thin Gaussian surface of thickness $2h$ and cross-sectional area A, that goes across the graphene sheet, we have

$$A\left[E_z(h) - E_z(-h)\right] = 2AE_z(h) = 4\pi \int d\mathbf{r}\ \rho(\mathbf{r}). \tag{2.26}$$

Here, $\rho(\mathbf{r}) = -n(\mathbf{r}) + n_+(\mathbf{r})$ is the total charge density, $-n(\mathbf{r})$ is the charge density due to the electrons, and $n_+(\mathbf{r}) = \sigma\delta(z)$ is the charge density due to the positive ion cores. Letting the thickness of the Gaussian surface go to zero, we get

$$\begin{aligned} &\lim_{h\to 0^+} 2AE_z(h) = \\ &-4\pi \lim_{h\to 0^+} \int_A d\mathbf{R} \int_{0-h}^{0+h} dz\ n(\mathbf{R}, z) + 4\pi \lim_{h\to 0^+} \int_A d\mathbf{R} \int_{0-h}^{0+h} dz\ \sigma\delta(z) \\ &\qquad = 4\pi A\sigma. \end{aligned} \tag{2.27}$$

So the magnitude of the electric field right next to the graphene sheet is given by

$$\lim_{h\to 0^+} E_z(h) = 2\pi\sigma. \tag{2.28}$$

[2]For a discussion of the electrodynamics of a charged plane using a "Gaussian pillbox", see [10].

Taking this boundary condition into account for (2.24) we calculate that

$$C_0 = (2\pi\sigma)^{-1/5}. \tag{2.29}$$

We now have an expression for the magnitude of the electric field in the vicinity of the graphene sheet

$$E_z(z) = \left[(2\pi\sigma)^{-1/5} + \zeta z/5\right]^{-5} \tag{2.30}$$

Integrating (2.30) we obtain the electric potential in the vicinity of the graphene sheet

$$\Phi(z) = \frac{1}{4b(bz+c)^4}, \tag{2.31}$$

where $b = \zeta/5$ and $c = (2\pi\sigma)^{-1/5}$. Now that we have an expression for $\Phi(z)$, (2.8) gives an expression for the electron density n as a function of the distance z from the sheet, namely

$$n(z) = \left(\frac{1}{2b}\right)^{3/2} \frac{1}{3\pi^2} \frac{1}{(bz+c)^6}. \tag{2.32}$$

Figure 2.1 shows this analytical Thomas-Fermi electron density as a function of the distance from the sheet, for $z \geq 0$. We can see that the TF electron density (2.32) has an inverse power decay and might overestimate the real electron density distribution because of its long range.

2.3 Minimizing Energy Functional

We have shown that an analytical solution for the electron density may be found using the Thomas-Fermi (TF) model. Now we want to find approximations to the electron density using a Thomas-Fermi-Dirac (TFD) model, so we want to include the Thomas-Fermi and Dirac terms in the energy functional (2.1).

Motivated by the fact that electron density in atomic orbitals typically decays

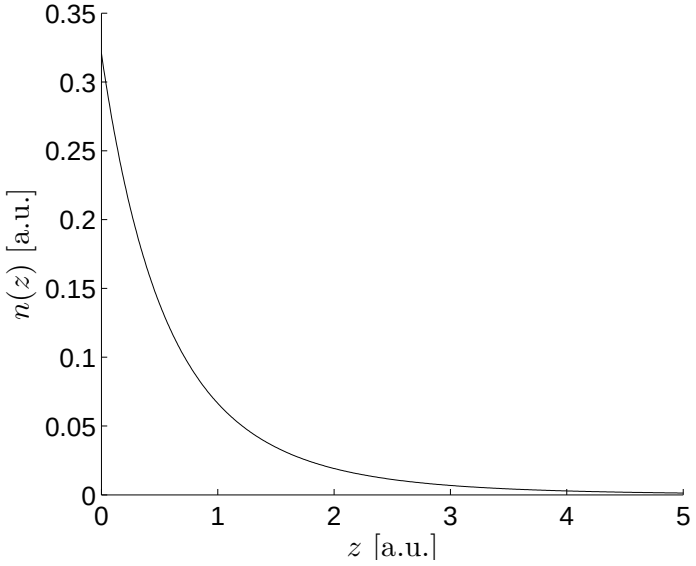

Figure 2.1: Analytical TF electron density for graphene. We plot the electron density as a function of the distance from the sheet.

exponentially with distance, we represent the electron density around a graphene sheet by using exponential approximations of the form

$$n(\mathbf{r}) = n_0 e^{-|z|/\lambda}, \tag{2.33}$$

where n_0 is a constant, z is the distance from the graphene sheet, and λ is a free parameter that we may choose so that (2.33) approximates well the electron density. In the TFD model, the electron density minimizes the energy functional

$$E\left[n\left(\mathbf{r}\right)\right] = \int d\mathbf{r}\left[C_F n^{5/3}(\mathbf{r}) - C_x n^{4/3}(\mathbf{r})\right]$$

$$+\frac{1}{2}\int d\mathbf{r}\int d\mathbf{r}'\frac{n(\mathbf{r})n(\mathbf{r}')}{|\mathbf{r}-\mathbf{r}'|} - \int d\mathbf{r}\; V_+(\mathbf{r})n\left(\mathbf{r}\right). \tag{2.34}$$

To find our approximation to the electron density for graphene, we must then minimize (2.34) with respect to the parameter λ in (2.33).

First we must express n_0 in (2.33) as a function of λ. The number of electrons per unit area is known from the neutrality condition, and it is given by

$$\sigma = n_0 \int_{-\infty}^{\infty} dz\ e^{-|z|/\lambda} = 2\lambda n_0, \tag{2.35}$$

so we have

$$n_0 = \frac{\sigma}{2\lambda}. \tag{2.36}$$

Now we may substitute (2.33) in (2.34) and minimize with respect to λ. The first two terms in (2.34) have the generic form

$$C_\alpha \int d\mathbf{r}\ \ [n(\mathbf{r})]^\alpha = C_\alpha \int d\mathbf{R} \int_{-\infty}^{\infty} dz\ n_0^\alpha\ e^{-\alpha|z|/\lambda} = 2C_\alpha \frac{\lambda}{\alpha}(n_0)^\alpha \int d\mathbf{R}, \tag{2.37}$$

and using (2.36) we may write them as

$$2AC_\alpha \frac{\lambda}{\alpha}\left(\frac{\sigma}{2\lambda}\right)^\alpha, \tag{2.38}$$

where

$$A \equiv \int d\mathbf{R}. \tag{2.39}$$

So, from the first and second terms in (2.34), we obtain the TF energy and exchange energy per unit area, respectively, as follows

$$2C_F \frac{3}{5}\lambda \left(\frac{\sigma}{2\lambda}\right)^{5/3} \text{and} \quad -2C_x \frac{3}{4}\lambda \left(\frac{\sigma}{2\lambda}\right)^{4/3}. \tag{2.40}$$

Now we look at the last two terms of the energy functional (2.34). These two terms represent the Coulomb interaction, and may be represented in terms of the total charge density $\rho(\mathbf{r})$, so that the total Coulomb interaction is written in the form

$$\frac{1}{2}\int d\mathbf{r} \int d\mathbf{r}'\ \frac{\rho(\mathbf{r})\rho(\mathbf{r}')}{|\mathbf{r}-\mathbf{r}'|}. \tag{2.41}$$

To write this term in a more useful form, we look further into the expression for the total charge density at $\mathbf{r}$, and write it as

$$\rho(\mathbf{r}) = \rho_e(\mathbf{r}) + \rho_n(\mathbf{r}), \tag{2.42}$$

where $\rho_e(\mathbf{r})$ represents the charge density due to the electrons and $\rho_n(\mathbf{r})$ represents the charge density due to the nuclear cores in the graphene sheet.[3] For a graphene sheet, we have

$$\rho_e(\mathbf{r}) = -n(\mathbf{r}) \quad \text{and} \quad \rho_n(\mathbf{r}) = \sigma\delta(z), \tag{2.43}$$

where $\delta(z)$ is the Dirac delta function.

It is useful to take the Fourier transform of (2.42), and we obtain this in the usual manner:

$$\tilde{\rho}(\mathbf{k}) = \int d\mathbf{r}\ e^{-i(\mathbf{k}\cdot\mathbf{r})}\rho(\mathbf{r}) = \sigma\int d\mathbf{r}\ e^{-i(\mathbf{k}\cdot\mathbf{r})}\left[\delta(z) - \frac{1}{2\lambda}e^{-|z|/\lambda}\right]. \tag{2.44}$$

We may express the vector $\mathbf{k}$ as $\mathbf{k} = (\mathbf{K}, k_z)$, where $\mathbf{K}$ is the component of $\mathbf{k}$ parallel to the graphene sheet and k_z is the component of $\mathbf{k}$ perpendicular to the graphene sheet. In the same way we may write $\mathbf{r} = (\mathbf{R}, z)$, with $\mathbf{R}$ and z being the components of $\mathbf{r}$ parallel and perpendicular to the sheet, respectively. Using this notation we may write (2.44) as

$$\tilde{\rho}(\mathbf{k}) = \sigma\int d\mathbf{R}\ e^{-i(\mathbf{K}\cdot\mathbf{R})}\int_{-\infty}^{\infty} dz\ e^{-ik_z z}\left[\delta(z) - \frac{1}{2\lambda}e^{-\frac{|z|}{\lambda}}\right]. \tag{2.45}$$

The z integral in (2.45) may be written

$$\int_{-\infty}^{\infty} dz\ e^{-ik_z z}\left[\delta(z) - \frac{1}{2\lambda}e^{-\frac{|z|}{\lambda}}\right] = 1 - \frac{1}{2\lambda}\int_{-\infty}^{\infty} dz\ e^{-ik_z z}e^{-\frac{|z|}{\lambda}}, \tag{2.46}$$

[3]Recall that, in our jellium model, these nuclear cores are approximated by a uniform charge distribution.

and we consider only the real part of $e^{-ik_z z} = \cos(k_z z) - i\sin(k_z z)$, because the imaginary part is odd and vanishes in the integral from $-\infty$ to ∞. The z integral then gives

$$1 - \frac{1}{2\lambda} \cdot 2 \int_0^\infty dz \ \cos(k_z z) e^{-|z|/\lambda} = 1 - \left(\frac{1}{\lambda^2 k_z^2 + 1} \right) = \frac{\lambda^2 k_z^2}{\lambda^2 k_z^2 + 1}. \tag{2.47}$$

Using (2.47) together with the fact that a two dimensional delta function may be written

$$\delta(\mathbf{K}) = \frac{1}{(2\pi)^2} \int d\mathbf{R} \ e^{-i(\mathbf{K}\cdot\mathbf{R})}, \tag{2.48}$$

we have that the Fourier transform of the charge density $\rho(\mathbf{r})$ is given by

$$\tilde{\rho}(\mathbf{k}) = \sigma(2\pi)^2 \delta(\mathbf{K}) \left(\frac{\lambda^2 k_z^2}{\lambda^2 k_z^2 + 1} \right). \tag{2.49}$$

Going back to our expression for the total Coulomb interaction, we may express the term $1/|\mathbf{r} - \mathbf{r}'|$ in (2.41) as

$$\frac{1}{|\mathbf{r} - \mathbf{r}'|} = \int d\mathbf{k} \ \frac{1}{(2\pi)^3} \frac{4\pi}{k^2} e^{i\mathbf{k}\cdot(\mathbf{r}-\mathbf{r}')}, \tag{2.50}$$

where $k = |\mathbf{k}| = \sqrt{K^2 + k_z^2}$, with $K = |\mathbf{K}|$. We may then write the Coulomb interaction term (2.41) as

$$\frac{1}{2} \int d\mathbf{r} \int d\mathbf{r}' \int d\mathbf{k} \ \frac{1}{(2\pi)^3} \frac{4\pi}{k^2} e^{i\mathbf{k}\cdot(\mathbf{r}-\mathbf{r}')} \rho(\mathbf{r}) \rho(\mathbf{r}'). \tag{2.51}$$

The $\mathbf{r}$ and $\mathbf{r}'$ integrals give the Fourier transform of the charge density, so we may write (2.51) as

$$\frac{1}{2} \frac{1}{(2\pi)^3} 4\pi \int d\mathbf{k} \ |\tilde{\rho}(\mathbf{k})|^2 \frac{1}{k^2}. \tag{2.52}$$

Now we may substitute $\tilde{\rho}(\mathbf{k})$ by its expression (2.49) and write (2.52) as

$$\frac{1}{2}8\pi^2\sigma^2\int d\mathbf{k}\,|\delta(\mathbf{K})|^2\,\frac{\lambda^4 k_z^4}{(\lambda^2 k_z^2+1)^2 k^2}. \tag{2.53}$$

For notational convenience we let

$$\Theta = \frac{1}{2}8\pi^2\sigma^2, \tag{2.54}$$

to abbreviate the constant in front of the integral. We also use (2.48) to express the two dimensional delta function in our Coulomb interaction (2.53), so we write (2.53) as

$$\Theta\int d\mathbf{k}\;\frac{1}{(2\pi)^4}\int d\mathbf{R}\;e^{-i(\mathbf{K}\cdot\mathbf{R})}\int d\mathbf{R}'\;e^{i(\mathbf{K}\cdot\mathbf{R}')}\frac{\lambda^4 k_z^4}{\lambda^2 k_z^2+1}\frac{1}{k^2} \tag{2.55}$$

or

$$\Theta\int d\mathbf{k}\;\frac{1}{(2\pi)^4}\int d\mathbf{R}\int d\mathbf{R}'\;e^{-i\mathbf{K}\cdot(\mathbf{R}-\mathbf{R}')}\frac{\lambda^4 k_z^4}{\lambda^2 k_z^2+1}\frac{1}{(K^2+k_z^2)}. \tag{2.56}$$

Since we are dealing with an infinite graphene sheet, we are interested only in the energy per unit area, so we do not consider the integral with respect to $\mathbf{R}$ over the area of the sheet.

For the integral over $\mathbf{R}'$ we have

$$\int d\mathbf{R}'\;e^{-i\mathbf{K}\cdot(\mathbf{R}-\mathbf{R}')} = (2\pi)^2\delta(\mathbf{K}), \tag{2.57}$$

so that the total Coulomb interaction[4] (2.56) may be written

$$\Theta\frac{1}{(2\pi)^4}\int d\mathbf{k}\;(2\pi)^2\delta(\mathbf{K})\frac{\lambda^4 k_z^4}{(\lambda^2 k_z^2+1)^2}\frac{1}{(K^2+k_z^2)} =$$

[4]Here we are considering the total Coulomb energy per unit area, since we are not considering the integral with respect to $\mathbf{R}$ in (2.56).

$$\Theta\frac{1}{(2\pi)^4}\int d\mathbf{K}\int_{-\infty}^{\infty}dk_z\ (2\pi)^2\delta(\mathbf{K})\frac{\lambda^4k_z^4}{(\lambda^2k_z^2+1)^2}\frac{1}{(K^2+k_z^2)}=$$

$$\Theta\frac{1}{(2\pi)^2}\int_{-\infty}^{\infty}dk_z\ \frac{\lambda^4k_z^2}{(\lambda^2k_z^2+1)^2}=\Theta\frac{1}{(2\pi)^2}\lambda\frac{\pi}{2}=\frac{\pi\sigma^2\lambda}{2}. \tag{2.58}$$

Using (2.40) and (2.58), we express the total energy per unit area for our graphene sheet as

$$E\left[n(\mathbf{r})\right]=2C_F\frac{3}{5}\lambda\left(\frac{\sigma}{2\lambda}\right)^{5/3}-2C_x\frac{3}{4}\lambda\left(\frac{\sigma}{2\lambda}\right)^{4/3}+\frac{\pi\sigma^2\lambda}{2}. \tag{2.59}$$

We want to minimize (2.59) with respect to our parameter λ. Differentiating (2.59) with respect to λ, multiplying it by $\lambda^{5/3}$, and setting the result equal to zero, we get the quintic equation

$$-\frac{4C_F}{5}\left(\frac{\sigma}{2}\right)^{5/3}+\frac{C_x}{2}\left(\frac{\sigma}{2}\right)^{4/3}\lambda^{1/3}+\frac{\pi\sigma^2}{2}\lambda^{5/3}=0. \tag{2.60}$$

We solve this equation numerically using Newton's method and find a zero at $\lambda\approx 0.6357$ a.u. [5] Using this value for λ we have a TFD exponential approximation of the form (2.33) to the electron density of graphene. We call this the TFD exponential approximation. Figure 2.2 shows this TFD exponential approximation to the electron density as a function of the distance from the sheet.

2.4 Least Squares Minimization

The Thomas-Fermi method gives an analytical electron density for graphene. Using a Thomas-Fermi-Dirac approach, we found an exponential approximation to the electron density by minimizing the energy functional (2.34).

We have found another exponential approximation of the form (2.33) by choosing a value of λ that minimizes the error with respect to the analytical TF electron

[5] This is the only real root of (2.60), so it is the one we consider for an approximation of the form (2.33).

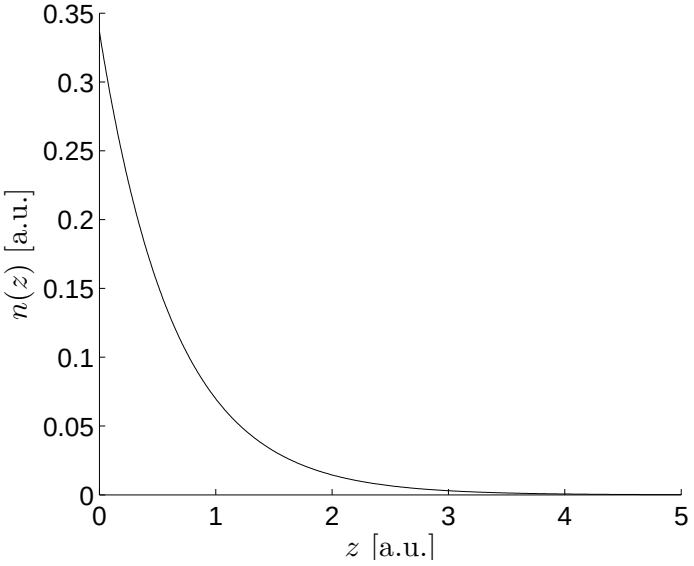

Figure 2.2: TFD exponential approximation to graphene electron density. We plot the electron density as a function of the distance from the sheet.

density.

By numerically minimizing the least squares error between the exponential approximation and the analytical TF electron density, we found a value of $\lambda \approx 0.7$. Using this λ in (2.33) we get what we call the least squares (LS) exponential approximation to the electron density. Figure 2.3 shows this LS exponential approximation to the electron density as a function of the distance from the sheet.

2.5 Molière Approximation

We have also computed the electron density distribution for graphene using the Molière approximation. Molière found that a single atom's electrostatic potential may be approximated by a function of the form [11] :

$$\Phi_1(\mathbf{r}) = \frac{Z_1}{r}\varphi(r/a_m), \tag{2.61}$$

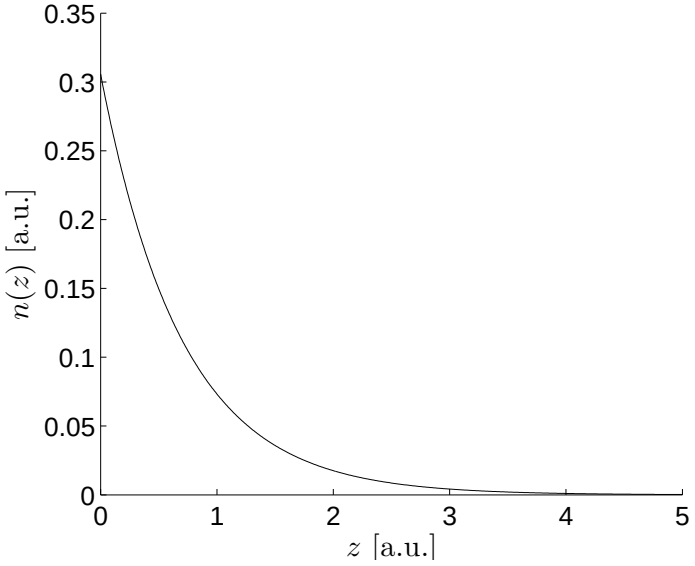

Figure 2.3: LS exponential approximation to graphene electron density. We plot the electron density as a function of the distance from the sheet.

where Z_1 is the nuclear charge, $\varphi(r/a_m)$ is a screening function that accounts for the electron density around the nucleus, and a_m is a screening length. The screening function is given by

$$\varphi(r/a_m) = \sum_{i=1}^{3} \alpha_i e^{-\beta_i r/a_m}, \tag{2.62}$$

where $\{\alpha_i\} \approx \{0.1, 0.55, 0.35\}$ and $\{\beta_i\} \approx \{6.0, 1.2, 0.3\}$. In Thomas-Fermi theory, the screening length a_m in (2.62) is given by $a_m = (9\pi^2/128Z_1)^{1/3} \approx 0.8853Z_1^{-1/3}$ [11].

To find the electrostatic potential around a graphene sheet, we must sum the contributions of the electrostatic potentials of the individual atoms making the sheet. We use the jellium approximation, so we assume the atoms are smeared out to form a uniform distribution on the sheet. The total electrostatic potential due

to all the atoms in the sheet is then given by

$$\Phi(\mathbf{r}) = \int d\mathbf{r}' \; D(\mathbf{r}')\Phi_1(\mathbf{r}-\mathbf{r}'), \tag{2.63}$$

where $D(\mathbf{r}')$ is the atomic density distribution. By choosing a coordinate system where our sheet lays in the xy-plane, the atomic density distribution is

$$D(\mathbf{r}') = \sigma_a \delta(z'), \tag{2.64}$$

where σ_a is the surface atomic density in the sheet and z' is the distance from the sheet. Using (2.62) and (2.64) in (2.63) we have

$$\begin{aligned}
\Phi(\mathbf{r}) &= \int d\mathbf{r} \; \sigma_a \delta(z') \frac{Z_1}{|\mathbf{r}-\mathbf{r}'|} \sum_{i=1}^{3} \alpha_i e^{-\beta_i |\mathbf{r}-\mathbf{r}'|/a_m} \\
&= \int d\mathbf{R}' \int dz' \; \sigma_a \delta(z') \frac{Z_1}{\sqrt{|\mathbf{R}-\mathbf{R}'|^2 + (z-z')^2}} \sum_{i=1}^{3} \alpha_i e^{-\beta_i \sqrt{|\mathbf{R}-\mathbf{R}'|^2+(z-z')^2}/a_m} \\
&= \int d\mathbf{R} \; \frac{\sigma_a Z_1}{\sqrt{R^2+z^2}} \sum_{i=1}^{3} \alpha_i e^{-\beta_i \sqrt{R^2+z^2}/a_m} \\
&= \int_0^{\infty} dR \; R \int_{-\pi}^{\pi} d\theta \; \frac{\sigma_a Z_1}{\sqrt{R^2+z^2}} \sum_{i=1}^{3} \alpha_i e^{-\beta_i \sqrt{R^2+z^2}/a_m} \\
&= \int_0^{\infty} dR \; R \frac{2\pi\sigma_a Z_1}{\sqrt{R^2+z^2}} \sum_{i=1}^{3} \alpha_i e^{-\beta_i \sqrt{R^2+z^2}/a_m}.
\end{aligned} \tag{2.65}$$

Now we let $r = \sqrt{R^2+z^2}$, so $dr = R/\sqrt{R^2+z^2} \; dR$, and we have

$$\Phi(\mathbf{r}) = \int_{|z|}^{\infty} dr \; 2\pi\sigma_a Z_1 \sum_{i=1}^{3} \alpha_i e^{-\beta_i |r|/a_m}$$

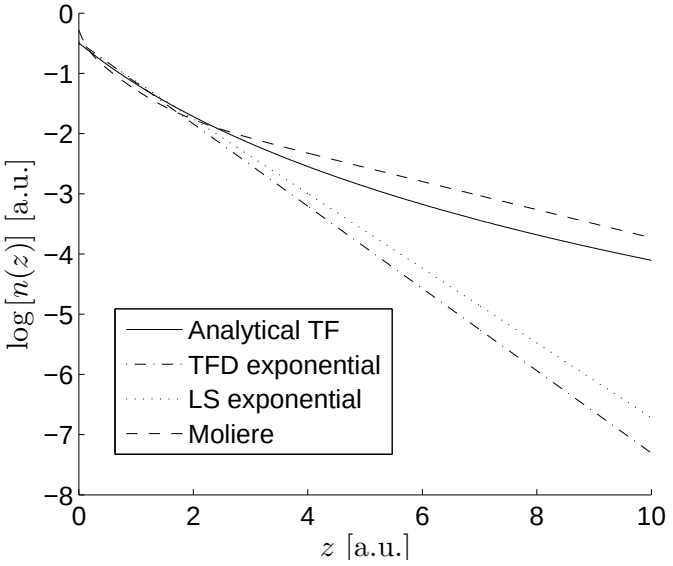

Figure 2.4: Graphene electron density obtained by different models. We plot the logarithm to base 10 of the electron density as a function of the distance from the sheet.

$$= 2\pi\sigma_a Z_1 a_m \sum_{i=1}^{3} \frac{\alpha_i}{\beta_i} e^{-\beta_i |z|/a_m}. \tag{2.66}$$

We are interested in finding the electron density distribution around the graphene sheet. From Poisson's equation (2.11) we have

$$n(\mathbf{r}) = \frac{1}{4\pi} \nabla^2 \Phi(\mathbf{r}). \tag{2.67}$$

Inserting the Laplacian of (2.66) into (2.67) we have what we call the Molière approximation to the electron density for graphene:

$$n(\mathbf{r}) = \frac{\sigma_a Z_1}{2a_m} \sum_{i=1}^{3} \alpha_i \beta_i e^{-\beta_i |z|/a_m}. \tag{2.68}$$

Figure 2.4 compares the various approximations to the electron density for graphene.

We can see how the TFD exponential density and the LS exponential density are much smaller than the analytical TF density, which has longer ranged inverse power decay. The Moliere electron density is given by a sum of exponentials, one of which is very long ranged, so at large distances from the sheet the plot shows it to be even higher than the analytical TF solution, although it will eventually drop below it at even farther distances.

2.6 Cruz Approximation

We now compute the electron density distribution for graphene using the approximation developed by Cruz *et al.* [12]. They found an expression for a single atom's electron density:

$$\rho_{at}(\mathbf{r}) = \sum_k \omega_k |\phi_k|^2, \tag{2.69}$$

where ω_k is the number of electrons in orbital k, and the sum is taken over all the occupied orbitals of the atom. In (2.69), ϕ_k is given by

$$\phi_k(r) = N_k r^{n_k - 1} e^{-\xi_k r}, \tag{2.70}$$

where N_k is a constant chosen so that

$$\int d\mathbf{r}\ |\phi_k(r)|^2 = 4\pi \int_0^\infty dr\ r^2 |\phi_k(r)|^2 = 1, \tag{2.71}$$

n_k is the principal quantum number of orbital k, and ξ_k is an orbital parameter.

The ground state of carbon has two $1s$ electrons, two $2s$ electrons, and two $2p$ electrons. For carbon, Cruz's model then gives

$$\rho_{at}(r) = \omega_{1s}|\phi_{1s}|^2 + \omega_{2s}|\phi_{2s}|^2 + \omega_{2p}|\phi_{2p}|^2, \tag{2.72}$$

where $\omega_{1s} = \omega_{2s} = \omega_{2p} = 2$; $n_{1s} = 1, n_{2s} = n_{2p} = 2$; and $\xi_{1s} \approx 5.5707$, $\xi_{2s} \approx 2.7034$, $\xi_{2p} \approx 1.2353$ [12]. We may write (2.72) as

$$\rho_{at}(r) = C_1 e^{-\lambda_1 r} + r^2 \left(C_2 e^{-\lambda_2 r} + C_3 e^{-\lambda_3 r} \right), \tag{2.73}$$

with $\lambda_1 \approx 11.14$, $\lambda_2 \approx 5.41$, $\lambda_3 \approx 2.47$, and

$$C_1 = \frac{2}{4\pi \int_0^\infty dr\ r^2 e^{-\lambda_1 r}} = \frac{\lambda_1^3}{4\pi}, \tag{2.74}$$

$$C_2 = \frac{2}{4\pi \int_0^\infty dr\ r^4 e^{-\lambda_2 r}} = \frac{\lambda_2^5}{48\pi}, \tag{2.75}$$

$$C_3 = \frac{2}{4\pi \int_0^\infty dr\ r^4 e^{-\lambda_3 r}} = \frac{\lambda_3^5}{48\pi}. \tag{2.76}$$

Finally, we have that the electron density distribution for a carbon atom is given by

$$\rho_{at}(r) = \frac{\lambda_1}{4\pi} e^{-\lambda_1 r} + \frac{r^2}{48\pi} \left(\lambda_2^5 e^{-\lambda_2 r} + \lambda_3^5 e^{-\lambda_3 r} \right), \tag{2.77}$$

which may be written as

$$\rho_{at}(r) = -\frac{\lambda_1^3}{4\pi} \frac{\partial}{\partial \lambda_1} \left(\frac{e^{-\lambda_1 r}}{r} \right) - \frac{\lambda_2^5}{48\pi} \frac{\partial^3}{\partial \lambda_2^3} \left(\frac{e^{-\lambda_2 r}}{r} \right) - \frac{\lambda_3^5}{48\pi} \frac{\partial^3}{\partial \lambda_3^3} \left(\frac{e^{-\lambda_3 r}}{r} \right). \tag{2.78}$$

To find the electron density distribution around a graphene sheet, we must sum the contribution of the electron densities of the individual atoms making the sheet. Again, we use the two-dimensional jellium approximation, so we assume the atoms are smeared out to form a uniform distribution on the sheet. The total density distribution due to all the atoms in the sheet is then given by

$$n(\mathbf{r}) = \int d\mathbf{r}'\ D(\mathbf{r}') \rho_{at}(\mathbf{r} - \mathbf{r}'), \tag{2.79}$$

where $D(\mathbf{r}')$ is the atomic density distribution. Choosing a coordinate system where our sheet lays in the xy-plane, the atomic density distribution is given by (2.64):

$$D(\mathbf{r}') = \sigma_a \delta(z'). \tag{2.80}$$

Using the result of (2.65) and (2.66), we may see that

$$\int d\mathbf{r}' \; D(\mathbf{r}') \frac{e^{-\lambda|\mathbf{r}-\mathbf{r}'|}}{|\mathbf{r}-\mathbf{r}'|} = \int d\mathbf{r}' \; \sigma_a \delta(z') \frac{e^{-\lambda|\mathbf{r}-\mathbf{r}'|}}{|\mathbf{r}-\mathbf{r}'|} = 2\pi\sigma_a \frac{e^{-\lambda|z|}}{\lambda}. \tag{2.81}$$

Using (2.81) in (2.78) we get

$$n(z) = -\frac{\sigma_a \lambda_1^3}{2} \frac{\partial}{\partial \lambda_1} \left(\frac{e^{-\lambda_1|z|}}{\lambda_1} \right) - \frac{\sigma_a \lambda_2^5}{24} \frac{\partial^3}{\partial \lambda_2^3} \left(\frac{e^{-\lambda_2|z|}}{\lambda_2} \right) - \frac{\sigma_a \lambda_3^5}{24} \frac{\partial^3}{\partial \lambda_3^3} \left(\frac{e^{-\lambda_3|z|}}{\lambda_3} \right), \tag{2.82}$$

which we call Cruz's approximation to the electron density distribution around a graphene sheet.

The Cruz model takes all six of carbon's electrons into account when calculating the electron density distribution. In figure 2.5 we compare the electron density for a graphene sheet calculated using Cruz's model as well as the TF analytical, TFD exponential, and Molière models. For these computations we have adapted the TF analytical, TFD exponential and Molière models to take into account all six of carbon's electrons in the calculation of the electron density.

Figure 2.6 compares the electron density for a graphene sheet using Cruz's model, the TFD exponential model for four electrons, the TF analytical model for six electrons, and the TF analytical model for four electrons. We can see that the Cruz electron density (2.82), which is given by a sum of exponentials multiplied by polynomials, gives an electron density which at some distances is above and at some distances is below the TFD single exponential approximation.

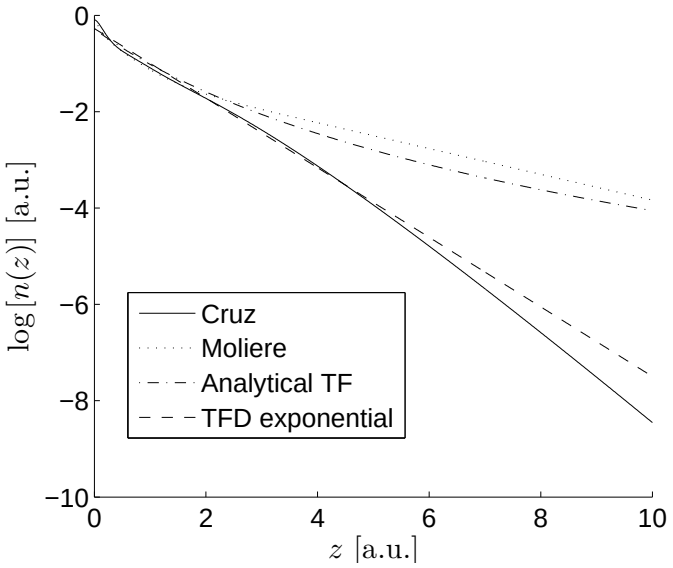

Figure 2.5: Graphene electron density obtained by different models. We plot the logarithm to base 10 of the electron density as a function of the distance from the sheet.

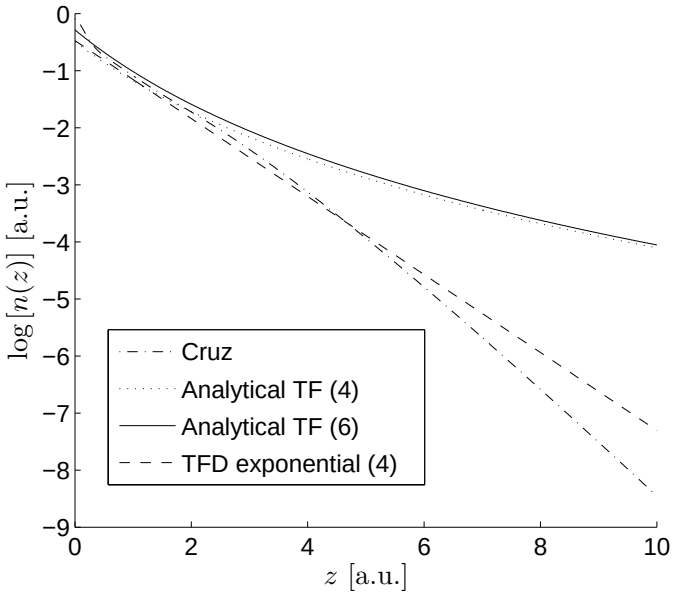

Figure 2.6: Graphene electron density obtained by different models. We plot the logarithm to base 10 of the electron density as a function of the distance from the sheet.

Chapter 3

Equilibrium Electron Density in Carbon Nanotubes

We are now interested in computing the three dimensional equilibrium electron density for carbon nanotubes. As we did for graphene, we shall use various models to calculate this electron density and then compare the results.

A carbon nanotube may be considered to be part of a graphene sheet that is rolled up to form a cylinder [13]. Analogously to our jellium model of graphene, we model a carbon nanotube as a cylinder with uniform charge density (representing the positive ion cores) surrounded by an electron gas. The surface charge density for the cylinder is the same as for graphene, namely, $\sigma \approx 0.428$ a.u.

3.1 Numerical Solution for Single-Walled Nanotubes

3.1.1 Thomas-Fermi Electron Density

Our goal is to find the electron density distribution around a single-walled nanotube (SWNT) of radius R_t. By symmetry, this equilibrium density will depend on only

the radial distance from the nanotube axis. Using a Thomas-Fermi (TF) model, we start with the TF equation (2.12). Writing this equation in cylindrical coordinates we get [1]

$$\frac{\partial^2 \Phi}{\partial r^2} + \frac{1}{r}\frac{\partial \Phi}{\partial r} = \xi \Phi^{3/2}, \tag{3.1}$$

where r is the perpendicular distance from the axis of the nanotube and ξ is defined in (2.14). We must solve this nonlinear second order differential equation subject to the following physical boundary conditions:

1. By symmetry requirements, the electric field must be zero at the nanotube axis, therefore
$$\left.\frac{\partial \Phi}{\partial r}\right|_{r=0} = 0. \tag{3.2}$$

2. The electric field and electron density must approach zero as $r \to \infty$, yielding
$$\lim_{r_0 \to \infty} \Phi(r_0) = 0. \tag{3.3}$$

3. The electric potential must be continuous across the nanotube wall, so we have
$$\Phi_{in}(R_t) = \Phi_{out}(R_t). \tag{3.4}$$

4. The electric field at the nanotube wall must have a discontinuity equal to 4π times the surface charge density:
$$\left.\frac{\partial \Phi_{in}}{\partial r}\right|_{r=R_t} = 4\pi\sigma + \left.\frac{\partial \Phi_{out}}{\partial r}\right|_{r=R_t}. \tag{3.5}$$

The first step in solving (3.1) numerically is to discretize the domain and derivatives. We choose a domain over which we want to compute the solution,

[1] In writing the Laplacian in cylindrical coordinates, we have assumed $\Phi(r, \phi, z) = \Phi(r)$, by symmetry.

say $r \in [0, R]$. We then partition this domain into N equal intervals defined by $(N+1)$ equally spaced points with separation distance Δr. The $(N+1)$ points are given by $r_n = n\Delta r$, where $n \in \{0, 1, 2, \ldots, N\}$. We then approximate the first derivative of Φ at r_n using a backward step

$$\frac{\partial \Phi(r_n)}{\partial r} \approx \frac{\Phi(r_n) - \Phi(r_{n-1})}{\Delta r}. \tag{3.6}$$

The second derivative of Φ at r_n is approximated using a forward step

$$\frac{\partial^2 \Phi(r_n)}{\partial r^2} \approx \frac{\Phi(r_{n+1}) - 2\Phi(r_n) + \Phi(r_{r_n-1})}{(\Delta r)^2}. \tag{3.7}$$

Now we may write our Thomas-Fermi equation as

$$\frac{\Phi(r_{n+1}) - 2\Phi(r_n) + \Phi(r_{r_{n-1}})}{(\Delta r)^2} + \frac{1}{r_n}\frac{\Phi(r_n) - \Phi(r_{n-1})}{\Delta r} = \xi \Phi(r_n)^{3/2}, \tag{3.8}$$

which is a discretized approximation to (3.1). At this point, we define Φ_n as the numerical approximation of $\Phi(r_n)$. We may then write (3.8) as

$$\frac{\Phi_{n+1} - 2\Phi_n + \Phi_{n-1}}{(\Delta r)^2} + \frac{1}{r_n}\frac{\Phi_n - \Phi_{n-1}}{\Delta r} = \xi \Phi_n^{3/2}, \tag{3.9}$$

and, solving for Φ_{n+1}, we get

$$\Phi_{n+1} = (\Delta r)^2 \left(\xi \Phi_n^{3/2} - \frac{1}{r_n}\frac{\Phi_n - \Phi_{n-1}}{\Delta r} \right) + 2\Phi_n - \Phi_{n-1}. \tag{3.10}$$

Using this numerical scheme, we may iteratively compute the solution at r_{n+1} when we know the solution at r_n and r_{n-1}.

The value Φ_0 of the potential at the origin is unknown. We have used a shooting method to search for a value of Φ_0 that makes the numerical solution satisfy the boundary conditions (3.2)-(3.5). Having found a value of Φ_0, we set $\Phi_1 = \Phi_0$, due

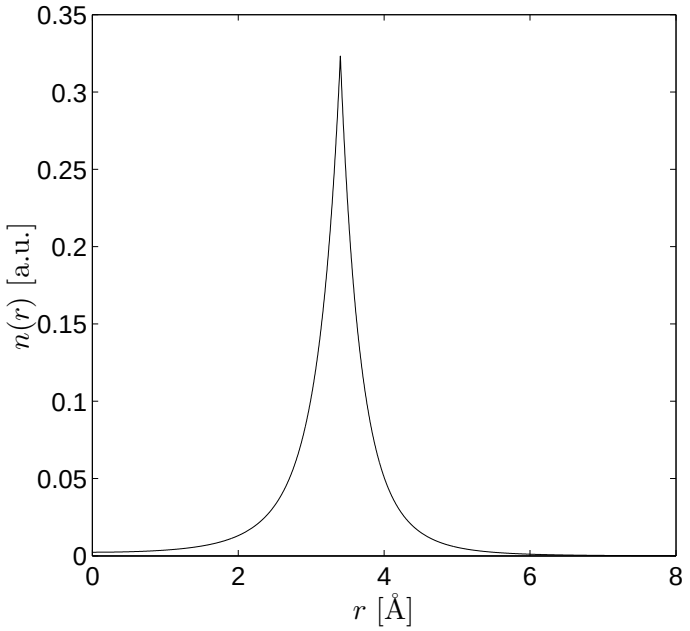

Figure 3.1: TF numerical electron density for a SWNT of radius $R_t = 3.4$ Å. We plot the electron density as a function of the distance from the nanotube axis.

to boundary condition (3.2), and we use the numerical scheme (3.10) to compute the solution for all $n \in \{2, 3, \ldots, N\}$.

The numerical solution was computed in this way for a nanotube of radius $R_t = 3.4$ Å. Having computed the potential Φ, we may compute the electron density using (2.8). We plot this numerical Thomas-Fermi electron density in figure 3.1.

Notice that when computing this numerical solution, in order to satisfy boundary condition (3.3), we need to set the potential $\Phi(r)$ and its derivative equal to zero at infinity. To actually do the numerical computation we need to choose a value which we will consider infinity. For the results shown in figure (3.1) we chose this value to be 2 times the radius of the nanotube. Later on we will compare results in which we choose this value to be different.

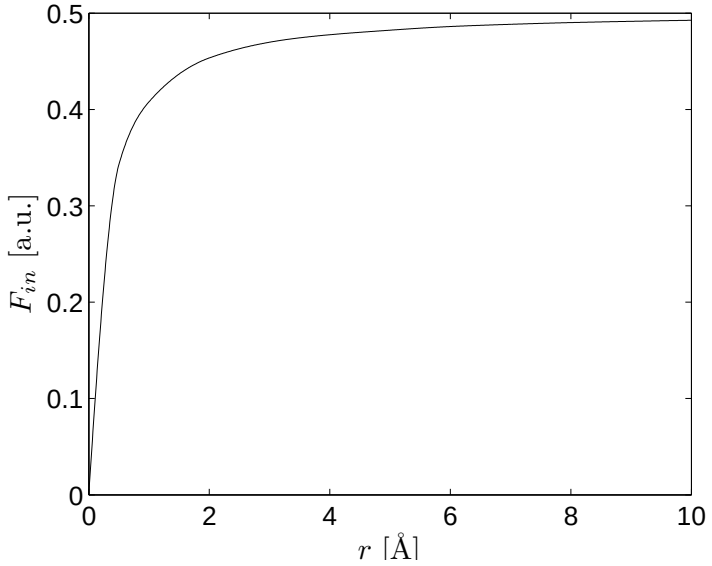

Figure 3.2: Fraction of electrons inside the tube as a function of the radius.

3.1.2 Electrons Inside and Outside the Nanotube

Using our TF numerical electron density, we have calculated the fraction of electrons inside and outside of a SWNT for different nanotube radii. We find, as expected, that for smaller radii, a smaller fraction of electrons is found inside the nanotube. As the radius increases, the density of electrons inside the nanotube approaches the density of electrons outside the nanotube. As the radius $R_t \to \infty$, we expect the nanotube electron density to approach that of the graphene sheet, so we have the same fraction of electrons on each side of the wall. Figure 3.2 shows the fraction F_{in} of electrons inside the tube for different radii.

3.1.3 Thomas-Fermi-Dirac Electron Density

We now use a Thomas-Fermi-Dirac (TFD) model to find the electron density distribution around a single-walled nanotube. We consider the Thomas-Fermi-Dirac

energy functional

$$E\left[n\left(\mathbf{r}\right)\right] = \int d\mathbf{r}\left[C_F n^{5/3}(\mathbf{r}) - C_x n^{4/3}(\mathbf{r})\right]$$

$$+\frac{1}{2}\int d\mathbf{r}\int d\mathbf{r}'\frac{n(\mathbf{r})n(\mathbf{r}')}{|\mathbf{r}-\mathbf{r}'|} - \int d\mathbf{r}V_+(\mathbf{r})n\left(\mathbf{r}\right). \tag{3.11}$$

We want to find the electron density $n(\mathbf{r})$ that minimizes (3.11). Performing a functional derivative we have

$$\frac{\delta E}{\delta n} = \frac{5}{3}C_F n^{2/3}(\mathbf{r}) - \frac{4}{3}C_x n^{1/3}(\mathbf{r}) - V_e(\mathbf{r}) - V_+(\mathbf{r}) = 0, \tag{3.12}$$

where

$$V_e(\mathbf{r}) = -\int d\mathbf{r}'\frac{n(\mathbf{r}')}{|\mathbf{r}-\mathbf{r}'|}. \tag{3.13}$$

The total electrostatic potential at point $\mathbf{r}$ is

$$\Phi(\mathbf{r}) = V_e(\mathbf{r}) + V_+(\mathbf{r}), \tag{3.14}$$

so we may write (3.12) as

$$\frac{5C_F}{3}n^{2/3}(\mathbf{r}) - \frac{4C_x}{3}n^{1/3}(\mathbf{r}) - \Phi(\mathbf{r}) = 0. \tag{3.15}$$

Now letting $X(\mathbf{r}) = n^{1/3}(\mathbf{r})$, we have the quadratic equation

$$\frac{5C_F}{3}X^2(\mathbf{r}) - \frac{4C_x}{3}X(\mathbf{r}) - \Phi(\mathbf{r}) = 0, \tag{3.16}$$

which we may solve for $X(\mathbf{r})$ to get

$$X(\mathbf{r}) = \frac{0.4C_x + \left[0.16C_x^2 + 0.6C_F\Phi(\mathbf{r})\right]^{1/2}}{C_F}. \tag{3.17}$$

We now write Poisson's equation

$$\nabla^2\Phi(\mathbf{r}) = \frac{\partial^2\Phi}{\partial r^2} + \frac{1}{r}\frac{\partial\Phi}{\partial r} = 4\pi n(\mathbf{r}) = 4\pi X^3(\mathbf{r}), \tag{3.18}$$

and we discretize the domain and derivatives as we did in (3.6) and (3.7), obtaining

$$\frac{\Phi(r_{n+1}) - 2\Phi(r_n) + \Phi(r_{r_{n-1}})}{(\Delta r)^2} + \frac{1}{r_n}\frac{\Phi(r_n) - \Phi(r_{n-1})}{\Delta r} = 4\pi X^3(r_n). \tag{3.19}$$

Again, we define Φ_n and X_n as the numerical approximations of $\Phi(r_n)$ and $X(r_n)$, respectively. So we write (3.19) as

$$\frac{\Phi_{n+1} - 2\Phi_n + \Phi_{n-1}}{(\Delta r)^2} + \frac{1}{r_n}\frac{\Phi_n - \Phi_{n-1}}{\Delta r} = 4\pi X_n^3. \tag{3.20}$$

Solving for Φ_{n+1} we have

$$\Phi_{n+1} = (\Delta r)^2\left(4\pi X_n^3 - \frac{1}{r_n}\frac{\Phi_n - \Phi_{n-1}}{\Delta r}\right) + 2\Phi_n - \Phi_{n-1}. \tag{3.21}$$

Using (3.17) we also write

$$X_n = \frac{0.4C_x + \left[0.16C_x^2 + 0.6C_F\Phi_n\right]^{1/2}}{C_F}. \tag{3.22}$$

We may use the numerical scheme (3.21) with (3.22) to iteratively compute the solution at r_{n+1} when we know the solution at r_n and r_{n-1}. We once again use a shooting method to find a value Φ_0 for the potential at the origin, such that the boundary conditions (3.2)-(3.5) are satisfied.

The numerical solution was computed in this way for a nanotube of radius $R_t = 3.4$ Å. Having computed the potential Φ, we may compute the electron density using (3.22) and $n = X^{1/3}$. In figure 3.3 we compare this numerical Thomas-Fermi-Dirac electron density with the numerical Thomas-Fermi electron density.

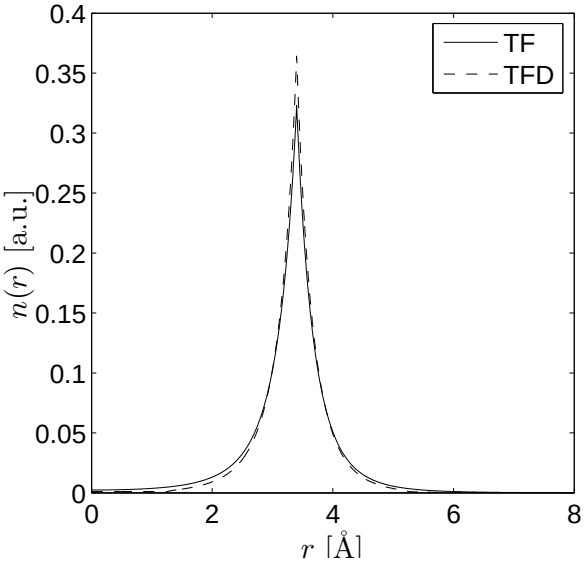

Figure 3.3: TF and TFD numerical electron densities for a SWNT of radius $R_t = 3.4$ Å. We plot the electron density as a function of the distance from the nanotube axis.

3.2 Molière Approximation

As we did for graphene in section 2.5, we now want to compute the electron density distribution for a nanotube using the Molière approximation. We had from (2.61) an expression for the total electrostatic potential of a single atom. We also had from (2.63) an expression for the total electrostatic potential of a configuration of atoms. We now work in cylindrical coordinates and the atomic density distribution $D(\mathbf{r}')$ in (2.63) is

$$D(\mathbf{r}') = \sigma_a \delta(r' - R_t), \tag{3.23}$$

where σ_a is the surface atomic density in the nanotube, r' is the radial coordinate and R_t is the nanotube radius. Using (2.61) and (3.23) in (2.63) we have

$$\Phi(\mathbf{r}) = \int d\mathbf{r}' \ \sigma_a \delta(r' - R_t) \frac{Z_1}{|\mathbf{r} - \mathbf{r}'|} \sum_{i=1}^{3} \alpha_i e^{-\beta_i |\mathbf{r}-\mathbf{r}'|/a_m}$$

$$= \int_0^\infty dr' \ r' \int_{-\infty}^\infty dz' \int_0^{2\pi} d\theta' \ \sigma_a \delta(r' - R_t) \ \times$$
$$\frac{Z_1}{\sqrt{r^2 + r'^2 - 2rr' \cos(\theta - \theta') + (z - z')^2}} \sum_{i=1}^{3} \alpha_i e^{-\beta_i \sqrt{r^2 + r'^2 - 2rr' \cos(\theta - \theta') + (z - z')^2}/a_m}$$

$$= \int_0^\infty dz \int_0^{2\pi} d\theta \ \frac{2\sigma_a Z_1 R_t}{\sqrt{r^2 + R_t^2 - 2rR_t \cos\theta + z^2}} \sum_{i=1}^{3} \alpha_i e^{-\beta_i \sqrt{r^2 + R_t^2 - 2rR_t \cos\theta + z^2}/a_m}. \tag{3.24}$$

We now let $\xi = \sqrt{r^2 + R_t^2 - 2rR_t \cos\theta + z^2}$, so that

$$z = \sqrt{\xi^2 - (r^2 + R_t^2 - 2rR_t \cos\theta)}, \quad \text{and} \quad dz = \frac{\xi \ d\xi}{\sqrt{\xi^2 - (r^2 + R_t^2 - 2rR_t \cos\theta)}}. \tag{3.25}$$

We may now write (3.24) as

$$\Phi(\mathbf{r}) = \int_0^{2\pi} d\theta \int_{\sqrt{r^2 + R_t^2 - 2rR_t \cos\theta}}^\infty d\xi \ \frac{2\sigma_a Z_1 R_t}{\sqrt{\xi^2 - (r^2 + R_t^2 - 2rR_t \cos\theta)}} \sum_{i=1}^{3} \alpha_i e^{-\beta_i \xi/a_m}, \tag{3.26}$$

or letting $h = \sqrt{r^2 + R_t^2 - 2rR_t \cos\theta}$,

$$\Phi(\mathbf{r}) = 2\sigma_a Z_1 R_t \int_0^{2\pi} d\theta \int_h^\infty d\xi \frac{1}{\sqrt{\xi^2 - h^2}} \sum_{i=1}^{3} \alpha_i e^{-\beta_i \xi/a_m}. \tag{3.27}$$

By making the change of variable $x = \xi/h$, we may write (3.27) as

$$\Phi(\mathbf{r}) = 2\sigma_a Z_1 R_t \int_0^{2\pi} d\theta \ \sum_{i=1}^{3} \alpha_i \int_1^{\infty} dx \ \frac{e^{-\beta_i x h/a_m}}{\sqrt{x^2-1}}$$

$$= 2\sigma_a Z_1 R_t \int_0^{2\pi} d\theta \ \sum_{i=1}^{3} \alpha_i K_0\left(\frac{\beta_i h}{a_m}\right), \tag{3.28}$$

where $K_0(\beta_i h/a_m)$ is the zeroth order modified Bessel function. We may write (3.28) as

$$\Phi(\mathbf{r}) = 4\sigma_a Z_1 R_t \int_0^{\pi} d\theta \ \sum_{i=1}^{3} \alpha_i K_0\left(\frac{\beta_i\sqrt{r^2+R_t^2-2rR_t\cos\theta}}{a_m}\right)$$

$$= 4\sigma_a Z_1 R_t \int_0^{\pi} d\theta \int_0^{\infty} d\xi \ \delta\left(\xi - \sqrt{r^2+R_t^2-2rR_t\cos\theta}\right) \sum_{i=1}^{3} \alpha_i K_0\left(\frac{\beta_i\xi}{a_m}\right)$$

$$= 4\sigma_a Z_1 R_t \int_0^{\infty} d\xi \sum_{i=1}^{3} \alpha_i K_0\left(\frac{\beta_i\xi}{a_m}\right) \int_0^{\pi} d\theta \ \delta\left(\xi - \sqrt{r^2+R_t^2-2rR_t\cos\theta}\right). \tag{3.29}$$

Now we let $t = \cos\theta$ and we use the property that a delta function of a function $g(x)$ may be written as

$$\delta\left(g(x)\right) = \sum_i \frac{\delta(x-x_i)}{|g'(x_i)|}, \tag{3.30}$$

where the x_i's are the zeros of $g(x)$. We may then write the integral over θ in (3.29) as

$$\int_0^{\pi} d\theta \ \delta\left(\xi - \sqrt{r^2+R_t^2-2rR_t\cos\theta}\right) = \frac{\xi}{rR_t}\int_{-1}^{1} dt \ \frac{\delta\left(t - \left(\frac{r^2+R_t^2-\xi^2}{2rR_t}\right)\right)}{\sqrt{1-t^2}}$$

$$= \frac{\xi}{rR_t}\frac{1}{\sqrt{1-\left(\frac{r^2+R_t^2-\xi^2}{2rR_t}\right)^2}} = \frac{2\xi}{\sqrt{(2rR_t)^2-(r^2+R_t^2-\xi^2)^2}}, \tag{3.31}$$

so that the total electrostatic potential of the nanotube is

$$\Phi(\mathbf{r}) = 4\sigma_a Z_1 R_t \int_{|r-R_t|}^{|r+R_t|} d\xi \, \frac{2\xi}{\sqrt{(2rR_t)^2 - (r^2 + R_t^2 - \xi^2)^2}} \sum_{i=1}^{3} \alpha_i K_0 \left(\frac{\beta_i \xi}{a_m} \right). \quad (3.32)$$

We may write the square root in the integrand as

$$\sqrt{(2rR_t)^2 - (r^2 + R_t^2 - \xi^2)^2} = \sqrt{[2rR_t + (r^2 + R_t^2 - \xi^2)]\,[2rR_t - (r^2 + R_t^2 - \xi^2)]}$$

$$= \sqrt{[(r + R_t)^2 - \xi^2]\,[\xi^2 - (r - R_t)^2]}, \quad (3.33)$$

so we get

$$\Phi(\mathbf{r}) = 4\sigma_a Z_1 R_t \int_{|r-R_t|}^{|r+R_t|} d\xi \, \frac{2\xi}{\sqrt{[(r + R_t)^2 - \xi^2]\,[\xi^2 - (r - R_t)^2]}} \sum_{i=1}^{3} \alpha_i K_0 \left(\frac{\beta_i \xi}{a_m} \right). \quad (3.34)$$

The integral in (3.34) has an analytic solution [14], so we get

$$\Phi(r) = 4\pi\sigma_a Z_1 R_t \sum_{i=1}^{3} \alpha_i I_0 \left(\frac{\beta_i r_<}{a_m} \right) K_0 \left(\frac{\beta_i r_>}{a_m} \right), \quad (3.35)$$

where I_0 and K_0 are the zeroth order modified Bessel functions, $r_< = \min(r, R_t)$, and $r_> = \max(r, R_t)$.

We are interested in finding the electron density distribution around the nanotube. From (2.11) we have

$$n(\mathbf{r}) = \frac{1}{4\pi} \nabla^2 \Phi(\mathbf{r}). \quad (3.36)$$

Taking the Laplacian of (3.35) we get

$$\nabla^2 \Phi(r) = \frac{1}{r} \frac{d}{dr} \left(r \frac{d\Phi(r)}{dr} \right)$$

$$= \frac{4\pi\sigma_a Z_1 R_t}{a_m^2} \sum_{i=1}^{3} \alpha_i \beta_i^2 I_0\left(\frac{\beta_i r_<}{a_m}\right) K_0\left(\frac{\beta_i r_>}{a_m}\right), \tag{3.37}$$

The Molière approximation to the electron density around a SWNT is then

$$n(r) = \frac{\sigma_a Z_1 R_t}{a_m^2} \sum_{i=1}^{3} \alpha_i \beta_i^2 I_0\left(\frac{\beta_i r_<}{a_m}\right) K_0\left(\frac{\beta_i r_>}{a_m}\right). \tag{3.38}$$

3.3 Least-Squares Minimization

The form of the Molière electron density (3.38) suggests that we can approximate the electron density of a SWNT by using functions of the form

$$n(r) = n_o \left[I_0\left(\frac{r_<}{a}\right) K_0\left(\frac{r_>}{b}\right)\right], \tag{3.39}$$

with $r_< = \min(r, R_t)$, and $r_> = \max(r, R_t)$, where r is the distance from the nanotube axis, and R_t is the radius of the nanotube. Both a and b in (3.39) are free parameters that may be chosen so that $n(r)$ approximates well the electron density distribution. Here, n_o is a normalization constant, that is fixed for any given a, b, and R_t. We call (3.39) the Bessel approximation.

In section 3.1, we computed numerically the electron density for a SWNT, using both a TF and a TFD method. Now we will find an analytical approximation to the electron density by using least-squares minimization. We assume an electron density of the form (3.39) and choose parameters a and b that minimize the least-squares error with respect to the numerical solution. This least-squares minimization is done numerically with respect to both the TF and TFD numerical electron densities. The two analytical approximations obtained are compared in figure 3.4.

In figure 3.5 we show the TF numerical electron density computed by setting the potential $\Phi(r)$ to be approximately zero at $r = 2R_t$ ($-\cdot-$) and at $r = 3R_t$ (——). We also show the Molière approximation to the electron density and the Bessel LS

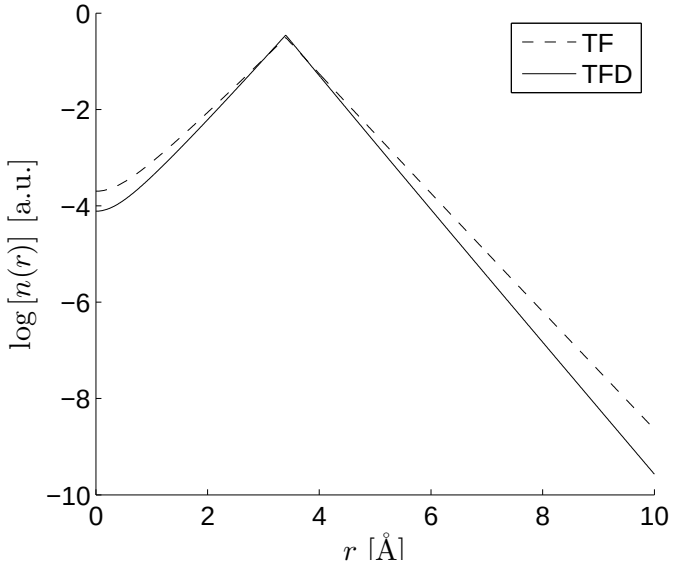

Figure 3.4: Bessel approximations (3.39) to electron density by least-squares minimization. We plot the logarithm to base 10 of the electron density as a function of the distance from the nanotube axis.

approximation minimized with respect to the numerical solution (I).

3.4 Minimizing Energy Functional

It is possible to obtain another analytical approximation to the electron density for a SWNT. Since equilibrium electron behavior for a single-walled nanotube is defined in terms of the functional (2.1), an analytical approximation to the equilibrium electron density may be found by inserting a trial function of the form (3.39) into the energy functional (2.1), and minimizing the functional with respect to the free parameters a and b. We have done this minimization by numerically evaluating the energy functional over a grid of values in a and b. We then choose the a and b values that give the minimum energy. Here, we have done this minimization by taking into account only the TF and Coulomb terms in (2.1) in order to obtain a TF electron

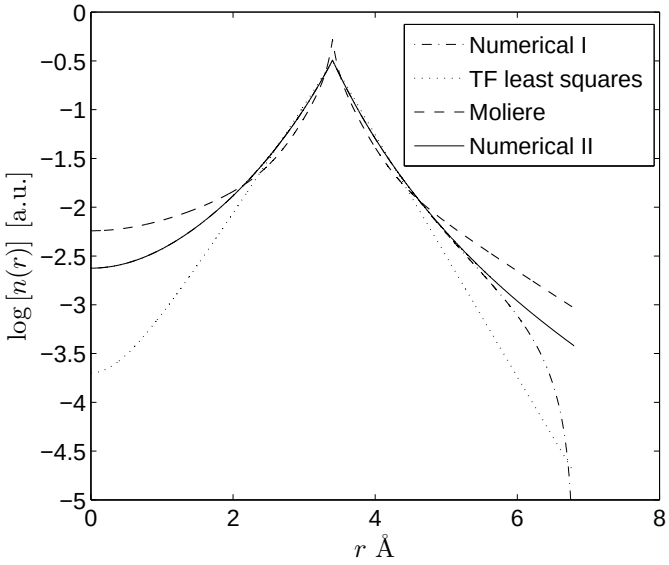

Figure 3.5: Electron density for a SWNT of radius $R_t = 3.4$ Å. We show the TF numerical electron density computed by setting the potential $\Phi(r)$ to be approximately zero at $r = 2R_t$ (I) and at $r = 3R_t$ (II). We also show the Molière approximation to the electron density and the Bessel LS approximation minimized with respect to the numerical solution (I).

density.

3.5 Multi-Walled Nanotubes

3.5.1 Numerical Solution

In section 3.1.1 we calculated the numerical TF electron density distribution for a single-walled nanotube. The numerical scheme we used was given by (3.10):

$$\Phi_{n+1} = (\Delta r)^2 \left(\xi \Phi_n^{3/2} - \frac{1}{r_n} \frac{\Phi_n - \Phi_{n-1}}{\Delta r} \right) + 2\Phi_n - \Phi_{n-1}. \tag{3.40}$$

Now we use this scheme together with boundary conditions (3.2)-(3.5) to calculate the numerical TF electron density distribution for a multi-walled nanotube. We have done this calculation for a 2-walled nanotube of inner radius $R_{t_1} = 3.4$ Å and outer radius $R_{t_2} = 6.8$ Å. We have also done this calculation for a 3-walled nanotube of radii $R_{t_1} = 3.4$ Å, $R_{t_2} = 6.8$ Å, and $R_{t_3} = 10.2$ Å. Figures 3.6 and 3.7 show these results.

3.5.2 Bessel Approximations

In sections 3.2–3.4 we found analytical Bessel approximations to the electron density distributions of single-walled nanotubes. We now consider these analytical Bessel approximations for single-walled nanotubes of radii R_{t_1}, R_{t_2}, and R_{t_3}. We use the superposition of these analytical Bessel approximations to model the electron density distribution of multi-walled nanotubes. The analytical Bessel approximations may be found using any of the methods discussed previously. Figure 3.8 compares the numerical TF electron density for a 3-walled nanotube with its analytical TF Bessel approximation obtained by minimization of the energy functional. The calculation was done for radii $R_{t_1} = 3.4$ Å, $R_{t_2} = 6.8$ Å, and $R_{t_3} = 10.2$ Å.

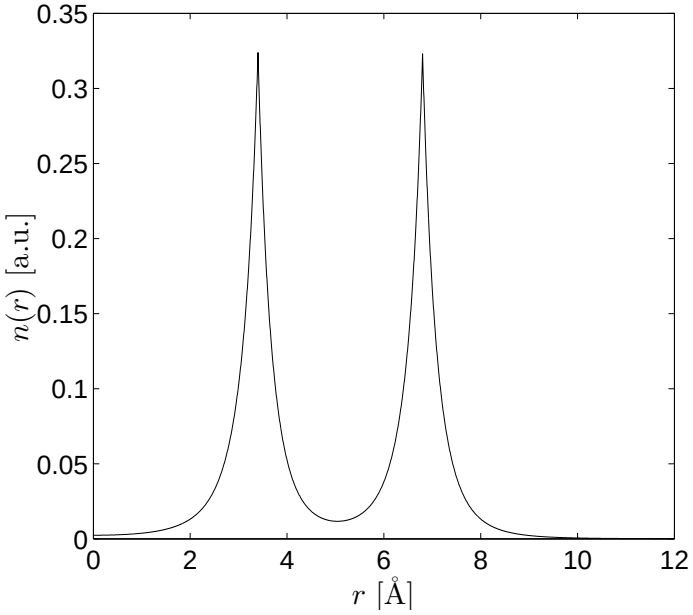

Figure 3.6: TF numerical electron density for a 2-walled nanotube of inner radius $R_{t_1} = 3.4$ Å and outer radius $R_{t_2} = 6.8$ Å. We plot the electron density as a function of the distance from the nanotube axis.

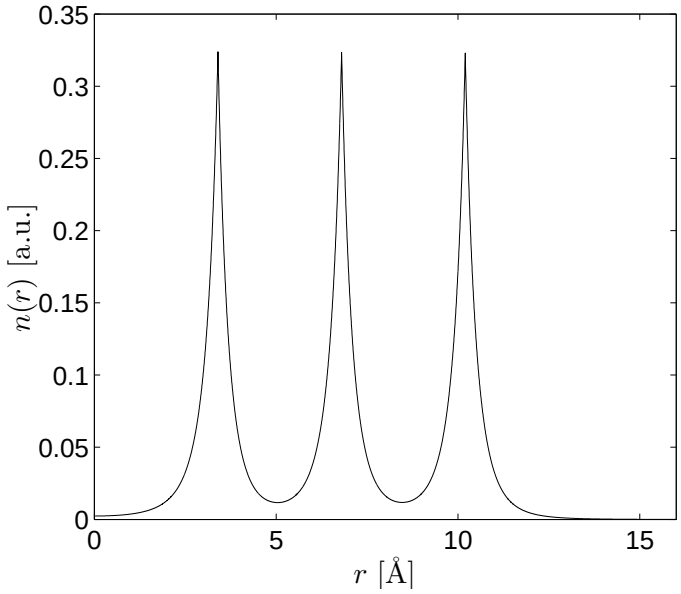

Figure 3.7: TF numerical electron density for 3-walled nanotube of radii $R_{t_1} = 3.4$ Å, $R_{t_2} = 6.8$ Å, and $R_{t_3} = 10.2$ Å. We plot the electron density as a function of the distance from the nanotube axis.

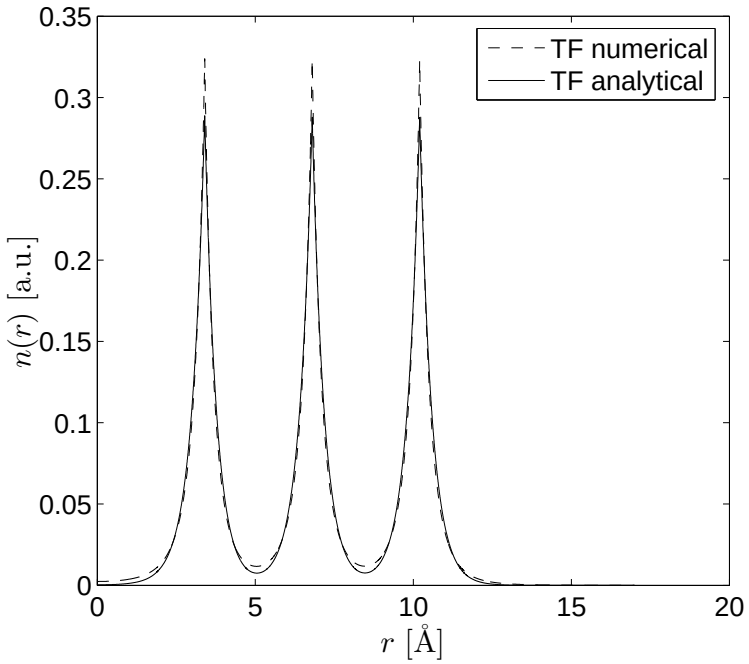

Figure 3.8: TF numerical electron density and its analytical TF Bessel approximation for 3-walled nanotube.

Chapter 4

Stopping Force

We will now be interested in studying ions moving parallel to a graphene sheet and experiencing forces due to the dynamic polarization of carbon valence electrons. When studying the energy loss of such ions, it is important to look at the force which directly opposes the ion's motion, called the stopping force (see figure 4.1). In this chapter, we develop the theory used to calculate the stopping force.

For an ion moving through an electron gas, the stopping force [1] is defined by

$$F_S(t) = -Z_1 \hat{\mathbf{v}} \cdot \mathbf{E}(\mathbf{r})\Big|_{\mathbf{r}=\mathbf{r}_0(t)}, \tag{4.1}$$

where Z_1 is the ion's electric charge, $\hat{\mathbf{v}} = \mathbf{v}(t)/v(t)$,[2] and $\mathbf{E}(\mathbf{r})$ is the induced electric field. We may write (4.1) as

$$F_S(t) = Z_1 \hat{\mathbf{v}} \cdot \vec{\nabla}\phi_{ind}(\mathbf{r}, t)\Big|_{\mathbf{r}=\mathbf{r}_0(t)}, \tag{4.2}$$

where $\phi_{ind}(\mathbf{r}, t)$ is the induced electric potential. Our goal is to find an expression

[1] Often incorrectly called "stopping power" in the literature.

[2] Here $\mathbf{v}(t) = d\mathbf{r}_0(t)/dt$ is the ion's velocity and $v(t)$ is $|\mathbf{v}(t)|$, i.e., the ion's speed.

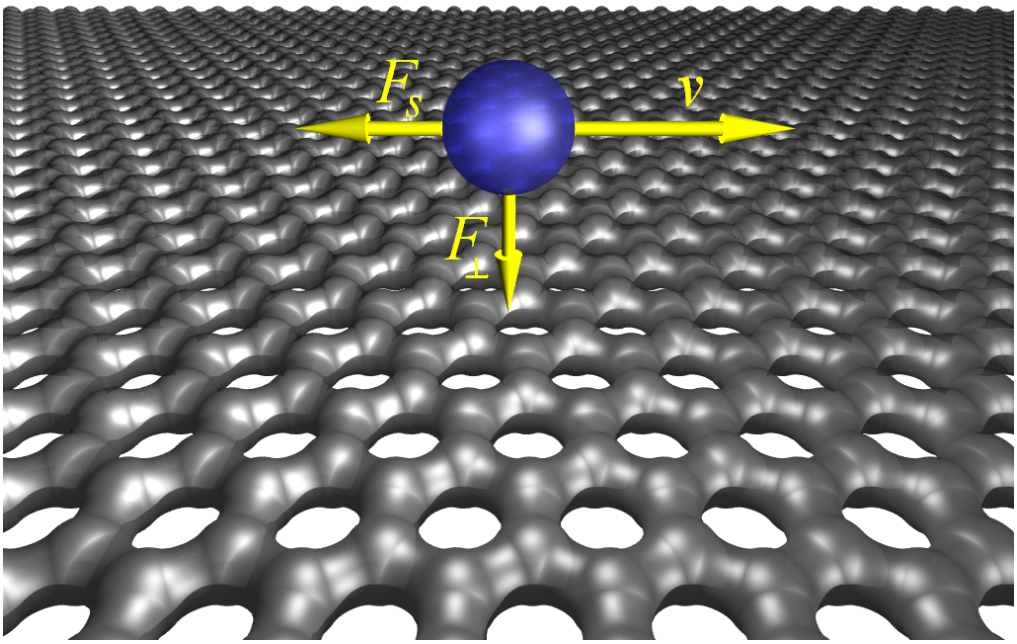

Figure 4.1: Ion moving parallel to a graphene sheet.

that we can use to calculate the stopping force for ions moving parallel to a graphene sheet.

4.1 Induced Electric Potential

Our first step in finding an expression for the stopping force that we can use is to find a way of expressing $\phi_{ind}(\mathbf{r}, t)$ in (4.2). The induced electric potential is given by

$$\phi_{ind}(\mathbf{r}, t) = \int d\mathbf{r}' \; \rho_{ind}(\mathbf{r}', t) V_c(\mathbf{r} - \mathbf{r}'), \tag{4.3}$$

where $\rho_{ind}(\mathbf{r}',t)$ is the induced charge density and $V_c(\mathbf{r}-\mathbf{r}') \equiv 1/|\mathbf{r}-\mathbf{r}'|$, is the Coulomb interaction. We know that the induced charge density is given by [15]

$$\rho_{ind}(\mathbf{r}',t) = \int d\mathbf{r}'' \int d\tau \ \left[\epsilon^{-1}(\mathbf{r}',\mathbf{r}'',t-\tau) - \delta(\mathbf{r}'-\mathbf{r}'')\delta(t-\tau)\right] \rho_{ext}(\mathbf{r}'',\tau), \quad (4.4)$$

where $\epsilon^{-1}(\mathbf{r}',\mathbf{r}'',t-\tau)$ is the inverse dielectric function of the medium and $\rho_{ext}(\mathbf{r}'',\tau)$ is the external charge density, which is the charge density of the ion alone. The term $[\epsilon^{-1}(\mathbf{r}',\mathbf{r}'',t-\tau) - \delta(\mathbf{r}'-\mathbf{r}'')\delta(t-\tau)]$ in (4.4) is called the density-density response function. Using (4.3) with (4.4) we may write

$$\begin{aligned}\phi_{ind}(\mathbf{r},t) = &\int d\mathbf{r}' \int d\mathbf{r}'' \int d\tau \ V_c(\mathbf{r}-\mathbf{r}') \\ &\times \ \left[\epsilon^{-1}(\mathbf{r}',\mathbf{r}'',t-\tau) - \delta(\mathbf{r}'-\mathbf{r}'')\delta(t-\tau)\right] \rho_{ext}(\mathbf{r}'',\tau), \end{aligned} \quad (4.5)$$

or using the notation $\mathbf{r} = (\mathbf{R}, z)$, [3]

$$\begin{aligned}\phi_{ind}(\mathbf{r},t) = &\int dz' \int dz'' \int d\mathbf{R}' \int d\mathbf{R}'' \int d\tau \ V_c(\mathbf{R}-\mathbf{R}';z-z') \\ \times \ &\left[\epsilon^{-1}(\mathbf{R}'-\mathbf{R}'';z',z'';t-\tau) - \delta(\mathbf{R}'-\mathbf{R}'')\delta(z'-z'')\delta(t-\tau)\right] \rho_{ext}(\mathbf{R}'',z'',\tau). \end{aligned} \quad (4.6)$$

In (4.6) we may write the inverse dielectric function in terms of its Fourier transform as

$$\epsilon^{-1}(\mathbf{R}'-\mathbf{R}'';z',z'';t-\tau) = \int \frac{d\mathbf{K}}{(2\pi)^2} \int \frac{d\omega}{2\pi} \ e^{i\mathbf{K}\cdot(\mathbf{R}'-\mathbf{R}'')} e^{-i\omega(t-\tau)} \epsilon^{-1}(\mathbf{K};z',z'';\omega), \quad (4.7)$$

and the term $\delta(\mathbf{R}'-\mathbf{R}'')\delta(t-\tau)$ as

$$\delta(\mathbf{R}'-\mathbf{R}'')\delta(t-\tau) = \int \frac{d\mathbf{K}}{(2\pi)^2} \int \frac{d\omega}{2\pi} \ e^{i\mathbf{K}\cdot(\mathbf{R}'-\mathbf{R}'')} e^{-i\omega(t-\tau)}, \quad (4.8)$$

[3] See p. 18.

so we get

$$\phi_{ind}(\mathbf{r},t) = \int dz' \int dz'' \int d\mathbf{R}' \int d\mathbf{R}'' \int d\tau \int \frac{d\mathbf{K}}{(2\pi)^2} \int \frac{d\omega}{2\pi}\ e^{i\mathbf{K}\cdot(\mathbf{R}'-\mathbf{R}'')-i\omega(t-\tau)}$$

$$\times\ V_c(\mathbf{R}-\mathbf{R}';z-z')\left[\epsilon^{-1}(\mathbf{K};z',z'';\omega)-\delta(z'-z'')\right]\rho_{ext}(\mathbf{R}'',z'',\tau). \tag{4.9}$$

We may also write the exponential in (4.9) as

$$e^{i\mathbf{K}\cdot(\mathbf{R}'-\mathbf{R}'')-i\omega(t-\tau)} = e^{i\mathbf{K}\cdot[\mathbf{R}-(\mathbf{R}-\mathbf{R}')-\mathbf{R}'']-i\omega(t-\tau)}, \tag{4.10}$$

so that the integral over $\mathbf{R}'$ becomes

$$\int d\mathbf{R}'\ e^{-i\mathbf{K}\cdot(\mathbf{R}-\mathbf{R}')}V_c(\mathbf{R}-\mathbf{R}';z-z') = V_c(\mathbf{K};z-z'). \tag{4.11}$$

The induced potential (4.9) may then be written as

$$\phi_{ind}(\mathbf{r},t) = \int dz' \int dz'' \int \frac{d\mathbf{K}}{(2\pi)^2}\ e^{i\mathbf{K}\cdot\mathbf{R}} \int \frac{d\omega}{2\pi}\ e^{-i\omega t}\ V_c(\mathbf{K};z-z')$$

$$\times\ \left[\epsilon^{-1}(\mathbf{K};z',z'';\omega)-\delta(z'-z'')\right]\int d\mathbf{R}'' \int d\tau\ e^{-i(\mathbf{K}\cdot\mathbf{R}'')}e^{i\omega\tau}\rho_{ext}(\mathbf{R}'',z'',\tau). \tag{4.12}$$

We write the velocity of a moving ion as $\mathbf{v}(t) = (\mathbf{V}, v_z)$, where $\mathbf{V} = (v_x, v_y)$ is the component of $\mathbf{v}$ in the xy-plane. For an ion of charge Z_1, moving at constant velocity $\mathbf{v}(t) \equiv (\mathbf{V}, v_z) = (\mathbf{V}, 0)$ parallel to the xy-plane, and at a distance b from the xy-plane, the charge density is given by

$$\rho_{ext}(\mathbf{R}'',z'',\tau) = Z_1\delta(\mathbf{R}''-\mathbf{V}\tau)\delta(z''-b). \tag{4.13}$$

In (4.12) the integrals over $\mathbf{R}''$ and τ then become

$$\int d\mathbf{R}'' \int d\tau\ e^{-i(\mathbf{K}\cdot\mathbf{R}'')}e^{i\omega\tau}\rho_{ext}(\mathbf{R}'',z'',\tau) = Z_1\int d\tau\ e^{-i(\mathbf{K}\cdot\mathbf{V}\tau)}e^{i\omega\tau}\delta(z''-b). \tag{4.14}$$

Using the exponential integral form of the Dirac delta function

$$\delta(\omega - \mathbf{K}\cdot\mathbf{V}) = \frac{1}{2\pi}\int d\tau\ e^{i\tau(\omega-\mathbf{K}\cdot\mathbf{V})}, \tag{4.15}$$

we write (4.14) as

$$\int d\mathbf{R}''\int d\tau\ e^{-i(\mathbf{K}\cdot\mathbf{R}'')}e^{i\omega\tau}\rho_{ext}(\mathbf{R}'',z'',\tau) = 2\pi Z_1\delta(\omega-\mathbf{K}\cdot\mathbf{V})\delta(z''-b). \tag{4.16}$$

Substituting (4.16) in (4.12) we get

$$\phi_{ind}(\mathbf{r},t) = \int dz'\int dz''\int \frac{d\mathbf{K}}{(2\pi)^2}\ e^{i\mathbf{K}\cdot\mathbf{R}}\int d\omega\ e^{-i\omega t}\ V_c(\mathbf{K};z-z')$$

$$\times\ \left[\epsilon^{-1}(\mathbf{K};z',z'';\omega) - \delta(z'-z'')\right] Z_1\delta(\omega-\mathbf{K}\cdot\mathbf{V})\delta(z''-b). \tag{4.17}$$

The integrals over ω and z'' may be done taking advantage of the delta functions. We get

$$\phi_{ind}(\mathbf{r},t) = \frac{Z_1}{(2\pi)^2}\int dz'\int d\mathbf{K}\ e^{i\mathbf{K}\cdot(\mathbf{R}-\mathbf{V}t)}V_c(\mathbf{K};z-z')\left[\epsilon^{-1}(\mathbf{K};z',b;\mathbf{K}\cdot\mathbf{V}) - \delta(z'-b)\right]. \tag{4.18}$$

4.2 Expressing the Coulomb Interaction

We now need an expression for $V_c(\mathbf{K};z-z')$ in (4.18). We know

$$V_c(\mathbf{r}-\mathbf{r}') = \frac{1}{|\mathbf{r}-\mathbf{r}'|} = \frac{1}{\sqrt{|\mathbf{R}-\mathbf{R}'|^2+(z-z')^2}} = \frac{1}{\sqrt{R_d^2+(z-z')^2}}, \tag{4.19}$$

where $\mathbf{R_d} \equiv \mathbf{R}-\mathbf{R}'$, and $R_d = |\mathbf{R_d}|$. Using Fourier transforms we have

$$V_c(\mathbf{K};z-z') = \int d\mathbf{R_d}\ e^{-i\mathbf{K}\cdot\mathbf{R_d}}V_c(\mathbf{r}-\mathbf{r}')$$

$$= \int_0^\infty dR_d \; R_d \int_{-\pi}^{\pi} d\theta \; \frac{e^{-iKR_d\cos\theta}}{\sqrt{(z-z')^2+R_d^2}}$$

$$= \int_0^\infty dR_d \; R_d \frac{2}{\sqrt{(z-z')^2+R_d^2}} \int_0^{\pi} d\theta \; \cos\left(KR_d\cos\theta\right). \tag{4.20}$$

Now we use the integral representation of the Bessel function of the first kind [16]

$$J_0(z) = \frac{1}{\pi}\int_0^{\pi} d\theta \; \cos\left(z\cos\theta\right), \tag{4.21}$$

and we write (4.20) as

$$V_c(\mathbf{K}; z-z') = 2\pi \int_0^\infty dR_d \; R_d \frac{1}{\sqrt{(z-z')^2+R_d^2}} J_0(KR_d)$$

$$= \frac{2\pi e^{-|z-z'|K}}{K}. \tag{4.22}$$

We may now substitute (4.22) into (4.18) and get

$$\phi_{ind}(\mathbf{r},t) = \frac{Z_1}{2\pi}\int dz' \int \frac{d\mathbf{K}}{K} \; e^{i\mathbf{K}\cdot(\mathbf{R}-\mathbf{V}t)} e^{-|z-z'|K} \left[\epsilon^{-1}(\mathbf{K}; z', b; \mathbf{K}\cdot\mathbf{V}) - \delta(z'-b)\right]. \tag{4.23}$$

4.3 Expressing the Stopping Force

In our expression for the stopping force (4.2), what we need is the gradient of $\phi_{ind}(\mathbf{r},t)$. Actually, because of the dot product of $\vec{\nabla}\phi_{ind}(\mathbf{r},t)$ with $\mathbf{v}(t)$ in (4.2), we care about only the component of $\vec{\nabla}\phi_{ind}(\mathbf{r},t)$ in the direction of $\mathbf{v}(t)$, that is, of $\mathbf{V}$.

From (4.23) we have [4]

$$\vec{\nabla}_{\mathbf{R}}\phi_{ind}(\mathbf{r},t) = \frac{Z_1}{2\pi}\int dz' \int \frac{d\mathbf{K}}{K}\,(i\mathbf{K})e^{i\mathbf{K}\cdot(\mathbf{R}-\mathbf{V}t)}\Big[\epsilon^{-1}(\mathbf{K},z',b,\mathbf{K}\cdot\mathbf{V})-\delta(z'-b)\Big]e^{-|z-z'|K}. \tag{4.24}$$

Using this equation, we write the stopping force (4.2) as

$$\begin{aligned} F_S &= Z_1\frac{\mathbf{v}(t)}{v(t)}\cdot\vec{\nabla}\phi_{ind}(\mathbf{r},t)\Big|_{\mathbf{r}=\mathbf{r}_0(t)} = Z_1\frac{\mathbf{v}(t)}{v(t)}\cdot\vec{\nabla}_{\mathbf{R}}\phi_{ind}(\mathbf{r},t)\Big|_{\mathbf{r}=\mathbf{r}_0(t)} \\ &= i\frac{(Z_1)^2}{2\pi v}\int dz' \int d\mathbf{K}\;(\mathbf{K}\cdot\mathbf{V})\Big[\epsilon^{-1}(\mathbf{K},z',b,\mathbf{K}\cdot\mathbf{V})-\delta(z'-b)\Big]\frac{e^{-|b-z'|K}}{K}. \end{aligned} \tag{4.25}$$

Notice that when we set $\mathbf{r} = \mathbf{r}_0(t)$, the first exponential from (4.24) vanishes because we have $\mathbf{R} = \mathbf{V}t$. This means that the stopping force is independent of time.

To write (4.25) in a more convenient form, we now introduce some notation. First of all, we are interested in studying an ion moving through an electron gas, and for simplicity we assume the ion to be moving parallel to the xy-plane and at a distance b from the xy-plane. To simplify things more, we may choose our coordinate system so that the ion moves parallel to the x-axis. We then have $\mathbf{V} = (v, 0)$, and since $\mathbf{K} = (K_x, K_y)$, [5] we may write $\mathbf{K}\cdot\mathbf{V} = K_x v$.

We had previously set $\omega = \mathbf{K}\cdot\mathbf{V}$ because of the delta function in (4.17), so we have $\omega = \mathbf{K}\cdot\mathbf{V} = K_x v$. Now we define $K_x \equiv \omega/v$ and $K_y \equiv q$, so $dK_x = d\omega/v$, $dK_y = dq$, and $d\mathbf{K} = dK_x dK_y = (1/v)d\omega dq$. We also have

$$K = \sqrt{K_x^2 + K_y^2} = \sqrt{\frac{\omega^2}{v^2} + q^2}, \tag{4.26}$$

---

[4] In (4.24), $\vec{\nabla}_{\mathbf{R}}\phi_{ind}(\mathbf{r},t)$ is the component of $\vec{\nabla}\phi_{ind}(\mathbf{r},t)$ in the $\mathbf{R}$ direction. We don't need the component in the z direction, since it will vanish when doing the dot product $\hat{\mathbf{v}}\cdot\vec{\nabla}\phi_{ind}(\mathbf{r},t)$ in (4.2).

[5] Recall $\mathbf{K}$ was the Fourier transform of $\mathbf{R} = (x, y)$.

and we know $z = b$ throughout the ion's trajectory.

Finally we may write the stopping force (4.25) as

$$F_S = i\frac{Z_1^2}{2\pi v}\int dz' \int dq \int d\omega\ \frac{\omega}{v}$$

$$\times \left[\epsilon^{-1}\left(z', b, \sqrt{q^2+\omega^2/v^2}, \omega\right) - \delta(z'-b)\right] \frac{e^{-|b-z'|\sqrt{q^2+\omega^2/v^2}}}{\sqrt{q^2+\omega^2/v^2}} \tag{4.27}$$

or

$$F_S = -\frac{Z_1^2}{2\pi v^2}\int dz' \int dq\ 2\int_0^\infty d\omega\ \omega \frac{e^{-|b-z'|\sqrt{q^2+\omega^2/v^2}}}{\sqrt{q^2+\omega^2/v^2}}$$
$$\times \mathrm{Im}\left[\epsilon^{-1}\left(z', b, q, \omega/v; \omega\right) - \delta(z'-b)\right], \tag{4.28}$$

where we have used the property that $\mathrm{Re}[\epsilon^{-1}(\omega)]$ is an even function of ω, and $\mathrm{Im}[\epsilon^{-1}(\omega)]$ is an odd function of ω. Equation (4.28) gives us an expression for the stopping force in terms of the inverse dielectric function.

4.4 Inverse Dielectric Function

To calculate the stopping force using (4.28), we need to know the inverse dielectric function. By using the high frequency approximation, Kitagawa derived an expression for the inverse dielectric function of a nonuniform electron gas with ground-state density $n(\mathbf{r})$ [6]. His inverse dielectric function is

$$\epsilon^{-1}(\mathbf{r}_1, \mathbf{r}_2, \omega) \cong \frac{\omega^2}{\omega^2 - \omega_p^2(\mathbf{r}_1)}\left[\delta(\mathbf{r}_1 - \mathbf{r}_2) - \frac{1}{\omega^2 - \omega_p^2(\mathbf{r}_2)}\frac{(\mathbf{r}_2 - \mathbf{r}_1)}{|\mathbf{r}_2 - \mathbf{r}_1|^3}\cdot\vec{\nabla} n(\mathbf{r}_1)\right], \tag{4.29}$$

where $\omega_p^2(\mathbf{r}) = 4\pi n(\mathbf{r})$ is the so-called local plasma frequency. We need to find the imaginary part of $\epsilon^{-1}(\mathbf{r}_1, \mathbf{r}_2, \omega)$ in order to calculate the stopping force. To do this, we first look at the factor $\omega^2/\left(\omega^2 - \omega_p^2(\mathbf{r}_1)\right)$ in the first term of $\epsilon^{-1}(\mathbf{r}_1, \mathbf{r}_2, \omega)$.

Letting $\omega \longrightarrow (\omega + i\eta)$ with $\eta \to 0^+$ to distinguish the real and imaginary parts, we write $\omega^2/\left(\omega^2 - \omega_p^2(\mathbf{r}_1)\right)$ as [6]

$$\frac{(\omega+i\eta)^2}{(\omega+i\eta)^2-\omega_p^2} = \frac{\omega^2-\eta^2+i2\omega\eta}{\omega^2-\eta^2+i2\omega\eta-\omega_p^2} = 1+\frac{\omega_p^2}{\omega^2-\eta^2+i2\omega\eta-\omega_p^2}$$

$$= 1+\frac{\omega_p^2\left(\omega^2-\eta^2-\omega_p^2\right)}{(\omega^2-\eta^2-\omega_p^2)^2+(2\omega\eta)^2} - i\frac{\omega_p^2 2\omega\eta}{(\omega^2-\eta^2-\omega_p^2)^2+(2\omega\eta)^2}. \tag{4.30}$$

Now letting $\eta \to 0^+$, we have

$$\frac{(\omega+i\eta)^2}{(\omega+i\eta)^2-\omega_p^2} \longrightarrow 1+P\left(\frac{\omega_p^2}{\omega^2-\omega_p^2}\right) - i\frac{\omega_p^2 2\omega\eta}{(\omega^2-\omega_p^2)^2+(2\omega\eta)^2}$$

$$= 1+P\left(\frac{\omega_p^2}{\omega^2-\omega_p^2}\right) - i\omega_p^2\,\mathrm{sign}(\omega)\pi\left[\frac{|\omega|2\eta/\pi}{(\omega^2-\omega_p^2)^2+(2|\omega|\eta)^2}\right], \tag{4.31}$$

where $P(\omega_p^2/(\omega^2-\omega_p^2))$ means we take the Cauchy principal part of $\omega_p^2/(\omega^2-\omega_p^2)$. Using the representation of the delta function

$$\delta(x) = \lim_{\gamma\to 0^+}\frac{1}{\pi}\frac{\gamma}{x^2+\gamma^2}\ , \tag{4.32}$$

we may write the right hand side of (4.31) as

$$1+P\left(\frac{\omega_p^2}{\omega^2-\omega_p^2}\right) - i\omega_p^2\,\mathrm{sign}(\omega)\pi\delta(\omega^2-\omega_p^2). \tag{4.33}$$

We may express the delta function in this expression as $\delta\left((\omega+\omega_p)(\omega-\omega_p)\right)$. Now we may use the property that a delta function of a function $g(x)$ may be written as

$$\delta\left(g(x)\right) = \sum_i \frac{\delta(x-x_i)}{|g'(x_i)|}\ , \tag{4.34}$$

---

[6] $\eta > 0$ to ensure that the density-density response function in (4.4) is causal, that is $\epsilon^{-1}(t-\tau) = 0$ for $\tau > t$ upon performing the inverse Fourier transform of $\epsilon^{-1}(\omega)$.

where the x_i's are the zeros of $g(x)$. So we have , as $\eta \to 0^+$,

$$\frac{(\omega+i\eta)^2}{(\omega+i\eta)^2-\omega_p^2} \longrightarrow 1 + P\left(\frac{\omega_p^2}{\omega^2-\omega_p^2}\right) - i\omega_p^2\,\mathrm{sign}(\omega)\pi\left[\frac{\delta(\omega-\omega_p)}{2\omega_p}+\frac{\delta(\omega+\omega_p)}{2\omega_p}\right] =$$

$$= 1 + P\left(\frac{\omega_p^2}{\omega^2-\omega_p^2}\right) - i\omega_p\frac{\pi}{2}\left[\delta(\omega-\omega_p)-\delta(\omega+\omega_p)\right]. \tag{4.35}$$

The second term in (4.29) has the factor

$$\frac{\omega^2}{\omega^2-\omega_p^2(\mathbf{r}_1)}\frac{1}{\omega^2-\omega_p^2(\mathbf{r}_2)} = -\frac{1}{(\omega_2^2-\omega_1^2)}\left[\frac{\omega^2}{(\omega^2-\omega_1^2)}-\frac{\omega^2}{(\omega^2-\omega_2^2)}\right], \tag{4.36}$$

where we have abbreviated $\omega_p^2(\mathbf{r}_1)$ and $\omega_p^2(\mathbf{r}_2)$ by ω_1^2 and ω_2^2, respectively.

As we did previously, we let $\omega \longrightarrow (\omega+i\eta)$ to distinguish the real and imaginary parts. Then, letting $\eta \to 0^+$, we use the result of (4.35) to write the right hand side of (4.36) as

$$\begin{aligned}
&-\frac{1}{\omega_2^2-\omega_1^2}\Bigg[\left\{1+P\left(\frac{\omega_1^2}{\omega^2-\omega_1^2}\right)-i\omega_1\frac{\pi}{2}\left[\delta(\omega-\omega_1)-\delta(\omega+\omega_1)\right]\right\}\\
&\qquad -\left\{1+P\left(\frac{\omega_2^2}{\omega^2-\omega_2^2}\right)-i\omega_2\frac{\pi}{2}\left[\delta(\omega-\omega_2)-\delta(\omega+\omega_2)\right]\right\}\Bigg]
\end{aligned}$$

$$\begin{aligned}
= \; & -\frac{1}{\omega_2^2-\omega_1^2}\Bigg\{P\left(\frac{\omega_1^2}{\omega^2-\omega_1^2}-\frac{\omega_2^2}{\omega^2-\omega_2^2}\right)\\
& -i\omega_1\frac{\pi}{2}\left[\delta(\omega-\omega_1)-\delta(\omega+\omega_1)\right]+i\omega_2\frac{\pi}{2}\left[\delta(\omega-\omega_2)-\delta(\omega+\omega_2)\right]\Bigg\}
\end{aligned}$$

$$\begin{aligned}
= \; & P\left(\frac{\omega^2}{(\omega^2-\omega_1^2)(\omega^2-\omega_2^2)}\right)-i\frac{\pi}{2}P\left(\frac{1}{\omega_2^2-\omega_1^2}\right)\\
& \times\Bigg\{-\omega_1\left[\delta(\omega-\omega_1)-\delta(\omega+\omega_1)\right]+\omega_2\left[\delta(\omega-\omega_2)-\delta(\omega+\omega_2)\right]\Bigg\},
\end{aligned} \tag{4.37}$$

where in the last step we have used

$$\frac{\omega_1^2}{\omega^2-\omega_1^2}-\frac{\omega_2^2}{\omega^2-\omega_2^2}=\frac{\omega^2(\omega_1^2-\omega_2^2)}{(\omega^2-\omega_1^2)(\omega^2-\omega_2^2)}. \tag{4.38}$$

The factors

$$\frac{\omega^2}{\omega^2-\omega_1^2} \quad \text{and} \quad \frac{\omega^2}{\omega^2-\omega_1^2}\frac{1}{\omega^2-\omega_2^2}\ , \tag{4.39}$$

in Kitagawa's inverse dielectric function (4.29), are given by (4.35) and (4.37), respectively. Taking the imaginary parts of (4.35) and (4.37) we may write the imaginary part of $\epsilon^{-1}(\mathbf{r}_1,\mathbf{r}_2,\omega)$ as

$$\begin{aligned}\mathrm{Im}\left[\epsilon^{-1}(\mathbf{r}_1,\mathbf{r}_2,\omega)\right] &= -\omega_p(\mathbf{r}_1)\frac{\pi}{2}\left[\delta\left(\omega-\omega_p(\mathbf{r}_1)\right)-\delta\left(\omega+\omega_p(\mathbf{r}_1)\right)\right]\delta(\mathbf{r}_1-\mathbf{r}_2)\\ &+\frac{\mathbf{r}_2-\mathbf{r}_1}{|\mathbf{r}_2-\mathbf{r}_1|^3}\cdot\vec{\nabla}n(\mathbf{r}_1)\left[\frac{\pi}{2}P\left(\frac{1}{\omega_p(\mathbf{r}_2)^2-\omega_p(\mathbf{r}_1)^2}\right)\Big(\omega_p(\mathbf{r}_2)\left[\delta(\omega-\omega_p(\mathbf{r}_2))-\delta(\omega+\omega_p(\mathbf{r}_2))\right]\right.\\ &\left.-\omega_p(\mathbf{r}_1)\left[\delta(\omega-\omega_p(\mathbf{r}_1))-\delta(\omega+\omega_p(\mathbf{r}_1))\right]\Big)\right].\end{aligned} \tag{4.40}$$

We consider an electron density that varies only in one dimension, and we write $\mathbf{r}_1=z'$, $\mathbf{r}_2=z$, and

$$\vec{\nabla}n(\mathbf{r}_1)=\frac{dn(z')}{dz'}\hat{\mathbf{e}}_z. \tag{4.41}$$

We also have

$$\frac{\mathbf{r}_2-\mathbf{r}_1}{|\mathbf{r}_2-\mathbf{r}_1|^3}=\vec{\nabla}_{\mathbf{r}_1}\frac{1}{|\mathbf{r}_1-\mathbf{r}_2|}=\vec{\nabla}_{\mathbf{r}_1}V_c(\mathbf{r}_1-\mathbf{r}_2)=\vec{\nabla}_{\mathbf{r}_1}V_c(\mathbf{R}_1-\mathbf{R}_2,z'-z) \tag{4.42}$$

so

$$\frac{\mathbf{r}_2-\mathbf{r}_1}{|\mathbf{r}_2-\mathbf{r}_1|^3}\cdot\vec{\nabla}n(\mathbf{r}_1)=\frac{\partial V_c(\mathbf{R}_1-\mathbf{R}_2,z'-z)}{\partial z'}\frac{dn(z')}{dz'}. \tag{4.43}$$

Taking the Fourier transform of (4.43) with respect to $\mathbf{R}_{d_{12}} \equiv \mathbf{R}_1 - \mathbf{R}_2$ we have

$$\int d\mathbf{R}_{d_{12}}\; e^{i\mathbf{K}\cdot(\mathbf{R}_1-\mathbf{R}_2)} \frac{\mathbf{r}_2-\mathbf{r}_1}{|\mathbf{r}_2-\mathbf{r}_1|^3}\cdot\vec{\nabla} n(\mathbf{r}_1)$$

$$= \frac{\partial V_c(\mathbf{K}, z'-z)}{\partial z'}\frac{dn(z')}{dz'}, \tag{4.44}$$

or using (4.22) for $V_c(\mathbf{K}, z'-z)$ we have

$$\int d\mathbf{R}_{d_{12}}\; e^{i\mathbf{K}\cdot(\mathbf{R}_1-\mathbf{R}_2)} \frac{\mathbf{r}_2-\mathbf{r}_1}{|\mathbf{r}_2-\mathbf{r}_1|^3}\cdot\vec{\nabla} n(\mathbf{r}_1)$$

$$= \frac{\partial}{\partial z'}\left(\frac{2\pi e^{-K|z'-z|}}{K}\right)\frac{dn(z')}{dz'} = 2\pi e^{-K|z'-z|}\frac{dn(z')}{dz'}\frac{z-z'}{|z-z'|}. \tag{4.45}$$

We may then use (4.40) to obtain the Fourier transform of the density-density response function

$$\begin{aligned}\mathrm{Im}\Big[\epsilon^{-1}(\mathbf{K}, z, b, \omega) - \delta(z'-b)\Big] &= -\omega_p(z')\frac{\pi}{2}\Big[\delta\left(\omega-\omega_p(z')\right) - \delta\left(\omega+\omega_p(z')\right)\Big]\delta(z'-b) \\ &\quad + \pi^2\frac{b-z'}{|b-z'|}e^{-|z'-b|K}\;\frac{dn(z')}{dz'}P\left(\frac{1}{\omega_p(b)^2-\omega_p(z')^2}\right) \\ \times\Big\{\omega_p(b)\left[\delta(\omega-\omega_p(b)) - \delta(\omega+\omega_p(b))\right] &- \omega_p(z')\left[\delta(\omega-\omega_p(z')) - \delta(\omega+\omega_p(z'))\right]\Big\}.\end{aligned} \tag{4.46}$$

4.5 Final Expression for Stopping Force

We may now use (4.46) with (4.26) in our expression (4.28) for stopping force. Substituting the first term of (4.46) in (4.28) we are left with the first term of our stopping force:

$$F_{S_1} = \frac{Z_1^2}{2v^2}\int dz' \int dq \int_0^\infty d\omega\; \omega \frac{e^{-|z-z'|\sqrt{q^2+\omega^2/v^2}}}{\sqrt{q^2+\omega^2/v^2}}$$

$$\times\ \omega_p(z')\left[\delta(\omega-\omega_p(z'))-\delta(\omega+\omega_p(z'))\right]\delta(z'-b) \tag{4.47}$$

Taking advantage of the delta functions to do the z' and ω integrals, we get [7]

$$F_{S_1}=\frac{(Z_1)^2}{v^2}\omega_p^2(b)\int_0^{q_{max}} dq\ \frac{e^{-|z-b|\sqrt{q^2+\omega_p^2(b)/v^2}}}{\sqrt{q^2+\frac{\omega_p^2(b)}{v^2}}}, \tag{4.48}$$

and since $z=b$ throughout the ion's trajectory,

$$F_{S_1}=\frac{(Z_1)^2}{v^2}\omega_p^2(b)\int_0^{q_{max}} dq\ \frac{1}{\sqrt{q^2+\frac{\omega_p^2(b)}{v^2}}}$$

$$=\frac{(Z_1)^2}{v^2}\omega_p^2(b)\left[\ln\left(q_{max}+\sqrt{q_{max}^2+\frac{\omega_p^2(b)}{v^2}}\right)-\ln\left(\frac{\omega_p(b)}{v}\right)\right]$$

$$=\frac{(Z_1)^2}{v^2}\omega_p^2(b)\ln\left(\frac{q_{max}v}{\omega_p(b)}+\sqrt{\frac{q_{max}^2v^2}{\omega_p(b)}+1}\right). \tag{4.49}$$

In the limit as $v\to\infty$, (4.49) corresponds to the well-known Bethe formula for stopping force in homogeneous media [17]. Substituting the second term of (4.46) in (4.28) we get the second term of our stopping force:

$$F_{S_2}=-\frac{(Z_1)^2\pi}{v^2}\int dz'\int dq\int_0^\infty d\omega\ \omega\frac{e^{-|z-z'|\sqrt{q^2+\omega^2/v^2}}}{\sqrt{q^2+\omega^2/v^2}}\frac{(b-z')}{|b-z'|}\ \times$$

$$e^{-|z'-b|\sqrt{q^2+\omega^2/v^2}}\frac{dn(z')}{dz'}P\left(\frac{1}{\omega_p^2(b)-\omega_p^2(z')}\right)\ \times$$

$$\left\{\omega_p(b)\left[\delta(\omega-\omega_p(b))-\delta(\omega+\omega_p(b))\right]-\omega_p(z')\left[\delta(\omega-\omega_p(z'))-\delta(\omega+\omega_p(z'))\right]\right\}. \tag{4.50}$$

[7] The integral in (4.48) is divergent if we take the upper limit to be infinity. For this reason we introduce a cutoff q_{max} corresponding the the maximum momentum transfer to an electron.

Taking advantage of the delta functions to do the ω integrals and using $\omega_p^2(z) = 4\pi n(z)$, we get

$$F_{S_2} = -\frac{(Z_1)^2}{2v^2}\int dz'\ \frac{d\omega_p^2(z')}{dz'}\frac{b-z'}{|b-z'|}P\left(\frac{1}{\omega_p^2(b)-\omega_p^2(z')}\right)$$

$$\times\ \left[\omega_p^2(b)\int_0^\infty dq\ \frac{e^{-2|z'-b|\sqrt{q^2+\omega_p^2(b)/v^2}}}{\sqrt{q^2+\omega_p^2(b)/v^2}} - \omega_p^2(z')\int_0^\infty dq\ \frac{e^{-2|z'-b|\sqrt{q^2+\omega_p^2(z')/v^2}}}{\sqrt{q^2+\omega_p^2(z')/v^2}}\right]. \tag{4.51}$$

Noting that the integrals over q in (4.51) are convergent, we get

$$F_{S_2} = -\frac{(Z_1)^2}{v^2}\frac{1}{2}\int dz'\ \frac{d\omega_p^2(z')}{dz'}\frac{b-z'}{|b-z'|}P\left(\frac{1}{\omega_p^2(b)-\omega_p^2(z')}\right)$$

$$\times\ \left[\omega_p^2(b)K_0\left(\frac{2\omega_p(b)}{v}|z'-b|\right) - \omega_p^2(z')K_0\left(\frac{2\omega_p(z')}{v}|z'-b|\right)\right], \tag{4.52}$$

where K_0 is the zeroth order modified Bessel function of the second kind.

The total stopping force is then given by the sum of (4.49) and (4.52):

$$F_S = F_{S_1} + F_{S_2}$$

$$= \frac{(Z_1)^2}{v^2}\omega_p^2(b)\ln\left(\frac{q_{max}v}{\omega_p(b)} + \sqrt{\frac{q_{max}^2v^2}{\omega_p(b)}+1}\right) - \frac{(Z_1)^2}{v^2}\frac{1}{2}\int dz'\ \frac{d\omega_p^2(z')}{dz'}\frac{b-z'}{|b-z'|}$$

$$\times P\left(\frac{1}{\omega_p^2(b)-\omega_p^2(z')}\right)\left[\omega_p^2(b)K_0\left(\frac{2\omega_p(b)}{v}|z'-b|\right) - \omega_p^2(z')K_0\left(\frac{2\omega_p(z')}{v}|z'-b|\right)\right]. \tag{4.53}$$

F_{S_1} is called the local stopping force and corresponds to the Bethe formula for stopping in a homogeneous medium. F_{S_2} is called nonlocal stopping force, and gives a correction to the local stopping force.

Chapter 5

Calculation of Stopping Force

Now that we have an expression for the stopping force (4.53), we go ahead and calculate it.

5.1 Stopping Force at Metal Surface

Before working with graphene, we are interested in calculating the stopping force for a particle moving next to a metal, for example aluminum, in order to compare our result with that of [18]. To use (4.53) we need an expression for the electron density near the aluminum surface. We use the Thomas-Fermi electron density distribution, fitted by simple analytical functions of the form

$$n(z) = \begin{cases} n_o - \frac{1}{2} n_o e^{\beta z}, & (z < 0) \\ \frac{1}{2} n_o e^{-\beta z}, & (z > 0) \end{cases} , \tag{5.1}$$

where z is the distance from the surface, n_o is the electron density in the bulk and β is a parameter that determines the electron tail. For aluminum $n_o \approx 2.69 \times 10^{-2}$ a.u. and $\beta \approx 1.24$ a.u. [18].

Using this electron density distribution together with (4.53), we compute the

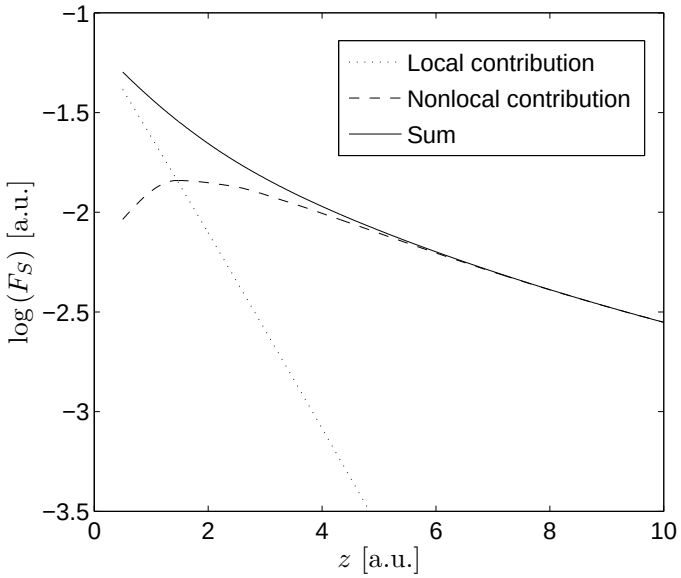

Figure 5.1: Stopping force for a proton of $v = 3.16$ a.u. moving parallel to an aluminum surface. The dotted line (·····) shows the first term of (4.53), called the local contribution. The dashed line (– –) shows the second term of (4.53), called the nonlocal contribution. The solid line (——) shows the sum of the local and nonlocal terms. We plot the logarithm to base 10 of the stopping force as a function of the distance from the metal surface.

stopping force for a proton of speed $v = 3.16$ a.u., for different distances z from the surface. In figure 5.1 we plot the first and second terms of (4.53) as well as their sum, reproducing the results of [18]. The first term (·····) is called the local contribution. The second term (– –) is a correction to the local contribution and is called the nonlocal contribution. It is clear from the figure that the nonlocal contribution is important at larger distances from the surface, while the local contribution is important near the surface.

5.2 Stopping Force Near a Graphene Sheet

Now we are interested in using the equilibrium electron density for graphene that we calculated in chapter 2, together with (4.53), to calculate the stopping force for an ion moving parallel to a graphene sheet.

Using the Thomas-Fermi analytical electron density for graphene (2.32), we compute the stopping force for a proton of speed $v = 3$ a.u., for different distances z from the surface. Figure 5.2 shows the contribution of each term of (4.53) to the total stopping force. Again, the first term (·····) is the local contribution and the second term (– –) is the correction to the local contribution, or the nonlocal contribution. Here we again see how the nonlocal term is important at larger distances from the surface, while the local term is important near the surface. We also compare our results with the stopping force calculated using a 2D-Fluid model for the electron gas on the graphene sheet [1] (–·–). The 2D-Fluid model approximates the electron distribution of graphene by a charged fluid confined to the two-dimensional plane of the sheet. We can see in figure 5.2 that the three-dimensional electron distribution of graphene greatly affects the stopping force on ions moving parallel to the sheet.

In figure 5.3 we compare the stopping force for a proton moving parallel to

[1] Refer to appendix B for a discussion of this 2D-Fluid model.

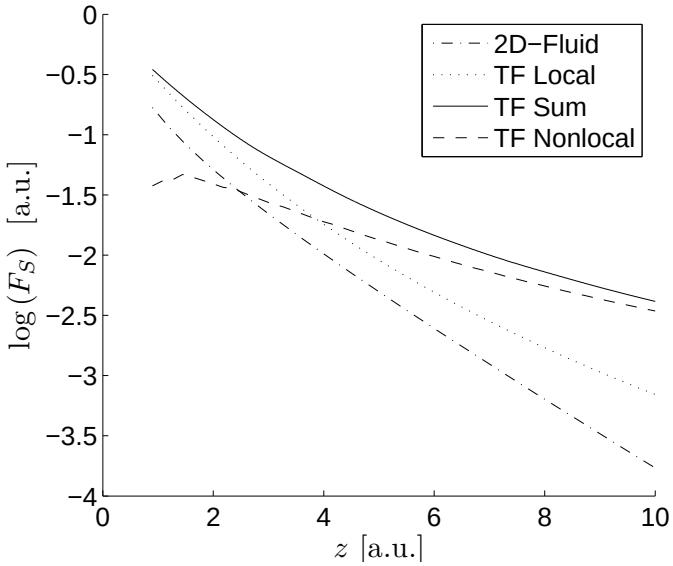

Figure 5.2: Stopping force for a proton of $v = 3$ a.u. moving parallel to a graphene sheet. The dotted line (·····) shows the first term of (4.53), called the local contribution. The dashed line (– –) shows the second term of (4.53), called the nonlocal contribution. The solid line (——) shows the sum of local and nonlocal contributions. The dashed-dotted line (–·–) is calculated using a 2D-Fluid model. We plot the logarithm to base 10 of the stopping force as a function of the distance from the sheet.

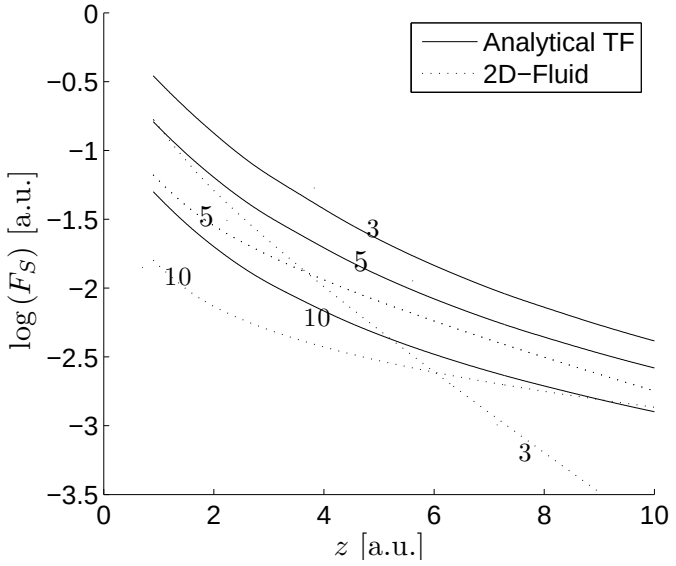

Figure 5.3: Stopping force for a proton moving parallel to graphene at speeds $v = 3$ a.u., $v = 5$ a.u., and $v = 10$ a.u. The solid line (——) is calculated using the TF analytical electron density for graphene. The dotted line (·····) is calculated using the 2D-Fluid model. We plot the logarithm to base 10 of the stopping force as a function of the distance from the sheet.

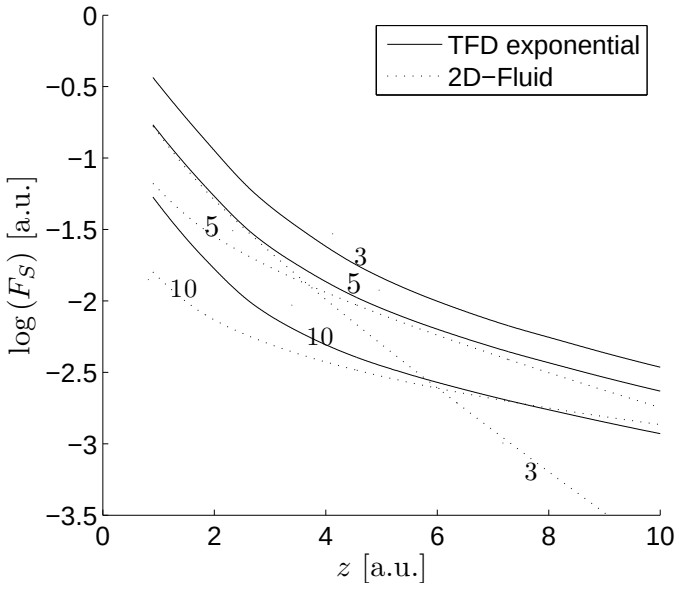

Figure 5.4: Stopping force for a proton moving parallel to graphene at speeds $v = 3$ a.u., $v = 5$ a.u., and $v = 10$ a.u. The solid line (——) is calculated using the TFD exponential approximation to the electron density for graphene. The dotted line (·····) is calculated using the 2D-Fluid model. We plot the logarithm to base 10 of the stopping force as a function of the distance from the sheet.

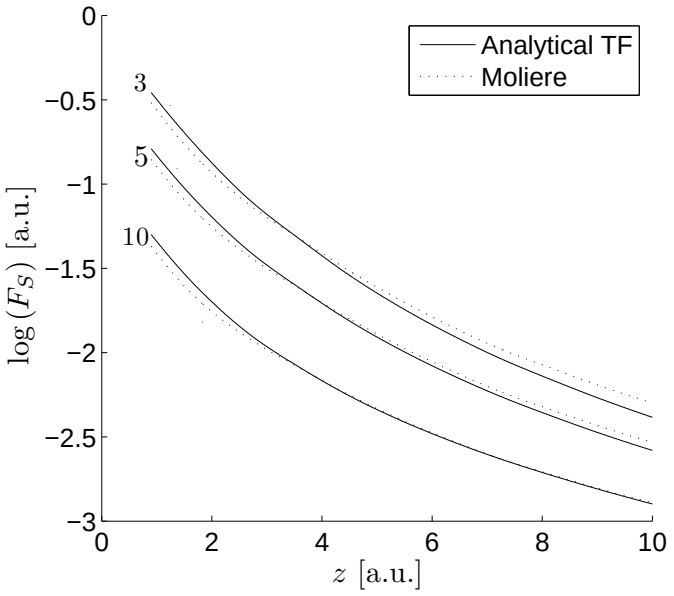

Figure 5.5: Stopping force for a proton moving parallel to graphene at speeds $v = 3$ a.u., $v = 5$ a.u., and $v = 10$ a.u. The solid line (——) is calculated using the TF analytical electron density for graphene. The dotted line (·····) is calculated using the Molière approximation to the electron density. We plot the logarithm to base 10 of the stopping force as a function of the distance from the sheet.

graphene at speeds $v = 3$ a.u., $v = 5$ a.u., and $v = 10$ a.u. The stopping force is calculated using the analytical TF electron density as well as the 2D-Fluid model. We again see how the stopping force is much greater when we don't restrict the electron density of graphene to the plane of the sheet. We also see how the stopping force is smaller for ions moving at higher speeds.

Figure 5.4 also compares the stopping force for a proton moving parallel to a graphene sheet. The calculations shown are done using the TFD exponential approximation to the electron density (2.33) as well as the 2D-Fluid model.

We also calculate the stopping force using the Molière approximation to the electron density. We compare this with the stopping force calculated using the analytical TF electron density and the TFD exponential approximation to the electron

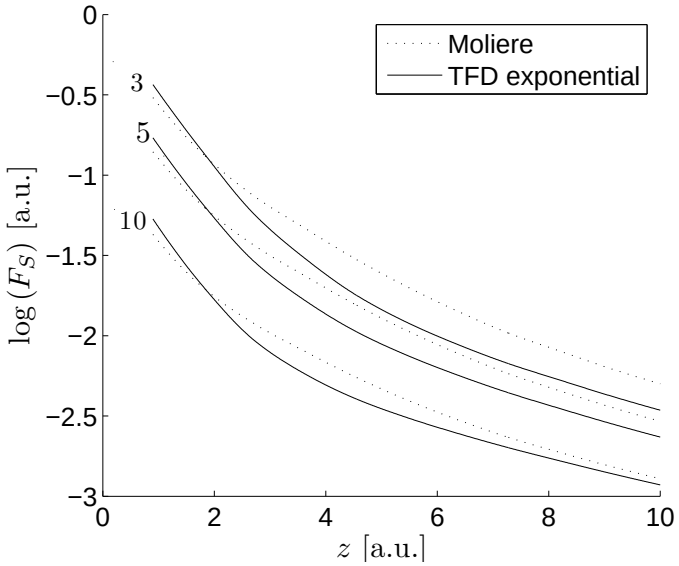

Figure 5.6: Stopping force for a proton moving parallel to graphene at speeds $v = 3$ a.u., $v = 5$ a.u., and $v = 10$ a.u. The solid line (——) is calculated using the TFD exponential approximation to the electron density. The dotted line (·····) is calculated using the Molière approximation to the electron density. We plot the logarithm to base 10 of the stopping force as a function of the distance from the sheet.

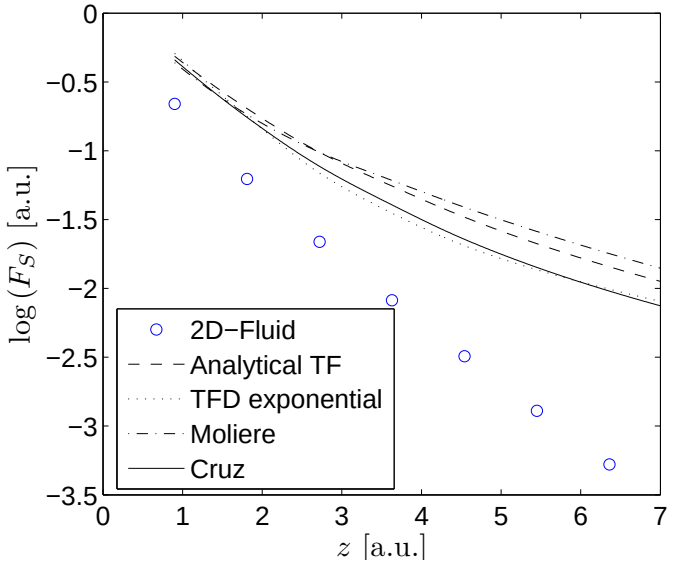

Figure 5.7: Stopping force for a proton moving parallel to graphene at speed $v = 3$ a.u. The dashed line (– –) is calculated using the analytical TF electron density for graphene. The dotted line (·····) is calculated using the TFD exponential approximation to the electron density. The dashed-dotted line (–·–) is calculated using the Molière approximation to the electron density. The solid line (——) is calculated using the Cruz approximation to the electron density. The circles (o o o) are calculated using a 2D-Fluid model. We plot the logarithm to base 10 of the stopping force as a function of the distance from the sheet.

density. The results are shown in figures 5.5 and 5.6. We can see how at close distances to the sheet, the stopping force calculated using the Molière electron density is smaller than the stopping force calculated using the TF and TFD electron densities. At larger distances from the sheet, where the Molière electron density is larger than the TF and TFD electron densities, the stopping force calculated using the Molière electron density is larger.

In figure 5.7 we show the stopping force for a proton moving parallel to a graphene sheet at speed $v = 3$ a.u. The stopping force is calculated using five different models for the electron density. Since Cruz's model takes into account all

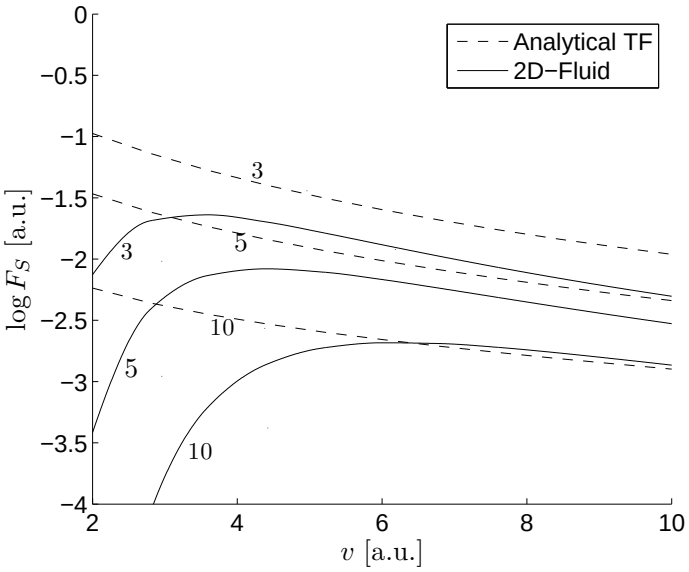

Figure 5.8: Stopping force for a proton moving parallel to graphene at distance $d = 3$ a.u., $d = 5$ a.u., and $d = 10$ a.u. from the sheet. The dotted line (·····) is calculated using the Analytical TF electron density for graphene. The solid line (——) is calculated using the 2D-Fluid model. We plot the logarithm to base 10 of the stopping force as a function of the proton's speed.

six of carbon's electrons in the calculation of the electron density, all models in this plot have been adjusted to include all of carbon's six electrons when calculating the electron density.

Now we study the dependence of the stopping force on the velocity of the moving ion. In figure 5.8 we show the stopping force as a function of the proton's speed, for a proton moving parallel to graphene at distances $d = 3$ a.u., $d = 5$ a.u., and $d = 10$ a.u. from the sheet. The stopping force is calculated using the analytical TF electron density (2.32) as well as the 2D-Fluid model. We see how the stopping force is smaller for ions moving farther from the sheet, and we can also notice the large effect of having a three-dimensional electron density distribution, especially at smaller speeds.

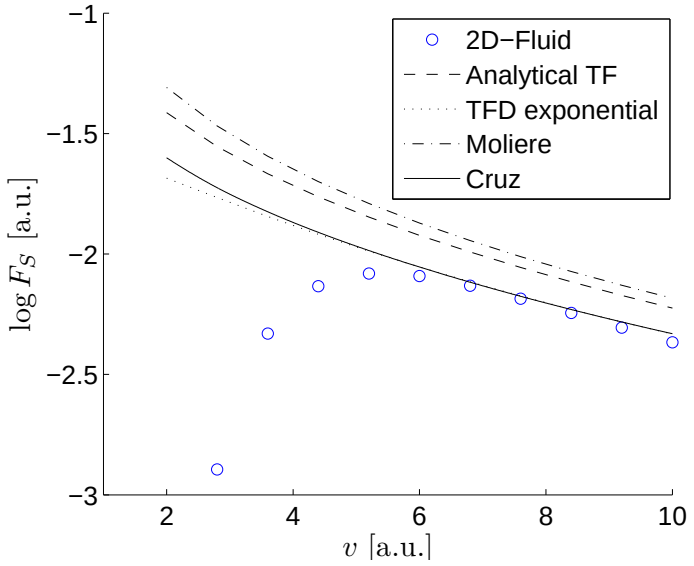

Figure 5.9: Stopping force for a proton moving parallel to graphene at distance $d = 3$ a.u. The dashed line (– –) is calculated using the analytical TF electron density for graphene. The dotted line (·····) is calculated using the TFD exponential approximation to the electron density. The dashed-dotted line (–·–) is calculated using the Molière approximation to the electron density. The solid line (——) is calculated using the Cruz approximation to the electron density. The circles (o o o) are calculated using the 2D-Fluid model. We plot the logarithm to base 10 of the stopping force as a function of the proton's speed.

In figure 5.9 we show the stopping force for a proton moving parallel to a graphene sheet and at distance $d = 3$ a.u. from the sheet. The stopping force is calculated using 5 different models for the electron density. All models in this plot have been adjusted to include all of carbon's six electrons when calculating the electron density. We plot the logarithm to base 10 of the stopping force as a function of the proton's speed. We can again see the large effect of having a three-dimensional electron density distribution, especially at smaller speeds.

Chapter 6

Image Force

When investigating ions moving parallel to a graphene sheet, it is also of interest to study the force which bends the ion's trajectory towards the sheet, called the image force (see figure 6.1). This force plays a major role in the study of ion channeling. In the present chapter we develop the theory used to calculate the image force.

Our goal is to derive a formula that we can use to compute the image force for ions moving parallel to a graphene sheet. For an ion moving through an electron gas, the dynamical image force is defined as the force perpendicular to its motion. Choosing our graphene sheet to lay in the xy-plane, we consider an ion of charge Z_1, moving at constant velocity $\mathbf{v} \equiv (\mathbf{V}, v_z) = (\mathbf{V}, 0)$ parallel to the xy-plane, and at a distance b from the xy-plane, so that the image force is given by

$$F_\perp = -Z_1 \frac{\partial \phi_{ind}}{\partial z}\bigg|_{z=b,\ \mathbf{R}=\mathbf{V}t}, \tag{6.1}$$

where ϕ_{ind} is the induced electric potential at the ion's position. To calculate the

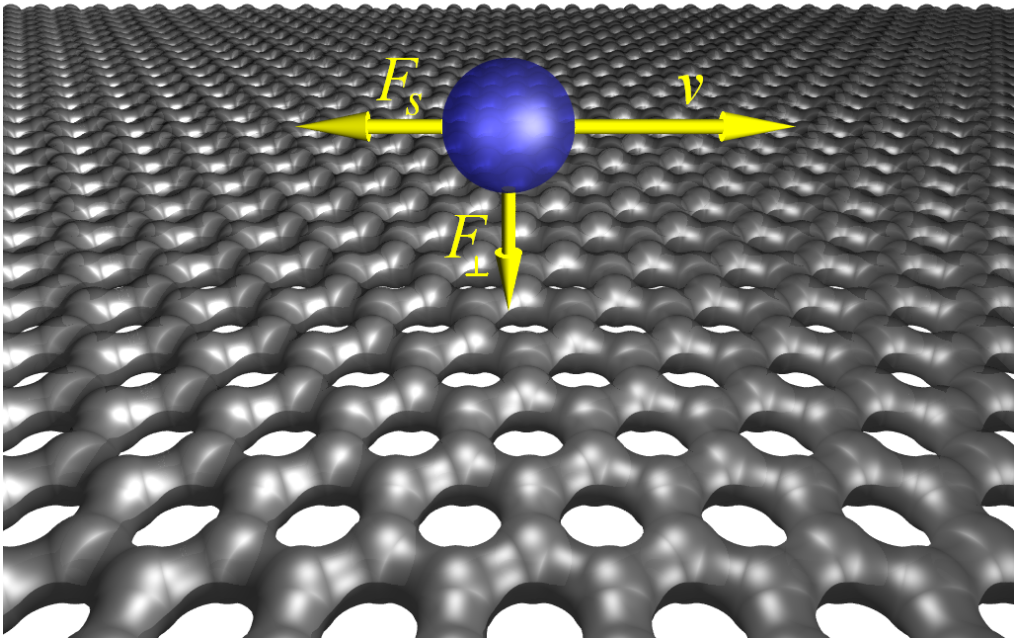

Figure 6.1: Ion moving parallel to a graphene sheet.

image force we need an expression for ϕ_{ind} in (6.1). We had from (4.23) that

$$\phi_{ind}(\mathbf{r},t) = \frac{Z_1}{2\pi}\int dz' \int \frac{d\mathbf{K}}{K}\; e^{i\mathbf{K}\cdot(\mathbf{R}-\mathbf{V}t)} e^{-|z-z'|K}\left[\epsilon^{-1}(\mathbf{K};z',b;\mathbf{K}\cdot\mathbf{V}) - \delta(z'-b)\right]. \tag{6.2}$$

Here we have that $e^{i\mathbf{K}\cdot(\mathbf{R}-\mathbf{V}t)} = 1$, since $\mathbf{R} = \mathbf{V}t$. The induced potential at the ion's position is then

$$\phi_{ind}(z) = \frac{Z_1}{2\pi}\int dz' \int \frac{d\mathbf{K}}{K}\; e^{-|z-z'|K}\left[\epsilon^{-1}(\mathbf{K};z',b;\mathbf{K}\cdot\mathbf{V}) - \delta(z'-b)\right]. \tag{6.3}$$

Now we need an expression for the inverse dielectric function in (6.3). We had from

(4.29) that the inverse dielectric function is given by

$$\epsilon^{-1}(\mathbf{r}_1,\mathbf{r}_2,\omega) \cong \frac{\omega^2}{\omega^2-\omega_p^2(\mathbf{r}_1)}\left[\delta(\mathbf{r}_1-\mathbf{r}_2) - \frac{e^2}{m}\frac{1}{\omega^2-\omega_p^2(\mathbf{r}_2)}\frac{(\mathbf{r}_2-\mathbf{r}_1)}{|\mathbf{r}_2-\mathbf{r}_1|^3}\cdot\vec{\nabla}n(\mathbf{r}_1)\right], \tag{6.4}$$

with $\omega_p^2(\mathbf{r}) = 4\pi n(\mathbf{r})$. If we consider the electron density to vary only in one dimension, we have from (4.45) that

$$\int d\mathbf{R}_{d_{12}}\; e^{i\mathbf{K}\cdot(\mathbf{R}_1-\mathbf{R}_2)}\frac{\mathbf{r}_2-\mathbf{r}_1}{|\mathbf{r}_2-\mathbf{r}_1|^3}\cdot\vec{\nabla}n(\mathbf{r}_1) = 2\pi e^{-K|z'-z|}\frac{dn(z')}{dz'}\frac{z-z'}{|z-z'|}, \tag{6.5}$$

so we may write the Fourier transform of our inverse dielectric function as

$$\epsilon^{-1}(\mathbf{K},z',z,\omega) \cong \frac{\omega^2}{\omega^2-\omega_p^2(z')}\delta(z'-z)$$

$$-\frac{1}{2}\frac{\omega^2\;\mathrm{sign}(z-z')}{\left[\omega^2-\omega_p^2(z')\right]\left[\omega^2-\omega_p^2(z)\right]}\frac{d\omega_p^2(z')}{dz'}e^{-|z-z'|K}. \tag{6.6}$$

Now we may substitute (6.6) into (6.3) and write the induced potential as

$$\phi_{ind}(z) = \frac{Z_1}{2\pi}\int\frac{d\mathbf{K}}{K}\int dz'\; e^{-|z-z'|K}\left[\frac{\omega^2}{\omega^2-\omega_p^2(z')}\delta(z'-b)\right.$$

$$\left.-\frac{1}{2}\frac{\omega^2\;\mathrm{sign}(b-z')}{\left[\omega^2-\omega_p^2(z')\right]\left[\omega^2-\omega_p^2(b)\right]}\frac{d\omega_p^2(z')}{dz'}e^{-|b-z'|K} - \delta(z'-b)\right], \tag{6.7}$$

where $\omega = \mathbf{K}\cdot\mathbf{V}$. The first and third terms inside the integral may be evaluated taking advantage of the delta function. We then have

$$\phi_{ind}(z) = \frac{Z_1}{2\pi}\int\frac{d\mathbf{K}}{K}\left[\frac{\omega^2}{\omega^2-\omega_p^2(b)}e^{-|z-b|K}\right.$$
$$\left.+\left(\int dz'\;\frac{e^{-|z-z'|K}}{2}\frac{\omega^2\;\mathrm{sign}(z'-b)}{\left[\omega^2-\omega_p^2(z')\right]\left[\omega^2-\omega_p^2(b)\right]}\frac{d\omega_p^2(z')}{dz'}e^{-|b-z'|K}\right) - e^{-|z-b|K}\right]. \tag{6.8}$$

Now we must obtain $\partial\phi_{ind}/\partial z$ to calculate the image force (6.1). When differentiating (6.8) with respect to z, the first and last terms go to zero, since

$$\frac{\partial}{\partial z}\Big[e^{-|z-b|K}\Big]_{z=b} = \lim_{h\to 0}\frac{e^{-|b+h/2-b|K} - e^{-|b-h/2-b|K}}{h} = 0. \tag{6.9}$$

We then have

$$\left.\frac{\partial\phi_{ind}}{\partial z}\right|_{z=b,\ \mathbf{R}=\mathbf{V}t} = \frac{Z_1}{2\pi}\int d\mathbf{K}\int dz' \frac{\omega^2 e^{-2|b-z'|K}}{2\left[\omega^2-\omega_p^2(z')\right]\left[\omega^2-\omega_p^2(b)\right]}\frac{d\omega_p^2(z')}{dz'}. \tag{6.10}$$

The image force is then

$$F_\perp = -Z_1\left.\frac{\partial\phi_{ind}}{\partial z}\right|_{z=b,\ \mathbf{R}=\mathbf{V}t} =$$

$$-\frac{(Z_1)^2}{4\pi}\int d\mathbf{K}\int dz'\ \frac{e^{-2|b-z'|K}\omega^2}{\left[\omega^2-\omega_p^2(z')\right]\left[\omega^2-\omega_p^2(b)\right]}\frac{d\omega_p^2(z')}{dz'} \tag{6.11}$$

It is easy to see that

$$\frac{\omega^2}{\left[\omega^2-\omega_p^2(z')\right]\left[\omega^2-\omega_p^2(b)\right]} = \frac{1}{\omega_p^2(z')-\omega_p^2(b)}\left(\frac{\omega_p^2(z')}{\omega^2-\omega_p^2(z')} - \frac{\omega_p^2(b)}{\omega^2-\omega_p^2(b)}\right), \tag{6.12}$$

so we may rewrite (6.11) as

$$F_\perp = -Z_1\left.\frac{\partial\phi_{ind}}{\partial z}\right|_{z=b,\ \mathbf{R}=\mathbf{V}t} =$$

$$-\frac{(Z_1)^2}{4\pi}\int d\mathbf{K}\int dz'\ \frac{d\omega_p^2(z')}{dz'}\frac{e^{-2|b-z'|K}}{\omega_p^2(z')-\omega_p^2(b)}\left(\frac{\omega_p^2(z')}{\omega^2-\omega_p^2(z')} - \frac{\omega_p^2(b)}{\omega^2-\omega_p^2(b)}\right). \tag{6.13}$$

We may also write (6.13) as

$$F_\perp(b) = -\frac{(Z_1)^2}{4\pi}\int_{-\infty}^{\infty} dz'\ \frac{d\omega_p^2(z')}{dz'}\frac{1}{\omega_p^2(z')-\omega_p^2(b)}$$

$$\times \ [G(z'-b,z') - G(z'-b,b)]\,, \tag{6.14}$$

where

$$G(x,y) = \int d\mathbf{K}\ e^{-2K|x|}\ P\int_{-\infty}^{\infty} d\omega\ \delta(\omega - \mathbf{K}\cdot\mathbf{V})\frac{\omega_p^2(y)}{\omega^2-\omega_p^2(y)}. \tag{6.15}$$

6.1 Simplifying $G(x,y)$

Now we want to write $G(x,y)$ in (6.14) in a more useful form. First we write (6.15) as

$$G(x,y) = \int_0^{\infty} dK\ Ke^{-2K|x|}\ P\int_{-\infty}^{\infty} d\omega\ \frac{\omega_p^2(y)}{\omega^2-\omega_p^2(y)}\int_{-\pi}^{\pi} d\theta\ \delta(\omega - KV\cos\theta). \tag{6.16}$$

Now we use the property of delta functions

$$\delta(cx) = \frac{1}{|c|}\delta(x) \tag{6.17}$$

and we have

$$G(x,y) = \int_0^{\infty} dK\ Ke^{-2K|x|}\ P\int_{-\infty}^{\infty} d\omega\ \frac{\omega_p^2(y)}{\omega^2-\omega_p^2(y)}\ 2\int_0^{\pi} d\theta\ \frac{1}{KV}\delta\left(\frac{\omega}{KV}-\cos\theta\right). \tag{6.18}$$

We define $\tau \equiv \cos\theta$, so $d\tau = -\sin\theta\ d\theta$, and making the change of variable in the θ integral, we have

$$G(x,y) = 4\int_0^{\infty} dK\ \frac{1}{V}e^{-2K|x|}\ P\int_0^{\infty} d\omega\ \frac{\omega_p^2(y)}{\omega^2-\omega_p^2(y)}\int_{-1}^{1} d\tau\ \frac{\delta(\frac{\omega}{KV}-\tau)}{\sqrt{1-\tau^2}}. \tag{6.19}$$

The τ integral becomes

$$\int_{-1}^{1} d\tau \ \frac{\delta(\frac{\omega}{KV} - \tau)}{\sqrt{1-\tau^2}} = \frac{1}{\sqrt{1-\frac{\omega^2}{(KV)^2}}} = \frac{KV}{\sqrt{(KV)^2-\omega^2}}, \tag{6.20}$$

where we must have $(KV)^2 \geq \omega^2$, so we may write (6.19) as

$$G(x,y) = 4\int_0^\infty dK \ \frac{1}{V} e^{-2K|x|} \ P\int_0^\infty d\omega \ \frac{\omega_p^2(y)}{\omega^2-\omega_p^2(y)} \frac{KV}{\sqrt{(KV)^2-\omega^2}} H(K^2V^2-\omega^2), \tag{6.21}$$

where the unit step function, $H(K^2V^2-\omega^2)$, guarantees that $(KV)^2 \geq \omega^2$.

Now we define $u_p \equiv \omega_p/(KV)$ and $u \equiv \omega/(KV)$, so that $du = d\omega/(KV)$. Using these changes of variable, the ω integral in (6.21) gives

$$\int_0^{KV} d\omega \frac{\omega_p^2(y)}{\omega^2-\omega_p^2(y)} \frac{KV}{\sqrt{(KV)^2-\omega^2}} = \int_0^1 du \ \frac{KVu_p^2(y)}{\left(u^2-u_p^2(y)\right)\sqrt{1-u^2}}$$

$$= -\frac{\pi}{2} \frac{KVu_p(y)}{\sqrt{u_p^2(y)-1}}, \tag{6.22}$$

where we need $u_p^2(y) > 1$. We may now write (6.21) as

$$G(x,y) = -2\pi \int_0^\infty dK \ Ke^{-2K|x|} \ \frac{u_p(y)H\left(u_p(y)-1\right)}{\sqrt{u_p^2(y)-1}}$$

$$= -2\pi \int_0^{\frac{\omega_p(y)}{V}} dK \ e^{-2K|x|} \ \frac{\omega_p(y)}{V} \frac{1}{\sqrt{\frac{\omega_p^2(y)}{K^2V^2}-1}}, \tag{6.23}$$

$$= -2\pi \int_0^{\frac{\omega_p(y)}{V}} dK \ e^{-2K|x|} \ \frac{K}{\sqrt{1-\frac{K^2V^2}{\omega_p^2(y)}}}. \tag{6.24}$$

Now we define $\gamma \equiv (KV)/\omega_p(y)$, so that $K = \gamma\omega_p(y)/V$ and $dK = (\omega_p(y)/V)d\gamma$.

We then have

$$G(x,y) = -2\pi \left(\frac{\omega_p(y)}{V}\right)^2 \int_0^1 d\gamma\ \gamma\ \frac{e^{-2|x|\gamma\omega_p(y)/V}}{\sqrt{1-\gamma^2}}. \tag{6.25}$$

We also define the following function

$$g(x) = \int_0^1 d\gamma\ \gamma\ \frac{e^{-x\gamma}}{\sqrt{1-\gamma^2}} = 1 - \frac{\pi}{2}\left[I_1(x) - L_1(x)\right], \tag{6.26}$$

where I_1 and L_1 are the modified Bessel function of the first kind of order 1 and the modified Struve function of order 1, respectively. We may then write (6.25) as

$$G(x,y) = -2\pi \left(\frac{\omega_p(y)}{V}\right)^2 g\left(2|x|\frac{\omega_p(y)}{V}\right). \tag{6.27}$$

6.2 Final Expression for the Image Force

We had from (6.14) that the image force was given by

$$F_\perp(b) = -\frac{(Z_1)^2}{4\pi}\int_{-\infty}^{\infty} dz'\ \frac{d\omega_p^2(z')}{dz'}\frac{1}{\omega_p^2(z') - \omega_p^2(b)}\ \times$$

$$\left[G(z'-b,z') - G(z'-b,b)\right]. \tag{6.28}$$

Using (6.27) in (6.28) we have our final expression for the image force:

$$F_\perp(b) = \frac{(Z_1)^2}{2V^2}\int_{-\infty}^{\infty} dz'\ \frac{d\omega_p^2(z')}{dz'}\frac{1}{\omega_p^2(z') - \omega_p^2(b)}\ \times$$

$$\left[\omega_p^2(z')g\left(2|z'-b|\frac{\omega_p(z')}{V}\right) - \omega_p^2(b)g\left(2|z'-b|\frac{\omega_p(b)}{V}\right)\right], \tag{6.29}$$

with $\omega_p^2(z) = 4\pi n(z)$, and g defined in (6.26).

Chapter 7

Calculation of Image Force

Now that we have an expression for the image force (6.29), we go ahead and calculate it.

7.1 Image Force at Metal Surface

As we did for the stopping force, we are first interested in calculating the image force for a particle moving next to a metal, for example aluminum, in order to compare our result with that of [19]. To use (6.29) we need an expression for the electron density. We had from (5.1) an expression for the electron density near an aluminum surface:

$$n(z) = \begin{cases} n_o - \frac{1}{2} n_o e^{\beta z}, & (z < 0) \\ \frac{1}{2} n_o e^{-\beta z}, & (z > 0) \end{cases} , \tag{7.1}$$

where z is the distance from the surface, $n_o \approx 2.69 \times 10^{-2}$ a.u. and $\beta \approx 1.24$ a.u. [18].

Using this electron density distribution together with (6.29), we compute the image force for a proton of speed $v = 3.16$ a.u., for different distances z from the surface. Figure 7.1 shows these results, which reproduce those of [19].

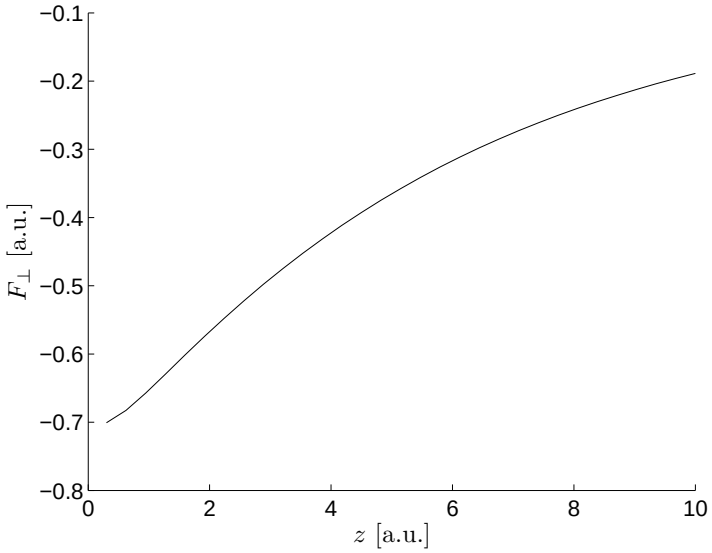

Figure 7.1: Image force for a proton of $v = 3.16$ a.u. moving parallel to an aluminum surface.

7.2 Image Force Near a Graphene Sheet

Now we are interested in using the equilibrium electron density for graphene that we calculated in chapter 2, together with (6.29), to calculate the image force for an ion moving parallel to a graphene sheet. In figure 7.2 we show the image force as a function of the distance from the sheet for a proton moving parallel to the sheet at speeds $v = 3$ a.u., $v = 5$ a.u., and $v = 10$ a.u. We compare the image force for a Thomas-Fermi analytical electron density (2.32) with the 2D-Fluid model. We can see how, as for the stopping force, the magnitude of the image force is smaller for ions moving a higher speeds. We can also see the considerable difference between the image force calculated calculated using a two-dimensional electron density and the image force calculated using a three-dimensional electron density.

Similarly, figures 7.3 and 7.4 show the image force as a function of the distance from the sheet for protons moving parallel to the sheet at speeds $v = 3$ a.u.,

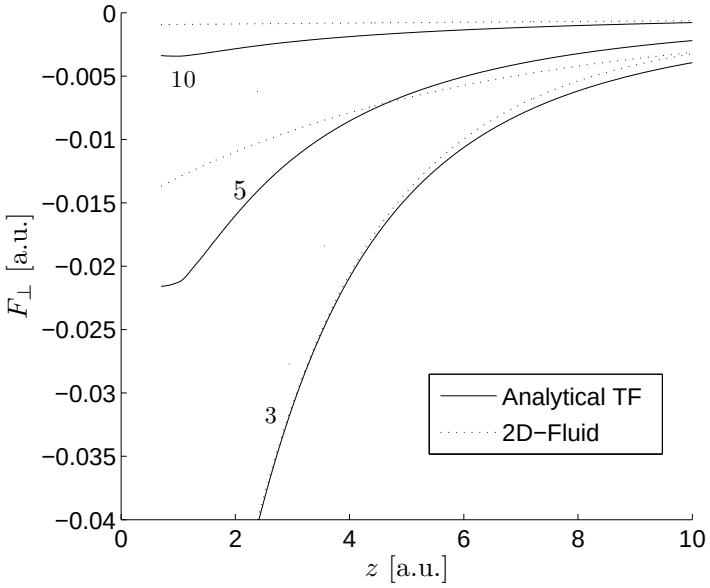

Figure 7.2: Image force for a proton moving parallel to graphene at speeds $v = 3$ a.u., $v = 5$ a.u., and $v = 10$ a.u. The solid line (——) is calculated using the TF analytical electron density for graphene. The dotted line (·····) is calculated using the 2D-Fluid model. We plot the image force as a function of the distance from the sheet.

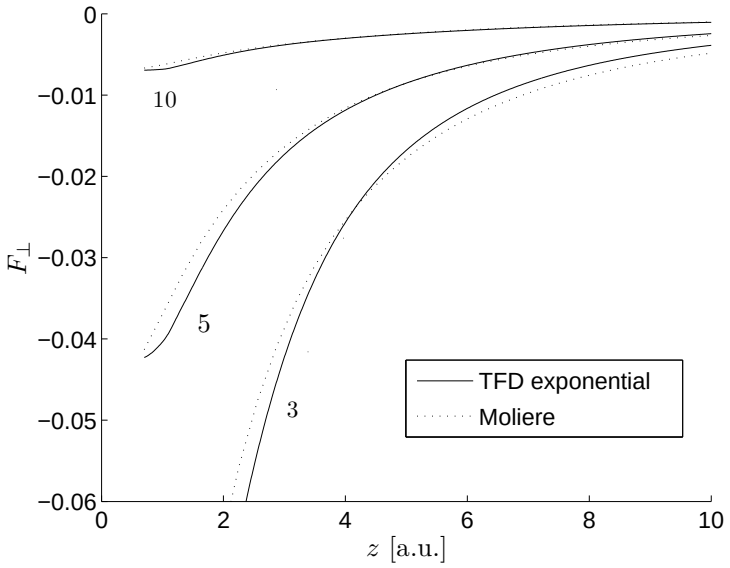

Figure 7.3: Image force for a proton moving parallel to graphene at speeds $v = 3$ a.u., $v = 5$ a.u., and $v = 10$ a.u. The solid line (——) is calculated using the TFD exponential approximation to the electron density. The dotted line (·····) is calculated using the Molière approximation to the electron density. We plot the image force as a function of the distance from the sheet.

$v = 5$ a.u., and $v = 10$ a.u. Figure 7.3 shows the image force calculated using a TFD exponential approximation to the electron density (2.33) and the image force calculated using a Molière approximation to the electron density (2.68). Figure 7.4 shows the image force calculated using the TF analytical electron density (2.32) and the image force calculated using Cruz's approximation to the electron density (2.82).

Now we study the dependence of the image force on the velocity of the moving ion. In figure 7.5 we show the image force as a function of the proton's speed, for a proton moving parallel to graphene at distances $d = 3$ a.u., $d = 5$ a.u., and $d = 10$ a.u. from the sheet. The image force is calculated using the TFD exponential approximation to the electron density (2.33) as well as the 2D-Fluid model.

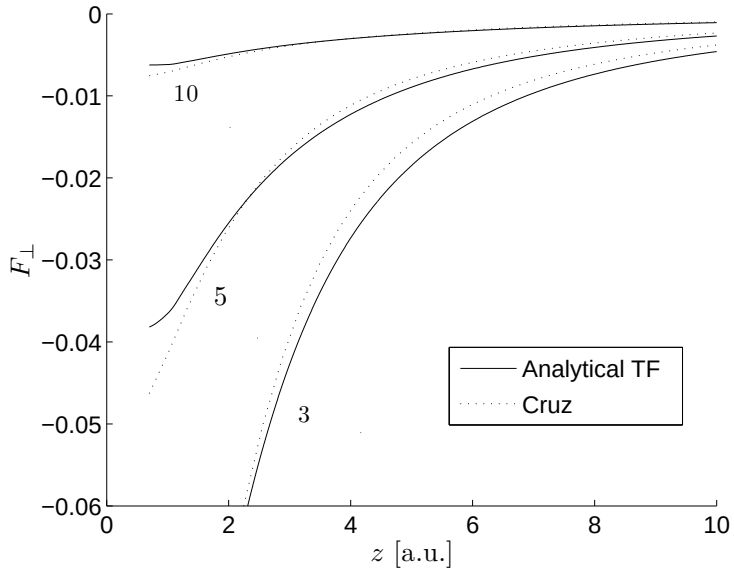

Figure 7.4: Image force for a proton moving parallel to graphene at speeds $v = 3$ a.u., $v = 5$ a.u., and $v = 10$ a.u. The solid line (——) is calculated using the TF analytical electron density for graphene. The dotted line (·····) is calculated using Cruz's approximation to the electron density. We plot the image force as a function of the distance from the sheet.

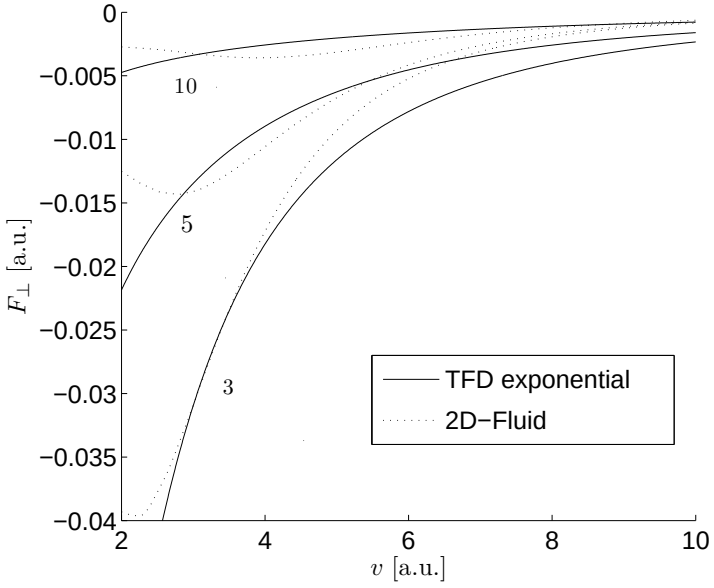

Figure 7.5: Image force for a proton moving parallel to graphene at distances $d = 3$ a.u., $d = 5$ a.u., and $d = 10$ a.u. from the sheet. The solid line (——) is calculated using the TFD exponential approximation to the electron density. The dotted line (·····) is calculated using the 2D-Fluid model. We plot the image force as a function of the proton's speed.

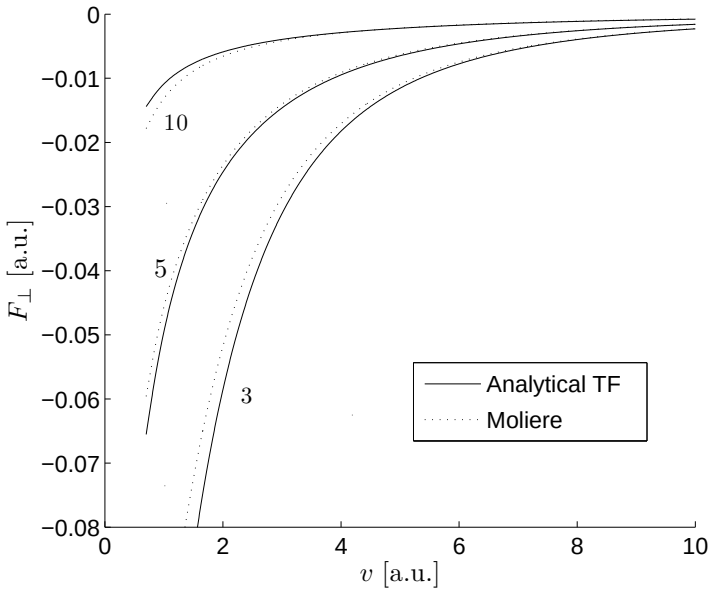

Figure 7.6: Image force for a proton moving parallel to graphene at distances $d = 3$ a.u., $d = 5$ a.u., and $d = 10$ a.u. from the sheet. The solid line (——) is calculated using the TF analytical electron density for graphene. The dotted line (·····) is calculated using the Molière approximation to the electron density. We plot the image force as a function of the proton's speed.

Similarly, figures 7.6 and 7.7 show the image force as a function of the proton's speed, for a proton moving parallel to graphene at distances $d = 3$ a.u., $d = 5$ a.u., and $d = 10$ a.u. from the sheet. Figure 7.6 shows the image force calculated using the TF analytical electron density (2.32) and the image force calculated using the Molière approximation to the electron density (2.68). Figure 7.7 shows the image force calculated using the TFD exponential approximation to the electron density (2.33) and the image force calculated using Cruz's approximation to the electron density (2.82).

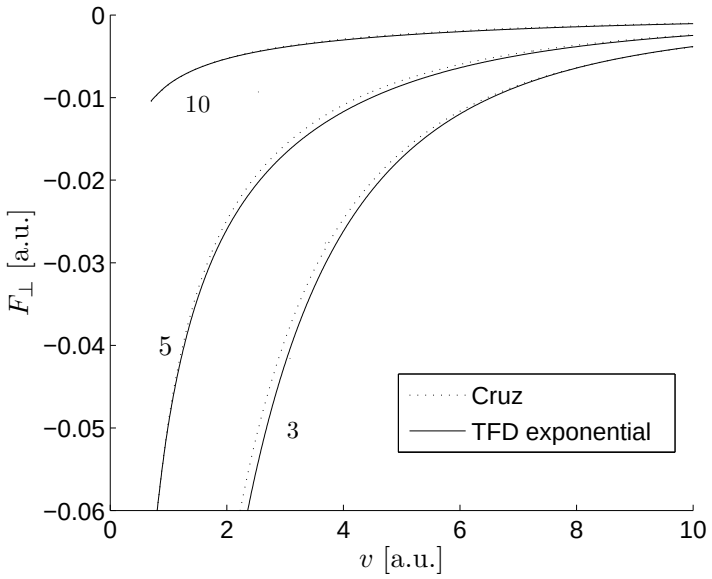

Figure 7.7: Image force for a proton moving parallel to graphene at distances $d = 3$ a.u., $d = 5$ a.u., and $d = 10$ a.u. from the sheet. The solid line (——) is calculated using the TFD exponential approximation to the electron density. The dotted line (·····) is calculated using Cruz's approximation to the electron density. We plot the image force as a function of the proton's speed.

Chapter 8

Concluding Remarks

8.1 Summary

In this work we have studied both graphene sheets and carbon nanotubes. We have analyzed the electron density distribution in these structures and how this affects the way fast moving ions interact with them.

In chapters 2 and 3 we calculated the three-dimensional equilibrium electron density for graphene and carbon nanotubes by using the generalized Thomas Fermi model in the jellium approximation where the carbon atoms are continuously distributed over, respectively, a single plane and a cylinder.

Next, we investigated fast ions moving parallel to a graphene sheet and experiencing forces due to the dynamic polarization of carbon valence electrons. First we studied the force which directly opposes the ion's motion, or the stopping force. In chapter 4 we developed the theory used to calculate the stopping force, and in chapter 5 we showed results for calculations of the stopping force using the three-dimensional electron density distribution of graphene.

Finally, we studied the force which bends the ion's trajectory towards the sheet, or the image force, which plays a major role in the study of ion channeling. In

chapter 6 we developed the theory used to calculate the image force, and in chapter 7 we showed results for calculations of the image force using the three-dimensional electron density distribution of graphene.

8.2 Conclusions

When studying the equilibrium electron density of graphene, we first found an analytical TF solution (2.32). This electron density had an inverse power decay, which might overestimate the real electron density because of its long range. We then found exponential approximations to the electron density by minimizing the TFD energy functional and by least squares minimization. Due to their faster decay, these exponential approximations gave us electron densities with much smaller tails than those of the analytical TF electron density. We also found other analytical approximations to the electron density distribution, first by using Poisson's equation together with the well-know Molière repulsive atomic potential, and then by generalizing Cruz's expression for a single atom's electron density to the case of a graphene sheet. We found that the Molière electron density was given by a sum of exponentials, one of which is very long ranged, so at large distances from the sheet it is even higher than the analytical TF solution. The Cruz electron density was given by a sum of exponentials multiplied by polynomials, and gives an electron density which at some distances is above and at some distances is below the TFD single exponential approximation. Since the Cruz model is designed from spherically averaged electron densities for all populated shells in a free carbon atom (two electrons in each of the 1s, 2s, and 2p shells), it is expected to provide the most realistic electron density dependence on the distance from graphene or the nanotube wall. However, it should be borne in mind that neither the Molière nor the Cruz approximation take into account electron hybridization that takes place

when carbon atoms form covalent bonds in graphene.

When studying the equilibrium electron density for carbon nanotubes, we first found numerical solutions using both a TF and a TFD model. As for graphene, we found that at large distances from the nanotube wall the TF density is larger than the TFD density. We also used a Molière approximation to the electron density and found how, like for graphene, it is higher than the TF solution at large distances from the nanotube wall.

In the second part of the thesis we studied ions moving parallel to graphene sheets. We calculated the stopping and image forces for these ions by using the three dimensional electron density distribution of graphene. We saw how the magnitude of stopping and image forces decreases with distance from the sheet and with the ion speed. In calculating the stopping force, we obtained an expression consisting of two terms, one called the local term, which corresponds to the well-known Bethe formula for stopping in a homogeneous medium, and one called the nonlocal term, which has a significant contribution to the stopping force at large distances from the graphene sheet.

We also compared our results for calculations of stopping and image force with calculations based on a two-dimensional hydrodynamic model of graphene, which approximates the electron distribution of graphene by a charged fluid confined to the two-dimensional plane of the sheet. We saw how considering a three-dimensional electron distribution for a graphene sheet has a considerable effect on the stopping and image forces for moving ions.

8.3 Future Work

The results obtained for interactions of ions with a single graphene sheet should be useful for a further analysis of ion channeling through carbon nanostructures. In

particular, it would be natural to extend our results for ions interacting with single graphene sheets to the case of multiple parallel planes of graphene, which form highly oriented pyrolytic graphite when stuck at a separation distance of about 3.4 Å.

On the other hand, rather intense studies of ion channeling through carbon nanotubes have been underway over the past several years. The main contribution of this thesis is in setting the stage for calculating both the stopping forces on ions channeling through nanotubes and the image forces which steer those ions towards the nanotube walls, in a manner which will be consistent with the models currently used for describing the repulsive interactions with the carbon atoms on the nanotube walls. For example, the recent results by Borka et al. [Phys. Rev. A, submitted] on proton channeling through short carbon nanotubes, where the image force was calculated by means of a 2D hydrodynamic model and the repulsive potential of carbon atoms by the Molière model, revealed a strong rainbow effect in the angular distributions of channeled protons. Since the ion trajectories are very sensitive to details of the interaction potentials, it will be important to reconsider this work by using the image force based on a dynamical polarization of the 3D electron density obtained from the Molière model. This project is already underway. It is expected that the results achieved will be used in promoting the rainbow effect in ion channeling through carbon nanotubes as a sensitive experimental technique for measuring the electron density in carbon nanotubes and other carbon nanostructures.

Appendix A

Inverse Dielectric Function

Here we derive Kitagawa's inverse dielectric function (4.29) from the 3-D fluid equations for an electron gas. When an ion moves through the electron gas, it perturbes the equilibrium electron density. We assume the flow of electrons in the perturbed state is irrotational, with velocity field

$$\mathbf{v}_f(\mathbf{r},t) = -\vec{\nabla}\psi(\mathbf{r},t), \tag{A.1}$$

where $\psi(\mathbf{r},t)$ is the potential function of the velocity field $\mathbf{v}_f(\mathbf{r},t)$. The electrostatic potential of the ion moving through the electron gas is given by

$$\phi_{ext}(\mathbf{r},t) = \int d\mathbf{r}'\ V_c(\mathbf{r}-\mathbf{r}')\rho_{ext}(\mathbf{r}',t), \tag{A.2}$$

where $V_c(\mathbf{r}-\mathbf{r}') = 1/|\mathbf{r}-\mathbf{r}'|$ is the Coulomb interaction and $\rho_{ext}(\mathbf{r}',t)$ is the charge density for the moving ion.

We then have that the total energy (Hamiltonian) of our electron gas is given by

$$H\left[n(\mathbf{r},t),\psi(\mathbf{r},t)\right] = G\left[n(\mathbf{r},t)\right] + \frac{1}{2}\int d\mathbf{r}\ n(\mathbf{r},t)|\vec{\nabla}\psi(\mathbf{r},t)|^2 +$$

$$\frac{1}{2}\int d\mathbf{r}\int d\mathbf{r}'\ V_c(\mathbf{r}-\mathbf{r}')n(\mathbf{r},t)n(\mathbf{r}',t) - \int d\mathbf{r}\ n(\mathbf{r},t)V_+(\mathbf{r}) - \int d\mathbf{r}\ n(\mathbf{r},t)\phi_{ext}(\mathbf{r},t), \quad \text{(A.3)}$$

where $n(\mathbf{r},t)$ is the perturbed electron density, $V_+(\mathbf{r})$ is the electrostatic potential produced by the positive ion cores, and $G\left[n(\mathbf{r},t)\right]$ is

$$G\left[n(\mathbf{r},t)\right] = \int d\mathbf{r}\ \left[C_F n^{5/3}(\mathbf{r}) + C_{vW}\frac{\left[\vec{\nabla}n(\mathbf{r})\right]^2}{n(\mathbf{r})} - C_x n^{4/3}(\mathbf{r})\right]. \quad \text{(A.4)}$$

As in section 2.1, the first two terms in (A.4) are the Thomas-Fermi kinetic energy functional and its von Weizsäcker correction, respectively. The third term is the Dirac exchange energy. The coefficients C_F, C_{vW}, and C_x are as given in section 2.1.

Treating n and ψ as conjugate variables, with Lagrangian

$$L = \int d\mathbf{r}\ n(\mathbf{r},t)\frac{\partial\psi(\mathbf{r},t)}{\partial t}\ -\ H\left[n(\mathbf{r},t),\psi(\mathbf{r},t)\right], \quad \text{(A.5)}$$

we use the variational principle and set

$$\delta\int_{t_1}^{t_2} dt\ L = 0. \quad \text{(A.6)}$$

Using (A.6) together with a normalization condition

$$\int d\mathbf{r}\ n(\mathbf{r},t) = N, \quad \text{(A.7)}$$

we get two equations:

$$\frac{\partial n}{\partial t} = \vec{\nabla}\cdot\left(n\vec{\nabla}\psi\right) \quad \text{(A.8)}$$

and

$$\frac{\partial\psi}{\partial t} + \gamma\psi + \mu = \frac{1}{2}|\vec{\nabla}\psi|^2 + \frac{\delta G}{\delta n} - \Phi(\mathbf{r},t). \quad \text{(A.9)}$$

The first equation is the continuity equation and the second equation gives an equation of motion for the electron fluid. The term $\gamma\psi$ is introduced to give friction. The term μ in (A.9) is a Lagrange multiplier arising from our normalization constraint (A.7). The total electrostatic potential $\Phi(\mathbf{r},t)$ is a solution to Poisson's equation

$$\nabla^2\Phi(\mathbf{r},t) = -4\pi\left[\rho_{ext}(\mathbf{r},t) + n_+(\mathbf{r}) - n(\mathbf{r})\right]. \tag{A.10}$$

Now we use perturbation theory assuming, $\rho_{ext}(\mathbf{r},t) \equiv \lambda\rho_{ext}(\mathbf{r},t)$, and expand quantities we will use in terms of a parameter λ:[1]

$$n(\mathbf{r},t) = n_0(\mathbf{r}) + \lambda n_1(\mathbf{r},t) + \cdots \tag{A.11}$$

$$\psi(\mathbf{r},t) = 0 + \lambda\psi_1(\mathbf{r},t) + \cdots \tag{A.12}$$

$$\Phi(\mathbf{r},t) = \Phi_0(\mathbf{r}) + \lambda\Phi_1(\mathbf{r},t) + \cdots \tag{A.13}$$

$$\frac{\delta G}{\delta n} = \left(\frac{\delta G}{\delta n}\right)_0 + \lambda\left(\frac{\delta G}{\delta n}\right)_1 + \cdots. \tag{A.14}$$

Using (A.11)-(A.14) together with (A.8)-(A.10) we may collect zeroth order terms and obtain our zeroth order equations:

$$\frac{\partial n_0}{\partial t} = 0 \tag{A.15}$$

$$\mu = \left(\frac{\delta G}{\delta n}\right)_0 - \Phi_0(\mathbf{r}) \tag{A.16}$$

$$\nabla^2\Phi_0(\mathbf{r}) = -4\pi\left[n_+(\mathbf{r}) - n_0(\mathbf{r})\right]. \tag{A.17}$$

[1]For now we assume that λ is a small parameter, but we will later set it equal to 1, since it is only a bookkeeping parameter.

Notice that if we take only the TF term in our expression (A.4) for $G\left[n(\mathbf{r},t)\right]$, then

$$\left(\frac{\delta G}{\delta n}\right)_0 = \frac{5}{3}C_F n_0^{2/3}(\mathbf{r}), \tag{A.18}$$

and (A.16) is equivalent to (2.7).[2] Also, (A.17) is equivalent to (2.10), so we see that the zeroth order equations (A.15)-(A.17) correspond exactly to the ground-state electron density problem solved in section 2.2.

To study the electron density perturbed by the moving ion, we again use (A.11)-(A.14) together with (A.8)-(A.10) and we collect first order terms to obtain our first order equations:

$$\frac{\partial n_1}{\partial t} = \vec{\nabla}\cdot\left(n_0\vec{\nabla}\psi_1\right) = \left(\vec{\nabla}n_0\cdot\vec{\nabla} + n_0\nabla^2\right)\psi_1 \tag{A.19}$$

$$\frac{\partial \psi_1}{\partial t} + \gamma\psi_1 = -\Phi_1 \tag{A.20}$$

$$\nabla^2\Phi_1 = -4\pi\left(\rho_{ext} - n_1\right). \tag{A.21}$$

For sake of simplicity we have dropped $(\delta G/\delta n)_1$ in (A.20). [3]

Defining the Fourier transform with respect to time,

$$n_1(\mathbf{r},t) = \int_{-\infty}^{\infty}\frac{d\omega}{2\pi}\; e^{-i\omega t}\tilde{n}_1(\mathbf{r},\omega) \tag{A.22}$$

and

$$\psi_1(\mathbf{r},t) = \int_{-\infty}^{\infty}\frac{d\omega}{2\pi}\; e^{-i\omega t}\tilde{\psi}_1(\mathbf{r},\omega), \tag{A.23}$$

we obtain

$$\frac{\partial n_1}{\partial t} = \int_{-\infty}^{\infty}\frac{d\omega}{2\pi}\; e^{-i\omega t}\left[-i\omega\tilde{n}_1(\mathbf{r},\omega)\right] \tag{A.24}$$

[2]The constant μ in (A.16), which is called the chemical potential, is zero in TF and TFD theory [20].

[3]By making this assumption we later recover Kitagawa's result in (A.42).

and

$$\frac{\partial \psi_1}{\partial t} = \int_{-\infty}^{\infty} \frac{d\omega}{2\pi}\; e^{-i\omega t}\left[-i\omega\tilde{\psi}_1(\mathbf{r},\omega)\right]. \tag{A.25}$$

Using (A.24) and (A.25), and taking the Fourier transform of our first order equations (A.19)-(A.21) we get

$$-i\omega\tilde{n}_1 = \left(\vec{\nabla} n_0 \cdot \vec{\nabla} + n_0\nabla^2\right)\tilde{\psi}_1 \tag{A.26}$$

$$(-i\omega + \gamma)\,\tilde{\psi}_1 = -\tilde{\Phi}_1 \tag{A.27}$$

$$\nabla^2\tilde{\Phi}_1 = -4\pi\left(\tilde{\rho}_{ext} - \tilde{n}_1\right). \tag{A.28}$$

Multiplying (A.26) by $(-i\omega + \gamma)$ and using (A.27) we get

$$\begin{aligned} -i\omega(-i\omega+\gamma)\tilde{n}_1 &= \left(\vec{\nabla} n_0 \cdot \vec{\nabla} + n_0\nabla^2\right)\left(-\tilde{\Phi}_1\right) \\ &= -\vec{\nabla} n_0 \cdot \vec{\nabla}\tilde{\Phi}_1 - n_0\nabla^2\tilde{\Phi}_1 \\ &= -\vec{\nabla} n_0 \cdot \vec{\nabla}\tilde{\Phi}_1 + 4\pi n_0\left(\tilde{\rho}_{ext} - \tilde{n}_1\right), \end{aligned} \tag{A.29}$$

where in the last step we have used (A.28). We now write (A.29) as

$$-\omega(\omega + i\gamma)\tilde{n}_1 = -\vec{\nabla} n_0 \cdot \vec{\nabla}\tilde{\Phi}_1 + \omega_p^2(\mathbf{r})\left(\tilde{\rho}_{ext} - \tilde{n}_1\right), \tag{A.30}$$

where $\omega_p^2(\mathbf{r}) = 4\pi n_0$. From (A.28) we also have

$$\tilde{\Phi}_1(\mathbf{r},\omega) = \int d\mathbf{r}'\; V_c(\mathbf{r}-\mathbf{r}')\left[\tilde{\rho}_{ext}(\mathbf{r}',\omega) - \tilde{n}_1(\mathbf{r}',\omega)\right]. \tag{A.31}$$

Using (A.30) and (A.31) we get the integral equation for $\tilde{n}_1(\mathbf{r},\omega)$:

$$\left[\omega_p^2(\mathbf{r}) - \omega(\omega+i\gamma)\right]\tilde{n}_1(\mathbf{r},\omega) \;=\; \omega_p^2(\mathbf{r})\tilde{\rho}_{ext}(\mathbf{r},\omega)$$

$$-\vec{\nabla}_{\mathbf{r}} n_0(\mathbf{r}) \cdot \vec{\nabla}_{\mathbf{r}} \int d\mathbf{r}' \; V_c(\mathbf{r}-\mathbf{r}') \left[\tilde{\rho}_{ext}(\mathbf{r}',\omega) - \tilde{n}_1(\mathbf{r}',\omega)\right]. \tag{A.32}$$

We assume $\vec{\nabla}_{\mathbf{r}} n_0(\mathbf{r})$ in (A.32) is small. We then solve for $\tilde{n}_1(\mathbf{r},\omega)$ and expand in small $\vec{\nabla}_{\mathbf{r}} n_0(\mathbf{r})$ to get[4]

$$\tilde{n}_1(\mathbf{r},\omega) = \frac{\omega_p^2(\mathbf{r})\tilde{\rho}_{ext}(\mathbf{r},\omega)}{\omega_p^2(\mathbf{r}) - \omega(\omega+i\gamma)}$$

$$-\lambda \frac{\vec{\nabla}_{\mathbf{r}} n_0(\mathbf{r})}{\omega_p^2(\mathbf{r}) - \omega(\omega+i\gamma)} \cdot \vec{\nabla}_{\mathbf{r}} \int d\mathbf{r}' \; V_c(\mathbf{r}-\mathbf{r}') \left[\tilde{\rho}_{ext}(\mathbf{r}',\omega) - \tilde{n}_1(\mathbf{r}',\omega)\right]. \tag{A.33}$$

We know that an expansion of $\tilde{n}_1(\mathbf{r},\omega)$ in small λ has the form

$$\tilde{n}_1(\mathbf{r},\omega) = \tilde{n}_1^{(0)}(\mathbf{r},\omega) + \lambda \tilde{n}_1^{(1)}(\mathbf{r},\omega) + \lambda^2 \tilde{n}_1^{(2)}(\mathbf{r},\omega) + \cdots, \tag{A.34}$$

so by solving iteratively (A.33) we get

$$\tilde{n}_1^{(0)}(\mathbf{r},\omega) = \frac{\omega_p^2(\mathbf{r})\tilde{\rho}_{ext}(\mathbf{r},\omega)}{\omega_p^2(\mathbf{r}) - \omega(\omega+i\gamma)} \tag{A.35}$$

and

$$\tilde{n}_1^{(1)}(\mathbf{r},\omega) = -\frac{\vec{\nabla}_{\mathbf{r}} n_0(\mathbf{r})}{\left[\omega_p^2(\mathbf{r}) - \omega(\omega+i\gamma)\right]} \cdot \vec{\nabla}_{\mathbf{r}} \int d\mathbf{r}' \; V_c(\mathbf{r}-\mathbf{r}') \left[\tilde{\rho}_{ext}(\mathbf{r}',\omega) - \tilde{n}_1^{(0)}(\mathbf{r}',\omega)\right]. \tag{A.36}$$

Substituting (A.35) in the right hand side of (A.36) we have

$$\tilde{n}_1^{(1)}(\mathbf{r},\omega) =$$

$$-\frac{\vec{\nabla}_{\mathbf{r}} n_0(\mathbf{r})}{\left[\omega_p^2(\mathbf{r}) - \omega(\omega+i\gamma)\right]} \cdot \vec{\nabla}_{\mathbf{r}} \int d\mathbf{r}' \; V_c(\mathbf{r}-\mathbf{r}') \tilde{\rho}_{ext}(\mathbf{r}',\omega) \left[1 - \frac{\omega_p^2(\mathbf{r}')}{\omega_p^2(\mathbf{r}') - \omega(\omega+i\gamma)}\right].$$

[4]Here we again assume that λ is a small parameter, but we will later set it equal to 1, since it is only a bookkeeping parameter.

$$= -\frac{\vec{\nabla}_{\mathbf{r}} n_0(\mathbf{r})}{\left[\omega_p^2(\mathbf{r}) - \omega(\omega + i\gamma)\right]} \cdot \vec{\nabla}_{\mathbf{r}} \int d\mathbf{r}' \; V_c(\mathbf{r} - \mathbf{r}') \frac{\omega(\omega + i\gamma)\tilde{\rho}_{ext}(\mathbf{r}', \omega)}{\left[\omega(\omega + i\gamma) - \omega_p^2(\mathbf{r}')\right]}. \tag{A.37}$$

We now set $\lambda = 1$ in (A.34) and to first order we have

$$\tilde{n}_1(\mathbf{r}, \omega) \approx \tilde{n}_1^{(0)}(\mathbf{r}, \omega) + \tilde{n}_1^{(1)}(\mathbf{r}, \omega). \tag{A.38}$$

Using (A.35) and (A.37), this gives

$$\tilde{n}_1(\mathbf{r}, \omega) = -\frac{\omega_p^2(\mathbf{r})\tilde{\rho}_{ext}(\mathbf{r}, \omega)}{\omega(\omega + i\gamma) - \omega_p^2(\mathbf{r})}$$

$$+ \frac{\vec{\nabla}_{\mathbf{r}} n_0(\mathbf{r})}{\left[\omega(\omega + i\gamma) - \omega_p^2(\mathbf{r})\right]} \cdot \vec{\nabla}_{\mathbf{r}} \int d\mathbf{r}' \; V_c(\mathbf{r} - \mathbf{r}') \frac{\omega(\omega + i\gamma)\tilde{\rho}_{ext}(\mathbf{r}', \omega)}{\left[\omega(\omega + i\gamma) - \omega_p^2(\mathbf{r}')\right]}. \tag{A.39}$$

By A.31, the total electrostatic potential due to ρ_{ext} and n_1 is given by

$$\tilde{\Phi}_1(\mathbf{r}, \omega) \equiv \int d\mathbf{r}' \; V_c(\mathbf{r} - \mathbf{r}') \left[\tilde{\rho}_{ext}(\mathbf{r}', \omega) - \tilde{n}_1(\mathbf{r}', \omega)\right]$$

$$= \int d\mathbf{r}' \int d\mathbf{r}'' \; V_c(\mathbf{r} - \mathbf{r}') \Bigg\{ \delta(\mathbf{r}' - \mathbf{r}'') \left[1 + \frac{\omega_p^2(\mathbf{r}')}{\omega(\omega + i\gamma) - \omega_p^2(\mathbf{r}')}\right]$$

$$- \frac{\vec{\nabla}_{\mathbf{r}'} n_0(\mathbf{r}')}{\omega(\omega + i\gamma) - \omega_p^2(\mathbf{r}')} \cdot \vec{\nabla}_{\mathbf{r}'} V_c(\mathbf{r}' - \mathbf{r}'') \frac{\omega(\omega + i\gamma)}{\omega(\omega + i\gamma) - \omega_p^2(\mathbf{r}'')} \Bigg\} \tilde{\rho}_{ext}(\mathbf{r}'', \omega). \tag{A.40}$$

Using (4.3) and (4.4) we also know that the total electrostatic potential may be expressed, by definition, as

$$\tilde{\Phi}_1(\mathbf{r}, \omega) \equiv \int d\mathbf{r}' \int d\mathbf{r}'' \; V_c(\mathbf{r} - \mathbf{r}') \epsilon^{-1}(\mathbf{r}', \mathbf{r}'', \omega) \tilde{\rho}_{ext}(\mathbf{r}'', \omega). \tag{A.41}$$

Be comparing (A.40) and (A.41) we see that

$$\epsilon^{-1}(\mathbf{r}', \mathbf{r}'', \omega) \cong$$

$$\frac{\omega(\omega+i\gamma)}{\omega(\omega+i\gamma)-\omega_p^2(\mathbf{r}')}\left[\delta(\mathbf{r}'-\mathbf{r}'')-\frac{1}{\omega(\omega+i\gamma)-\omega_p^2(\mathbf{r}'')}\frac{(\mathbf{r}''-\mathbf{r}')}{|\mathbf{r}''-\mathbf{r}''|^3}\cdot\vec{\nabla}_{\mathbf{r}'}n(\mathbf{r}')\right], \tag{A.42}$$

which is precisely (4.29) when we let $\omega^2 \longrightarrow \omega(\omega+i\gamma)$.

Appendix B

2D-Fluid Model

In chapters 5 and 7 we calculated the stopping and image forces acting on ions moving parallel to a graphene sheet. We compared calculations done using three-dimensional approximations to the electron density for graphene, with calculations done using a 2D-Fluid model. Here we show what this 2D-Fluid model is.

We model the electron density of a graphene sheet by a compressible charged fluid that is constrained to move in 2D on the neutralizing positively charged sheet. As given in equation (99) of [21] we have that for such a model, when we consider a particle moving parallel to a graphene sheet, the induced electrostatic potential at the particle's position is given by

$$\phi_{ind}(\mathbf{R},z,t) \equiv \int \frac{d\mathbf{K}}{(2\pi)^2} \int \frac{d\omega}{2\pi}\, e^{i(\mathbf{K}\cdot\mathbf{R}-\omega t)} \tilde{\phi}_{ind}(\mathbf{K},z,\omega)$$

$$= -\frac{Z_1}{2\pi} \int \frac{d\mathbf{K}}{K} e^{i\mathbf{K}\cdot(\mathbf{R}-\mathbf{V}t)} e^{-K(|z|+|b|)} \frac{2\pi K\sigma}{\Omega^2(K) - \mathbf{K}\cdot\mathbf{V}(\mathbf{K}\cdot\mathbf{V}+i\gamma)}, \tag{B.1}$$

where $\Omega^2(K) = 2\pi\sigma K + \alpha K^2$, $\alpha = \pi\sigma$, Z_1 is the particle's charge, σ is the surface charge density of the neutralizing positively charged sheet, and b is the particle's

distance from the sheet.[1] We had from (4.2) that the stopping force is given by

$$F_S(t) = Z_1 \frac{\mathbf{v}(t)}{v(t)} \cdot \vec{\nabla}\phi_{ind}(\mathbf{r},t)\Big|_{\mathbf{R}=\mathbf{V}t,\ z=b}. \tag{B.2}$$

As given in equation (103) of [21], we may use (B.1) together with (B.2) and write the stopping force as

$$F_S = -\frac{Z_1^2}{2}\sqrt{1-\alpha/v^2}\ \kappa_{min}^2(v)e^{-\kappa_{min}(v)|b|}\Big[K_0(\kappa_{min}(v)|b|) + K_1(\kappa_{min}(v)|b|)\Big], \tag{B.3}$$

where $\kappa_{min} \equiv 2\pi\sigma/(v^2-\alpha^2)$ and $v^2 > \alpha$. When the particle's speed is high enough and we have $v^2 >> \alpha$, we let $\alpha \to 0$ in (B.3), and we get

$$F_S = \frac{Z_1^2}{\Lambda^2}e^{-|b|/\Lambda}\left[K_0\left(\frac{|b|}{\Lambda}\right) + K_1\left(\frac{|b|}{\Lambda}\right)\right], \tag{B.4}$$

where $\Lambda = v^2/(2\pi\sigma)$. This expression is what we call the 2D-Fluid model for the stopping force.

Now we are interested in calculating the image force. We had from (6.1) that the image force is

$$F_\perp = -Z_1 \frac{\partial\phi_{ind}}{\partial z}\Big|_{z=b,\ \mathbf{R}=\mathbf{V}t}. \tag{B.5}$$

We may use (B.1) together with (B.5) to write the image force as [21]

$$F_\perp = -Z_1 \text{sign}(b)\int_0^{\kappa_{max}(v)} dK\ Ke^{-2K|b|}\frac{2\pi\sigma K}{\Omega(K)}\frac{1}{\sqrt{\Omega^2(K)-K^2v^2}}, \tag{B.6}$$

---

[1] Notice we are using the same notation we have defined earlier and used throughout this work, where a particle's position is given by $\mathbf{r} = (\mathbf{R}, z)$, a particle's velocity is given by $\mathbf{v} = (\mathbf{V}, v_z)$, and the Fourier coordinates of position are described by $\mathbf{k} = (\mathbf{K}, k_z)$. The magnitude of $\mathbf{k}$ is given by k, the magnitude of $\mathbf{K}$ is given by K, and so forth.

with

$$\kappa_{max}(v) = \begin{cases} \infty, & 0 < v < \sqrt{\alpha} \\ \frac{2\pi\sigma}{v^2-\alpha}, & v > \sqrt{\alpha} \end{cases} . \tag{B.7}$$

When the particle's speed is high enough and we have $v^2 >> \alpha$, we let $\alpha \to 0$ in (B.6), so that $\Omega^2 \to 2\pi\sigma K$ and $\kappa_{max} \to 2\pi\sigma/v^2$, and we get

$$F_\perp = \frac{Z_1^2}{\Lambda^2}\frac{\sqrt{\pi}}{2}\text{sign}(b)\frac{\partial}{\partial\xi}\left[\frac{e^{-2\xi}}{\sqrt{2\xi}}\text{erfi}(\sqrt{2\xi})\right]_{\xi=|b|/\Lambda}, \tag{B.8}$$

where $\Lambda = v^2/(2\pi\sigma)$, and

$$\text{erfi}(x) = \frac{2}{\pi}\int_0^x dt\ e^{t^2}. \tag{B.9}$$

Equation (B.8) is what we call the 2D-Fluid model for the image force.

Bibliography

[1] H. Kroto, J. Heath, S. O'Brien, R. Curl, and R. Smalley, "C_{60}: Buckminsterfullerene", *Nature* **318**, 162 (1985).

[2] S. Iijima, "Helical microtubules of graphitic carbon", *Nature* **354**, 354 (1991).

[3] B. Dumé, "Hottest topic in physics revealed", *Physics Web* (2006).

[4] X. Artrue, S. Fomin, N. Shul'Ga, K. Ispirian, and N. Zhevago, "Carbon nanotubes and fullerites in high-energy and x–ray physics", *Phys. Rep.* **412** (2005).

[5] Mukhopadyay and Lundqvist, "Density oscillations and density response in systems with nonuniform electron density", *Nuovo Cimento* **B 27** (1975).

[6] M. Kitagawa, "Calculation of the stopping power at the surface of a solid", *Nucl. Inst. & Meth. in Phys. Res.* **B 33**, 409 (1988).

[7] S. P. Apell, J. R. Sabin, and S. B. Trickey, "Surface stopping", *Phys. Rev. A* **56**(5), 3769 (Nov. 1997).

[8] E. Santos and A. Villagrá, "Thomas–Fermi calculation of the interlayer force in graphite", *Phys. Rev. B* **6**, 3134 (1972).

[9] E. Zaremba and H. C. Tso, "Thomas–Fermi–Dirac–von Weizsacker hydrodynamics in parabolic wells", *Phys. Rev. B* **49**(12), 8147 (Mar. 1994).

[10] D. Griffiths, *Introduction to Electrodynamics* (Prentice Hall, New Jersey, 1999).

[11] D. S. Gemmell, "Channeling and related effects in the motion of charged particles through crystals", *Rev. Mod. Phys.* **46**, 129 (1974).

[12] S. Cruz, C.Díaz-García, A.P.Pathak, and J.Soullard, "Pressure dependence of the mean excitation energy of atomic systems", *Nucl. Inst. & Meth. in Phys. Res.* **B 230**, 46 (2005).

[13] R. Saito, C.Dresselhaus, and M. Dresselhaus, *Physical Properties of Carbon Nanotubes* (Imperial College Press, London, 1998).

[14] A. Prudnikov, Y. Brychkov, and O. Marichev, *Integrals and Series* (1983).

[15] S. Lundqvist and N. H. March, eds., *Theory of the Inhomogeneous Electron Gas* (Plenum Press, New York, 1983).

[16] M. Abramowitz and I. Stegun, *Handbook of Mathematical Functions* (Dover, New York, 1972).

[17] J. D. Jackson, *Classical Electrodynamics* (John Wiley & Sons, Inc., New York, 1999), 3rd ed.

[18] Y. Ohtsuki, T. Tokioka, T. Iitaka, and M. Kitagawa, "Stopping power at metal surfaces", *Nucl. Inst. & Meth. in Phys. Res.* **B 67**, 53 (1992).

[19] H. Sakai, Y. Ohtsuki, and M. Kitagawa, "Calculation of the dynamical image potential at metal surfaces", *Surface Science* **283**, 84 (1993).

[20] R. G. Parr and W. Yang, *Density-Functional Theory of Atoms and Molecules* (Osford University Press, New York, 1989).

[21] A. L. Fetter, "Electrodynamics of a layered electron gas.", *Annals of Physics* **81**, 367 (1973).